REACTOR SPACE-TIME ANALYSIS AND EXPERIMENTS

A THESIS

Presented to

The Faculty of the Division of Graduate

Studies and Research

by

Gabriel Howard Weaver

In Partial Fulfillment

of the Requirements for the Degree

Doctor of Philosophy

in the School of Nuclear Engineering

Georgia Institute of Technology

October, 1971

In presenting the dissertation as a partial fulfillment of the requirements for an advanced degree from the Georgia Institute of Technology, I agree that the Library of the Institute shall make it available for inspection and circulation in accordance with its regulations governing materials of this type. I agree that permission to copy from, or to publish from, this dissertation may be granted by the professor under whose direction it was written, or, in his absence, by the Dean of the Graduate Division when such copying or publication is solely for scholarly purposes and does not involve potential financial gain. It is understood that any copying from, or publication of, this dissertation which involves potential financial gain will not be allowed without written permission.

7/25/68

REACTOR SPACE-TIME ANALYSIS AND EXPERIMENTS

Approved:

Chairman

Date approved by Chairman: Oct. 12, 1971

ACKNOWLEDGMENTS

Many people have assisted me in the work described in this thesis. The faculty members of the School of Nuclear Engineering, as well as other departments, have given assistance in their areas of specialization. Dr. Graham, my thesis advisor, has not only provided much technical assistance but has made many valuable suggestions on the composition and editing of the text of this thesis. The other members of my reading committee, Dr. J. D. Clement, Dr. L. J. Gallaher, and Dr. R. J. Johnson, have given help in particular areas and lent encouragement on the entire work as well. The School of Nuclear Engineering has contributed significant funds to the completion of this thesis. Additionally, it has made possible the able assistance of Mr. Billy D. Statham for the design and construction of the electronic control circuits, Mr. Mike Burke for mechanical design and construction of the experimental device, and Mr. John Alderman for advice on data acquisition.

The provision by the Rich Electronic Computer Center of the computer time necessary for the analytical work in this thesis is acknowledged. The Frank H. Neely Nuclear Research Center supplied reactor time and made available many of its personnel. I am especially appreciative of the licensing and scheduling assistance given by Messrs. Robert Kirkland and Frederick Apple. The reactor operators, Messrs. Sam Kirbo, Dean McDowell, John Moon, and Sonny Pruett, were very helpful, both from a design and operational viewpoint.

Special thanks are due to Mobesco, Inc. and to Mr. Stanley Beavers in particular for contributions to the design and implementation of the hydraulic system used in this work. Mrs. Lydia Geeslin edited and typed the final manuscript and did much to see that all the necessary forms, and so forth, were completed. Miss Martha Shoemaker devoted many long hours to preparing the figures in this work.

I am grateful to my friends Anthony Foltman and Dr. Donald Bridges. Difficulties encountered in this work were more easily overcome knowing that others were finding and solving similar problems. Mr. Foltman deserves special thanks since he participated very closely in all phases of this thesis work. He was of particular help in program debugging and mechanical design. Additionally, the photographs in this thesis were taken by him.

The Atomic Energy Commission, through its Traineeship Program, made it financially possible for me to remain in school to complete this work.

My wife, Liz, and children, Robert and David, deserve more than thanks for the sacrifices they made to permit this work to be completed. I especially appreciate the effort made by Liz to raise happy children without much fatherly help.

TABLE OF CONTENTS

TABLE OF CONTENTS (Concluded)

LIST OF TABLES

LIST OF TABLES (Concluded)

LIST OF ILLUSTRATIONS

LIST OF ILLUSTRATIONS (Continued)

LIST OF ILLUSTRATIONS (Concluded)

SUMMARY

The flux in the Georgia Tech Research Reactor, a heavy-water moderated and cooled research reactor fueled with highly-enriched uranium, was sampled 100 times per second at several positions in the core and reflector as the reactor was shut down with a special control-rod-like device. Part of this hydraulically-operated device fit into the central fuel element position of the reactor and inserted a control rod at selected speeds. Two different rods were used, one of aluminum, worth approximately 1.5 percent $\Delta k/k$, and one of stainless steel, worth approximately 8 percent $\Delta k/k$.

Two-dimensional, multi-group, cylindrical-geometry statics and associated kinetics models of the experiment were developed. These models varied the boundaries of the central regions axially to simulate the insertion of a control rod. A digital kinetics program based on this geometrical model and using a theta-weighting scheme to solve the spatially differenced (space-time) kinetics equations was developed. However, options in the kinetics program permitted any or all energy groups to be treated adiabatically.

The results of ten different experiments are reported. Each of these experiments was simulated both with the kinetics code operating in the purely space-time mode and in the purely adiabatic mode. These kinetics simulations were in fair agreement with the experimental results. The differences between analysis and experiment were primarily due to the

inability of the homogeneous statics model to accurately predict the static flux shapes and reactor multiplications of the heterogeneous reactor.

The purely space-time calculations were compared to the adiabatic ones. Significant differences were apparent for rapid insertions; however, for slow insertions these differences diminished. Also, it was found that space-time calculations on the thermal group in conjunction with adiabatic calculations for the fast group led to results which were in agreement with the treatment of both groups by the space-time approximation. This suggests the attractive possibility of using mixed methods to perform multigroup, 2-D kinetics calculations with substantially improved economy.

CHAPTER I

INTRODUCTION

Public safety has been one of the primary considerations of the nuclear community since the first nuclear reactor went critical in 1942.[1] The process of assuring reactor safety is complicated and requires the application of many scientific disciplines. This research is concerned primarily with one of these fields, the time dependent behavior of a nuclear reactor.

There are many ways of formulating reactor kinetics theory. These range from simple point reactor kinetics theory, requiring many assumptions and providing only limited accuracy, to Boltzmann transport theory, with few assumptions and great accuracy. The difficulty of obtaining solutions to practical problems increases as fewer assumptions are made. The result is that, for any given problem, there are many possible applications of theory, each with different assumptions, different degrees of accuracy, and different real costs for the solution. Anyone using reactor kinetics theory for safety analysis must make a difficult choice between the accuracy of a solution and its cost. These decisions become increasingly more complicated as the size of reactors increases since many of the assumptions of the simpler theories become less valid.[2] In addition, the safety analysis of large, liquid-cooled, fast reactors presents problems whose solution by the simpler theories is not appropriate.[3] Thus, the

decision on which theory to use in the safety analysis of a reactor must be based on experience with each of the alternatives and on comparisons between the predictions of these theories and experimental measurements. This research will provide additional analytical and experimental results to use in making these decisions.

The remainder of this chapter reviews kinetics theory and kinetics experiments. Finally, the specific objectives of this research are given.

Kinetics Theory

Kinetics theory has been reviewed by many authors. Henry[4] discusses several of the fundamental considerations of reactor kinetics while summarizing early developments in this field. Kerlin's[5] paper extends this discussion to include present reactor kinetics. Yasinsky[6] has published an excellent explanatory text on reactor kinetics.

Kinetics theory can be derived from Boltzmann transport theory; however, a simpler starting point is that of diffusion theory. Among the many different possible results of such derivations, point reactor kinetics is the simplest technique used in the analysis of reactor transients. Historically, this method assumed a homogeneous reactor with only one neutron energy group. In addition, it assumed that the leakage throughout the reactor can be represented by a single, space-independent buckling. Henry[7] relaxed these restrictions so that only the weighted average of quantities are required to be space and energy independent. Point reactor kinetics theory results in a simple set of coupled differential equations which can be solved readily.[8] This approach is adequate for the analysis

of reactors having normalized flux distributions which change only slightly with time; however, for large, loosely-coupled reactors, heterogeneous configuration changes, and fast reactor analysis, this approach becomes questionable.

Yasinsky and Henry[9] have reported numerical examples demonstrating that point reactor kinetics theory produces results significantly different from more exact calculations. Since one cannot predict in advance those cases where point reactor kinetics will be in error, importance has been attached to developing better methods. The adiabatic or instantaneous flux-tilt method is a technique that assures accurate kinetics predictions, given gradual spatial-flux-distribution changes. The adiabatic method assumes that the spatial distribution of the flux is given by that distribution which would be present in the equilibrium state of a reactor as it physically exists at any time. By choosing weighting functions and integrating the neutron balance equations over the volume of the reactor, one obtains a set of equations, similar to those of point reactor kinetics, which can be solved for the magnitude of the flux.[10] This method produces solutions more reasonable than those of point kinetics without greatly complicating the solution process. Adiabatic methods become inaccurate as the reactor parameters are varied rapidly. The numerical examples already referenced demonstrate this.

The modal method attempts to improve the adiabatic technique by allowing more freedom in the spatial flux distribution. This spatial flux distribution is assumed, at any time, to be a linear combination of several flux shapes, usually the fundamental and higher harmonics of the

equilibrium flux shape. By using different weighting functions, sets of coupled differential equations are obtained. The number of such equations increases directly as the number of flux shapes used. This method, as discussed by Kaplan,[11] Stacey,[12] and others, has many variations in the spatial functions and weighting techniques used. Yasinsky[13] has reported excellent agreement between this method and more exact methods. Its fundamental disadvantage is the ambiguous way in which flux shapes and weighting techniques are chosen.

The most exact kinetics method which can currently be applied is that of finite differences, sometimes referred to as the nodal method. This is a brute-force method which replaces a continuous reactor by a finite, discontinuous mesh. The leakage is approximated by a Taylor series expansion, enabling kinetics theory to be replaced by many coupled differential equations. Unlike other techniques, this method can be shown to approach the exact diffusion theory solution in the limit of small mesh separations. The development of the governing equations is well explained by Hansen.[14] The finite difference method can be broken into subsets, each using different numerical means to solve the same basic theoretical equation. Hansen has analyzed several of these numerical techniques. The one most often used is that of Henry and Vota.[15] This method uses a theta-differencing scheme[15,16] to set up the solution. This scheme is a current industry standard for kinetics work although it has a severe disadvantage in that it can only be used in two-energy-group problems.

Kinetics Experiments

Kinetics experiments range from the study of inherent noise in a

critical assembly,[17] to the study of reactor shutdown mechanisms during power excursions.[18]

These investigations can usually be categorized as transfer function experiments and real-time experiments. In the simplest form of transfer function experiments, one introduces into a system a perturbation consisting of a sinusoidal change. If the system is linear, then its response will be a sinusoidal function with the same frequency as the perturbation. However, this response may have a delay, or phase shift, and a different amplitude. The results of transfer function experiments are then the amplitude and phase shift of the response relative to a perturbation of the same frequency. A spatial transfer function experiment would consist of transfer functions for different frequencies, for a distribution of spatial locations of both the perturbation and the response.

Another type of experiment is the real-time experiment. Here, one measures the response produced by some perturbation. A spatial, real-time experiment would consist of measuring the response for a distribution of points during a perturbation of the system.

In a sense, real-time experiments encompass transfer function experiments since the actual transfer function experiment can be visualized as a real-time experiment. However, for a linear system, a complete set of transfer function experiments can be used to predict nonsinusoidal real-time experiments by using an inverse Fourier transform. It turns out that one does the experiment most easily compared with the theoretical model being used. Thus, for transfer function theory, transfer function experiments are more valuable, while for real-time theory, real-time

experiments are more valuable.

Before the real-time work is described, it is instructive to consider the transfer work which has been done and which provides a limit of the type of real-time experiments which might produce significant results. Early space-time transfer work was done on the NORA Reactor,[19] a D_2O-reflected experimental reactor. It was found that perturbations above 20 radians per second produce dramatic spatial effects. This work was extended by Johnson[20] on the Georgia Tech Research Reactor. A spatial dependence was found for frequencies greater than one cycle per second. These experiments show that it is not unreasonable to expect space-time effects at moderate perturbing frequencies.

Results have recently been reported on two real-time experiments. Diaz[21] at the University of Florida has reported data on the propagation of a neutron wave through an essentially one-dimensional subcritical assembly. The results were used to test a WIGL2[15] code. Good agreement was obtained; however, the theory was found to be sensitive to the transverse buckling.

Rydin[22] has reported flux-tilting experiments on a decoupled reactor shut down by a step-like insertion of a poison near one end. He obtained fair agreement between this experiment and calculations from a modal analysis. Since only one reactor transient was reported, it is difficult to analyze any trends in the experiment or theory.

These experiments have several gaps when used in testing kinetics theory. The more accurate data are in the transfer function field and are

not directly usable in testing kinetics codes. The limited amount of real-time experiments, though applicable, does not test important aspects of kinetics codes. For example, they do not continuously vary the reactor's configuration; therefore, in essence, they only test a code's ability to handle a changing spatial boundary condition. The experiments at the University of Florida also have the disadvantage of being one dimensional and thus too simple to adequately test present two-dimensional models.

Objectives of This Thesis

Kinetics theory, based on diffusion theory, is well understood. Theoreticians have advanced very elaborate techniques for solving kinetics problems. Present computational equipment is extended to its limit in finding numerical solutions to kinetics theory. In addition, there are very few experiments with which numerical results can be compared in order to test the validity of the theories. Henry,[23] Hansen,[24] and others have stressed the importance of obtaining practical experience with the existing theoretical methods and of proving these methods by comparisons with experiment. Such comparisons must be made before these more advanced techniques can be used for reactor safety investigations.

This research produced experimental results useful in testing kinetics theories. In particular, the neutron flux of the highly-enriched D_2O-moderated reactor was monitored at several points as the reactor was shut down with different absorbers at different poisoning rates. These data are contained in this work.

An analysis technique, based on finite differences, was developed. This method includes the capability of treating any or all energy groups

adiabatically. In conjunction with this, a computer program was written to implement these numerical techniques. Using a two-dimensional model, simulations of the experiments were made. These simulations are also reported.

Finally, a comparison of analysis and experiment was made. This comparison includes an examination of adiabatic and space-time calculations.

CHAPTER II

EXPERIMENTAL EQUIPMENT AND INSTRUMENTATION

The flux was monitored at several positions as the Georgia Tech Research Reactor[25,26] (GTRR) was shut down with a specially constructed control-rod-like device, henceforth called the control rod, operating in the center of the reactor. The experimental equipment and instrumentation which were used are described in this chapter. Experimental procedures and data reduction technique are given in Chapter III and Appendix B. The results of the experiment are examined in Chapter VI.

Reactor

The primary experimental facility was the GTRR. This is a heterogeneous, heavy-water-moderated and cooled, research reactor fueled with an alloy of aluminum and highly enriched uranium. The GTRR is operated under AEC license number R-97.

A perspective view of a fuel element is shown in Figure 1. The fuel elements each have 10 fuel plates containing 14.2 grams of U^{235} clad in aluminum. The fuel plates are encased in an aluminum box, one end of which seats into the reactor's coolant flow divider or plenum. The other end is attached to a shield plug which supports the fuel element such that the fueled regions have about two feet of moderator on either end.

The heavy-water moderator and coolant is contained within a cylindrical aluminum vessel approximately six feet in diameter and ten feet

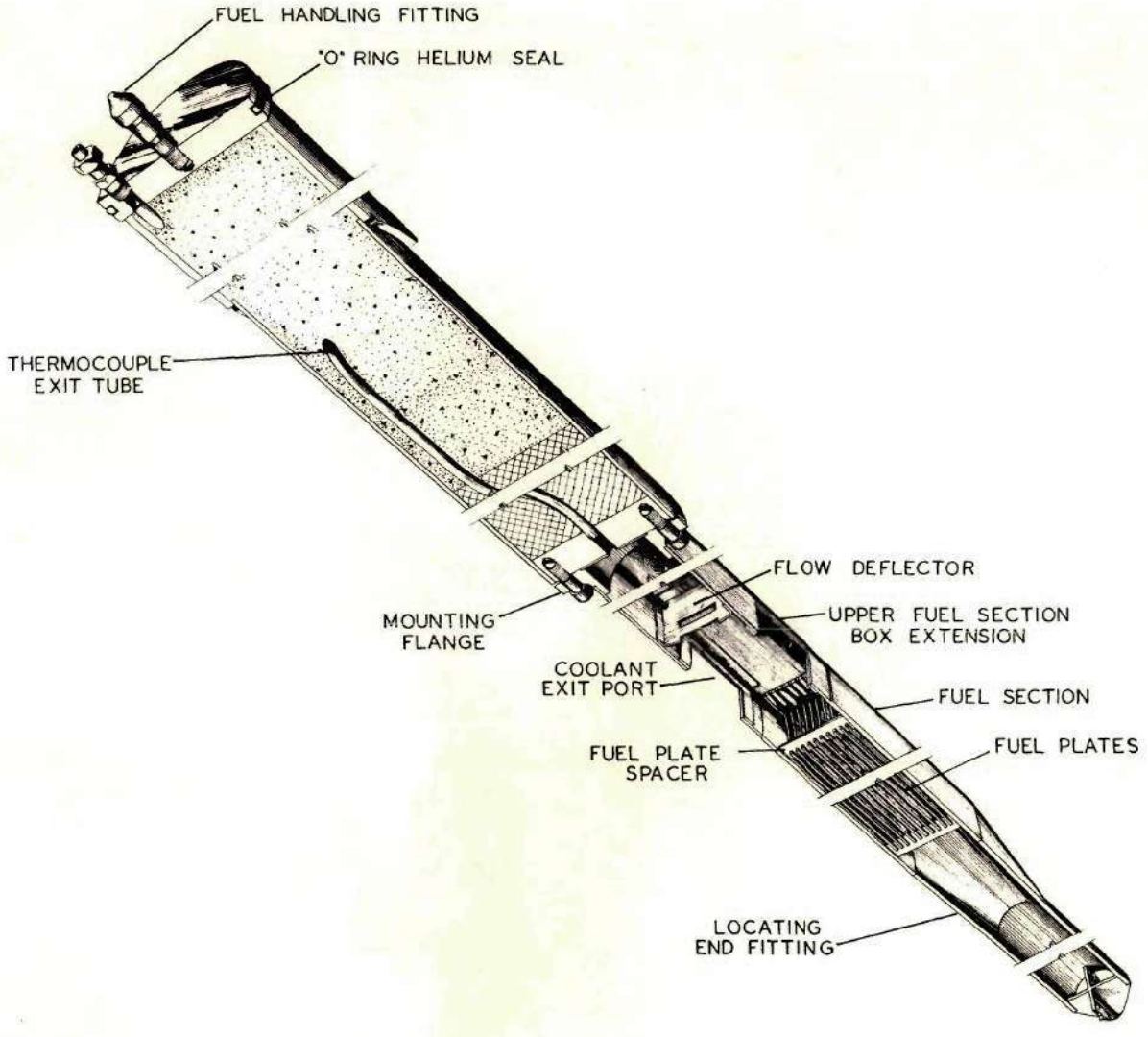

Figure 1. Perspective of a Fuel Assembly.

high. This vessel contains a grid which can hold as many as nineteen fuel elements in a six-inch triangular pitch. Figure 2 shows a horizontal section of the GTRR. Vertical penetrations V-1 through V-19 are fuel element positions. Vertical penetrations V-20 through V-23, also shown in this figure, are in the core lattice, but are not designed to accept fuel elements.

The GTRR is controlled by four shim-safety blades. The active part of these blades is made of aluminum-clad cadmium. These blades pivot from the upper edge of the reactor vessel. When fully withdrawn their center line is 6° below the horizontal. When fully inserted, it is 61° below the horizontal. Figure 3 shows the relationship between the fuel elements and the shim-safety blades. Control is also obtained with a regulating rod located in the heavy-water reflector. This rod has much less effect than a shim-safety blade and is used to make fine adjustments in the reactor multiplication.

The reactor vessel is contained in a cup-like graphite reflector. This graphite reflector is about two feet thick and extends radially and beneath the reactor vessel. Figures 2 and 4 show the sizes and positions of these components. It can be seen that the graphite is extended outward to those external positions requiring neutrons. A lead thermal shield 3 1/2 inches thick surrounds the active regions of the core. A high-density-concrete biological shield protects the environment from core radiations.

In order to produce reactor transients which were amenable to analysis with a two-dimensional kinetics program, it was necessary to insert

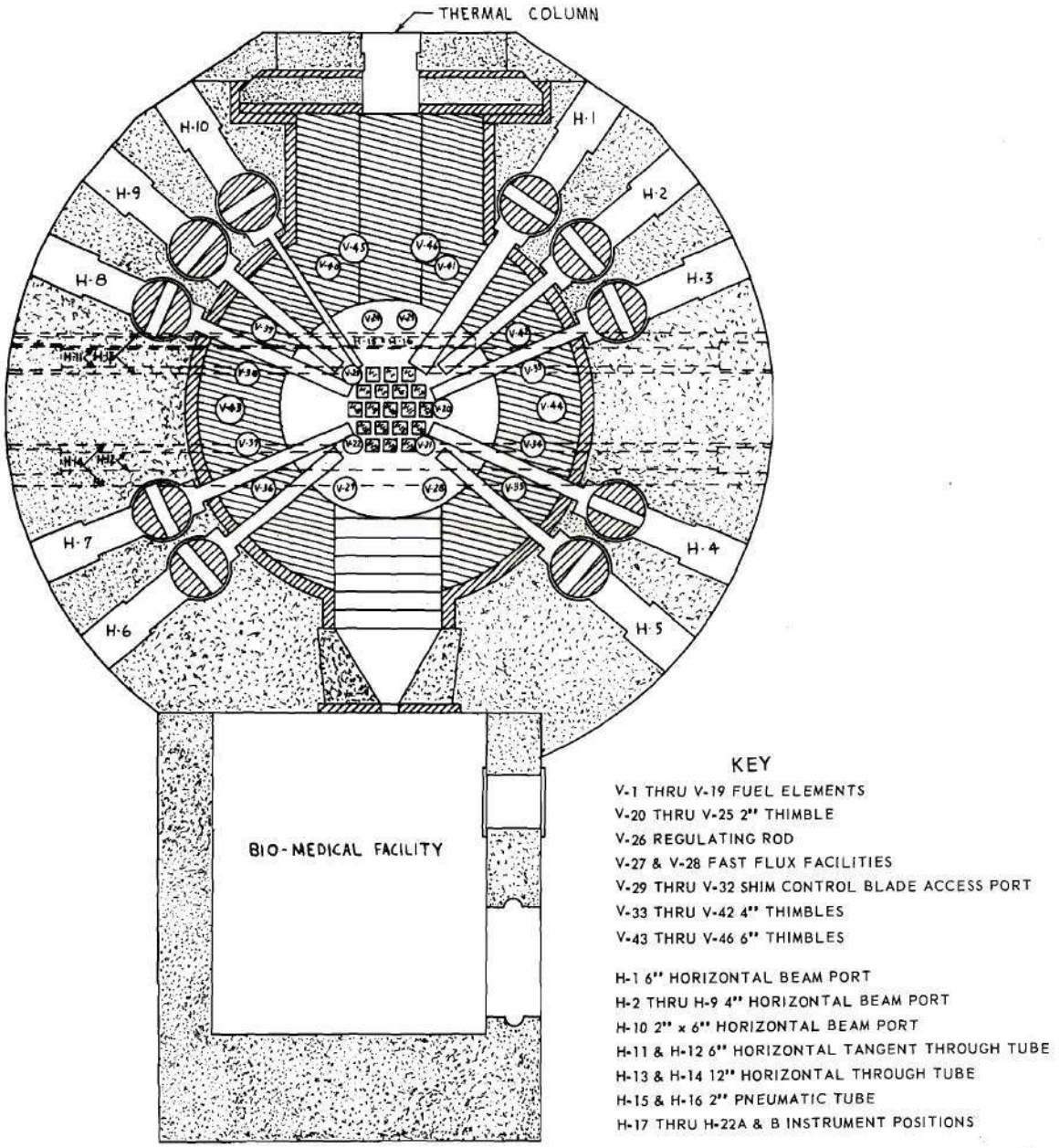

Figure 2. Horizontal Section of the GTRR at the Core Mid-Plane.

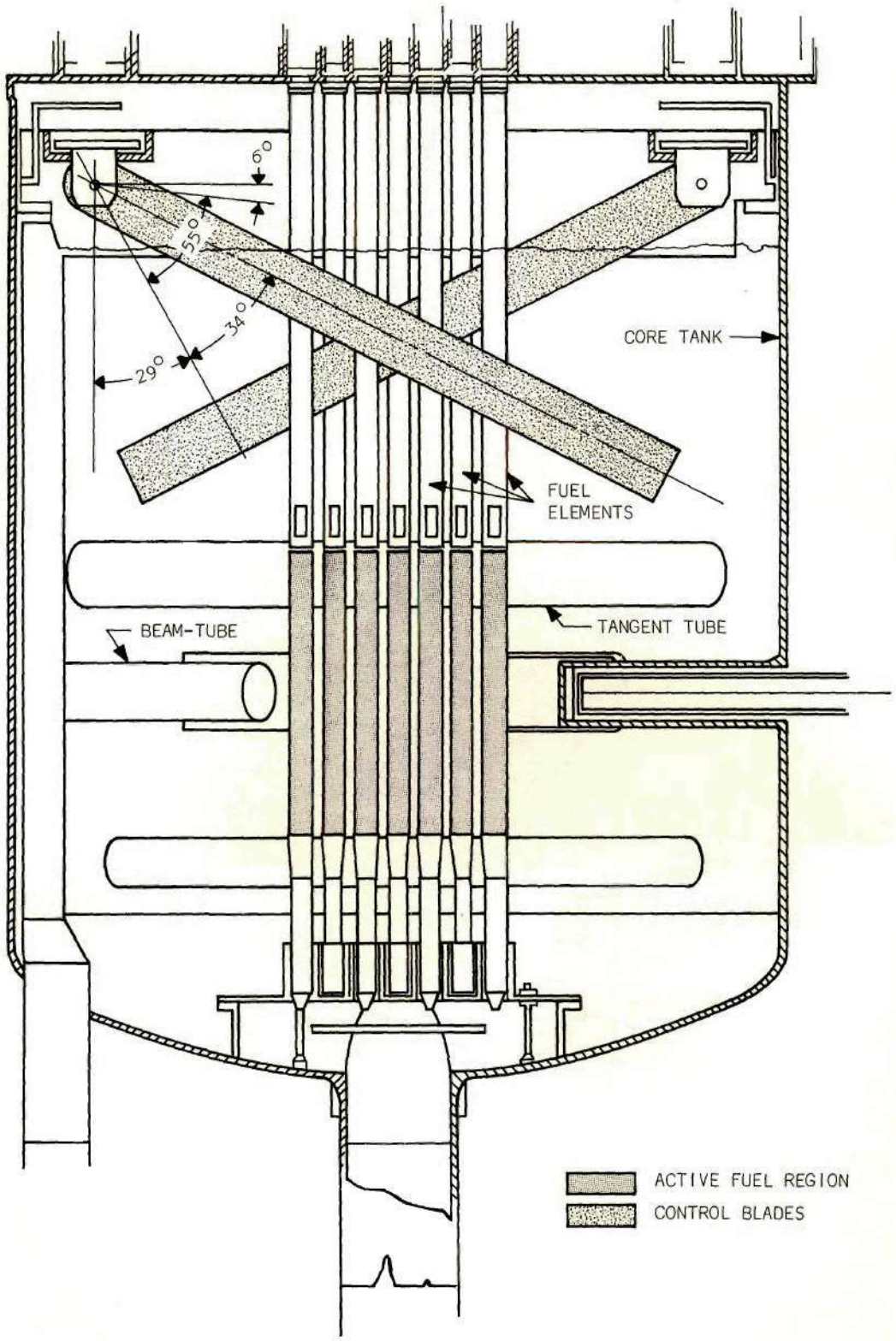

Figure 3. Vertical Section Through the GTRR Core Tank Showing a Banked Shim-Safety Blade Configuration.

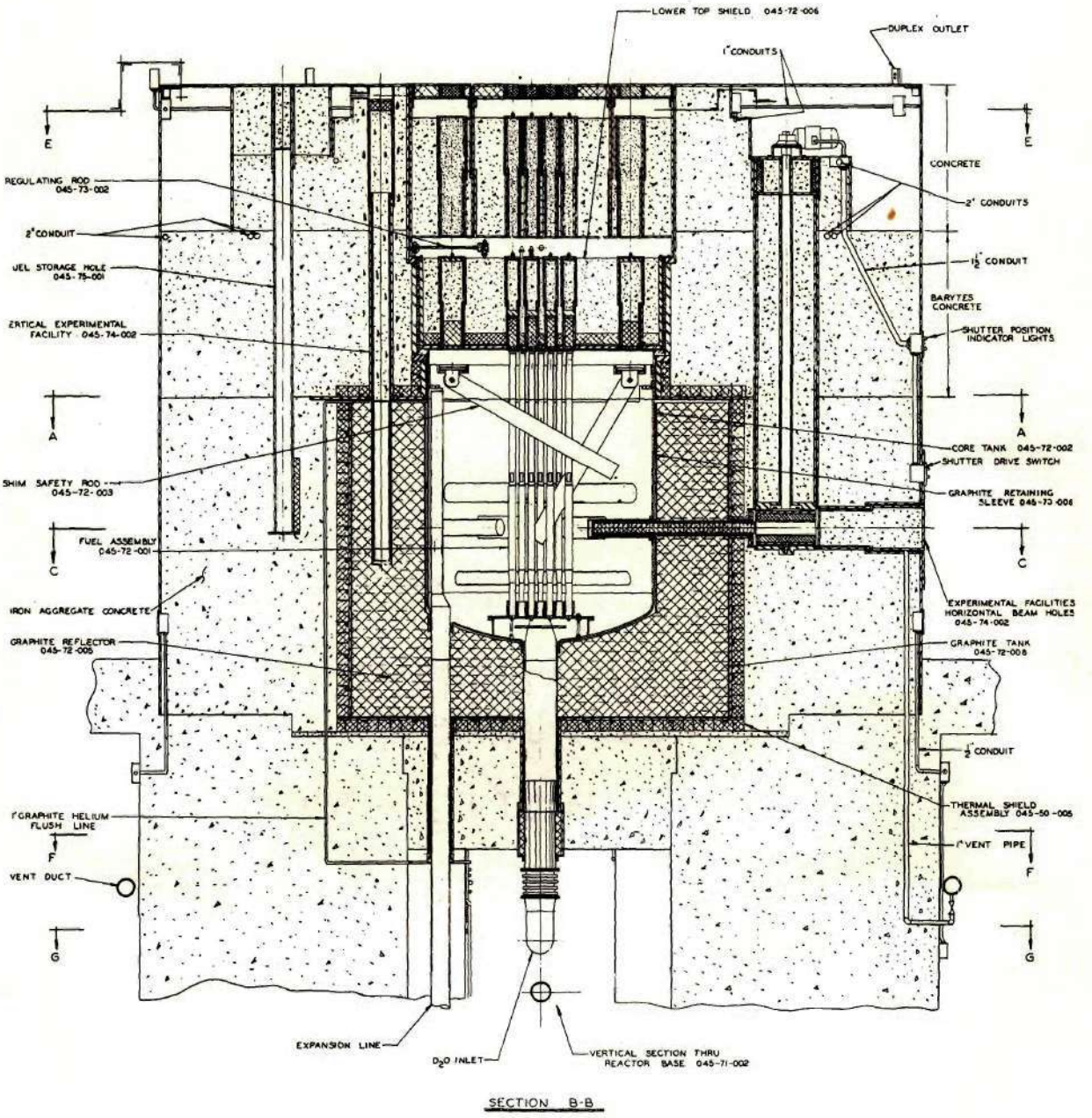

Figure 4. A Vertical Section Through the GTRR

an experimental assembly into the center of the core. Before this device is described, a few of its design criteria will be reviewed. Since safety was a main consideration, all kinetics runs were such as to reduce the GTRR's power level. In addition, an attempt was made to perform experiments whose geometry was simple enough to facilitate testing two-dimensional kinetics programs. The experimental assembly was designed for versatility, in that geometry, rates of perturbation, and control rod compositions were readily varied. Finally, the assembly was made simple to install, operate, and remove.

The experimental device was basically a hydraulically driven control rod fitting into the central fuel element position. It separates into four basic subsystems. These are:

1. Control Rod Assembly
2. Link and Instrumentation Unit
3. Hydraulic Drive
4. Control and Monitoring System.

Control Rod Assembly

The control rod assembly fits into any fuel element position, but was used in the central position, V-10, in order to approximate two-dimensional geometry. A cut-away view of the device is shown in Figure 5 and photographs are given in Figures 6 and 7. The two control rods used in the experiments each have a diameter of two inches and are thirty inches long. One is made of type 304 stainless steel and the other of type 6061 aluminum. The vertical dimensions are such that the bottom of the control rod is three inches above the fueled region of the core when

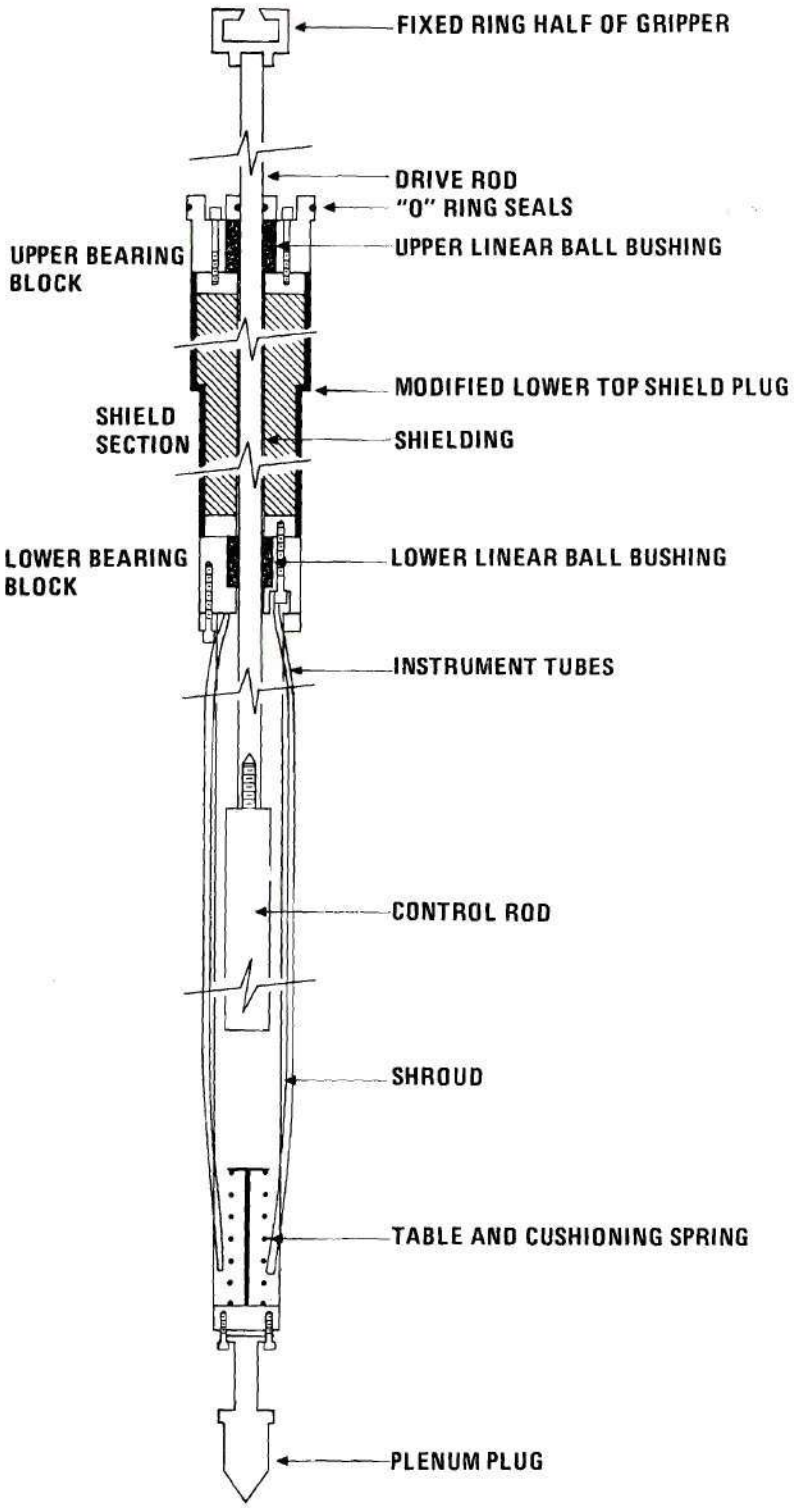

Figure 5. Cutaway View of the Control Rod Assembly.

Figure 6. Assembled Control Rod Assembly.

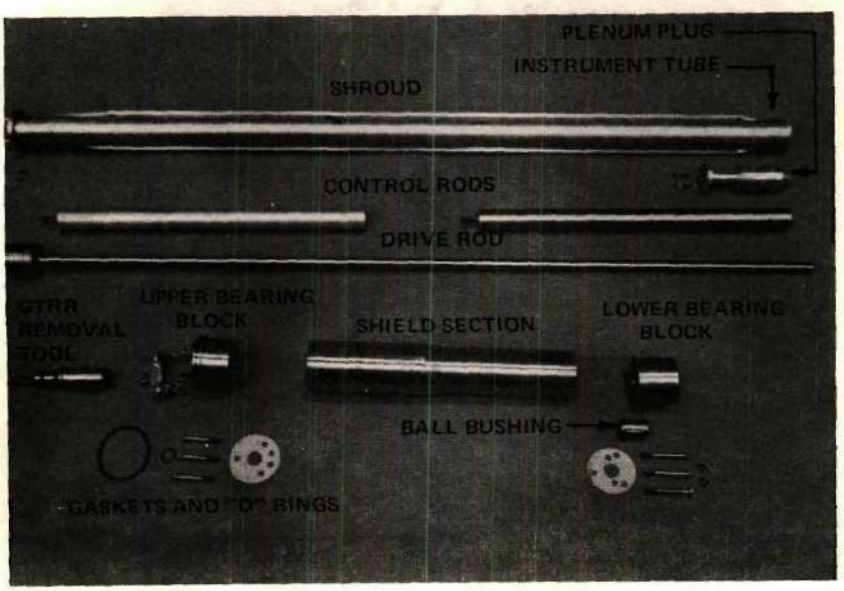

Figure 7. Disassembled Control Rod Assembly

it is fully withdrawn. When the control rod is fully inserted, it centers on the core and has about three inches extending outside either end of the fueled region.

The control rod is screwed into a one-inch-diameter stainless-steel drive rod. The other end of this drive rod is attached through a remote gripper to the hydraulic drive system. The remote gripper is a double-cam, rotary-solenoid-operated device consisting of a ring and a latch. The ring of the gripper is fastened to the drive rod while the latch is indirectly connected to the hydraulic piston rod. A spring holds the latch to a neutral position so that it can be inserted through the ring. Current to the solenoid cams three balls in the latch outward so that separation is prevented. This keeps the drive rod attached to the hydraulic system as long as current is applied to the solenoid.

The drive rod is guided by the low friction, stainless steel, recirculating ball bushings. The bushings are contained in bearing blocks which bolt onto the shield section. The three-inch-diameter, .035-inch-wall aluminum shroud slides over the control rod and bolts into the lower bearing block. The lower part of the shroud contains a spring loaded table which holds the control rod above the full-in position in order to facilitate remote latching, but which allows the control rod to be driven further in on the application of force from the hydraulic drive system. The plenum plug prevents loss of coolant through the plenum and holds the lower end of the assembly stationary. The shield section with bearing blocks supports the assembly just as a fuel element is supported by its shield plug. Two instrument tubes permit insertion of detectors into the

experimental assembly. "O" rings and gaskets maintain a helium seal above the core. Of interest is the dynamic "O" ring seal which provides a helium barrier between the core and the drive shaft even though this drive shaft moves at speeds of several feet per second.

This control rod assembly satisfies the previously mentioned design criteria. The control rod assembly fits into the center of a basically cylindrical core and moves vertically. The control rods are easily changed to vary their nuclear properties. This control rod assembly is easily inserted and removed from the reactor since it is designed to fit the GTRR's insertion and removal tools.

Assembly of the control rod can be visualized by the steps in the process:

1. The bearing blocks are bolted to the shield section and the drive rod inserted.

2. The fixed ring of the gripper is bolted onto the drive rod and the control rod is screwed on.

3. The shroud and plenum plug are then bolted on, completing the assembly.

Link and Instrumentation Unit

One purpose of the link and instrumentation unit is to couple the control rod assembly to the hydraulic drive. This is necessary since the control rod assembly is inside the reactor, while the hydraulic system is on the upper face of the reactor. In addition, this unit contains all non-nuclear instrumentation for the experiment. Figure 8 is a photograph of this device, disassembled. The aluminum support tube is supported by

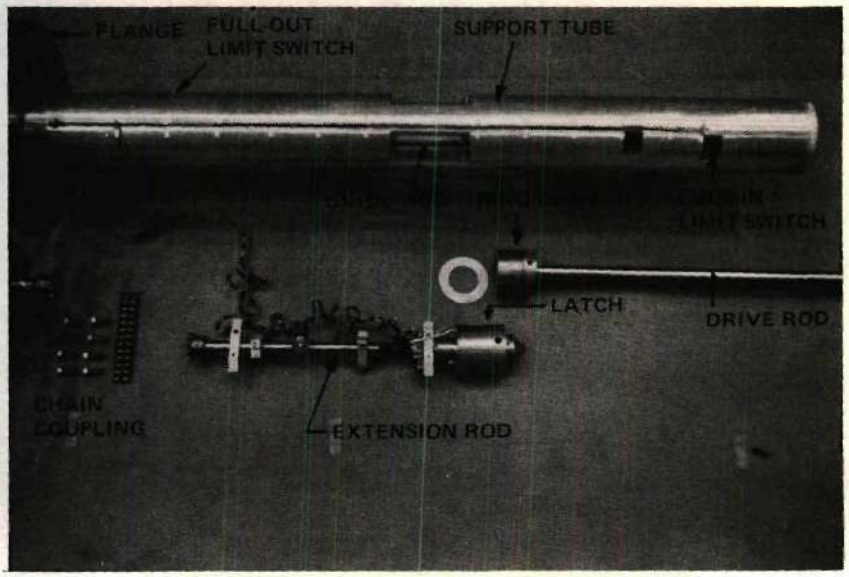

Figure 8. Disassembled Link and Instrumentation Unit.

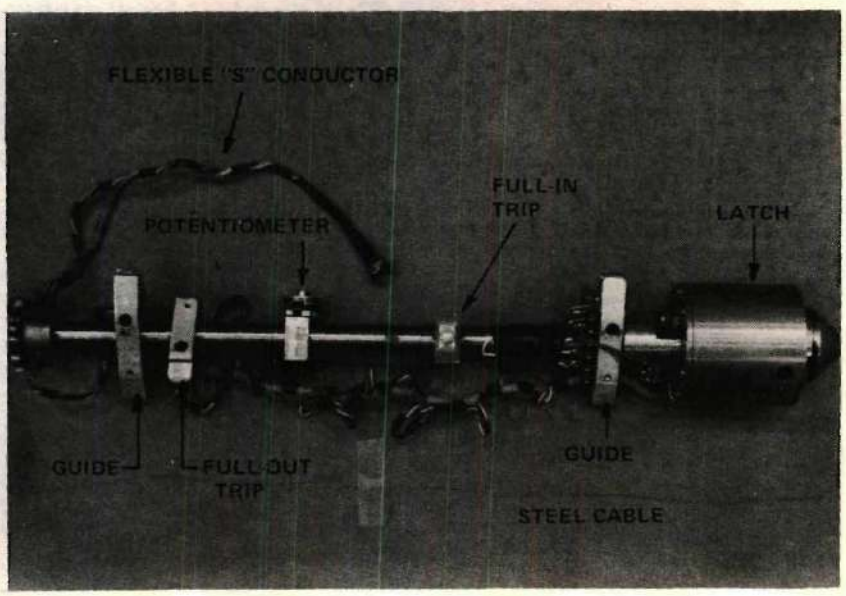

Figure 9. Extension Rod.

the flange and extends through a vertical penetration to within six inches of the top of the control rod assembly. The extension rod, shown in Figure 9, is used to join the hydraulic piston rod to the drive rod. It is joined to the piston rod by a small chain coupling. This coupling is easy to connect and provides a limited amount of vertical and angular flexibility. The other end of the extension rod is attached to the latch part of the remote gripper. Guides are fastened to the extension rod. These guides have notched ends which fit onto stainless steel guide rods on the inside of the support tube and which maintain a fixed angular orientation between the extension rod and the aluminum tube.

The instrumentation is provided by three limit switches and a ten-turn potentiometer. Two of the limit switches are located in the wall of the support tube; when closed by the trip arms on the extension rod they indicate the full-out and full-in positions of the control rod. The other limit switch is on the latch of the remote gripper and closes whenever this part of the gripper engages the ring fixed to the drive rod in the control rod assembly. The potentiometer is fixed to the extension rod and has a one-inch-diameter pulley attached to it. When assembled, this pulley has a thin steel cable wrapped around it and fastened to the ends of the support tube. Thus, any relative movement of the extension rod will create a unique reading on the potentiometer. The electrical signals from these devices as well as the power to the solenoid must be brought to the face of the reactor. The end-point limit switches have their wires channeled along the outside of the support tube to the top. The rotary solenoid in the latch of the remote gripper, the engaged limit

switch, and the potentiometer have their leads carried along a flexible conductor to the top of the reactor. The flexible conductor is made by attaching "S" shaped conductors to a natural gum rubber tube. As the tube stretches, the "S"'s flatten out and as it contracts, they enlarge. Such an arrangement allows for a 3:1 stretched to unstretched ratio. The signal leads lie in a groove on top of the flange so that the hydraulic system's drive cylinder can be bolted flush to the top.

The four slots at the center of the aluminum tube are used to make adjustments to the extension rod whenever the unit is assembled with the hydraulic cylinder. A slot near the top is used to set the resistance of the continuous position potentiometer to zero when the control rod is fully withdrawn.

Hydraulic Drive

The hydraulic drive provides the motive force for the control rod. Part of this drive is a hydraulic cylinder having a stroke of 30 inches. The time required for full extension can be varied from 2 seconds to 1,000 seconds. The time required for full retraction is preset at 1,000 seconds. The piston rod of this hydraulic cylinder is attached, via the chain coupling, to the extension rod of the link and instrumentation unit. The hydraulic cylinder bolts directly to the flange on this unit. Figure 10 is a schematic of this system using the symbols defined in reference 27. Figure 11 is a photograph of the hydraulic system without the cylinder and attached valves. Figure 12 is a photograph of the cylinder attached to the link and instrumentation unit. A more detailed description of the hydraulic drive can be found in Appendix A.

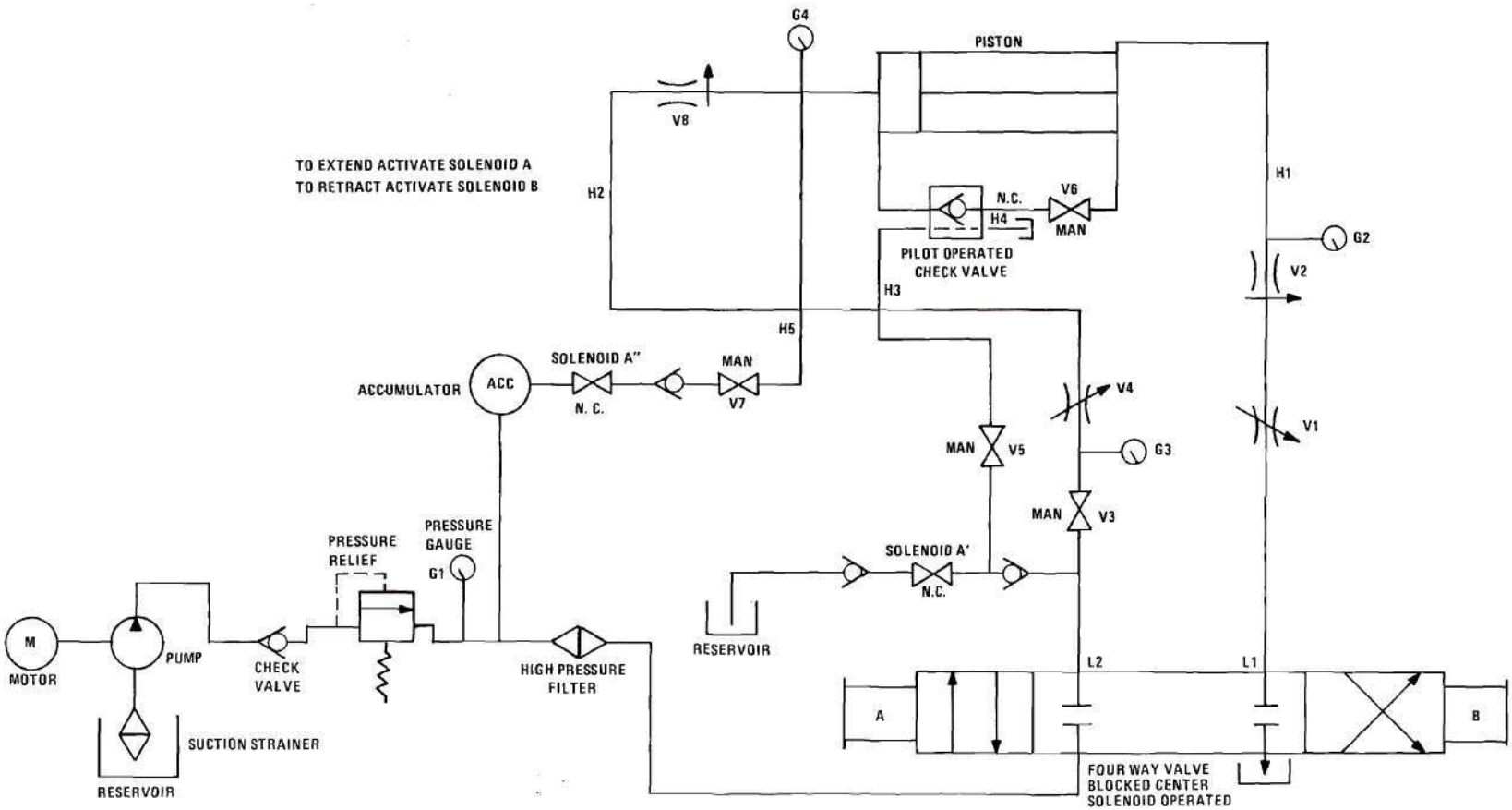

Figure 10. Schematic of the Hydraulic Drive.

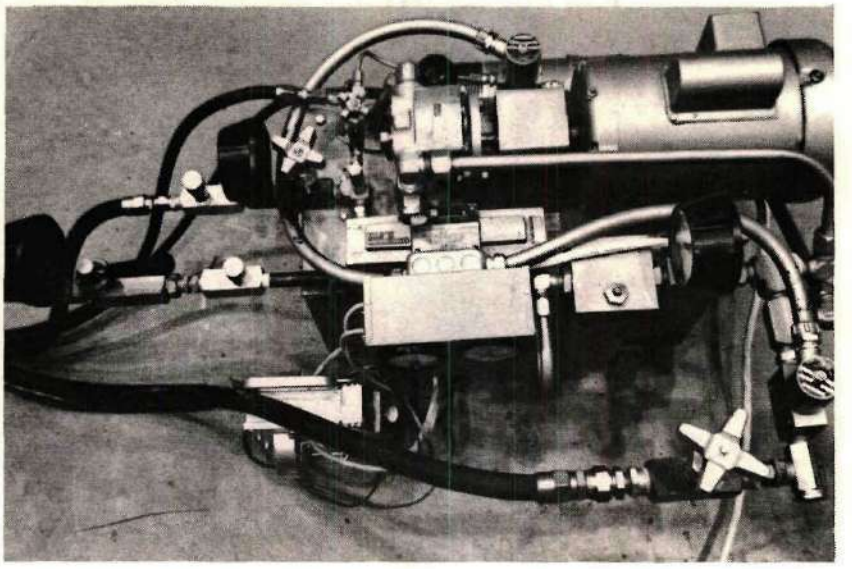

Figure 11. Hydraulic System.

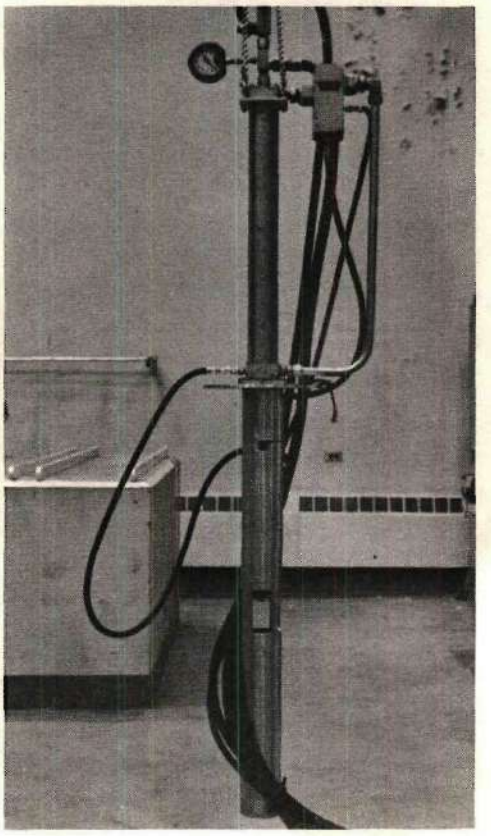

Figure 12. Hydraulic Cylinder Attached to the Link and Instrumentation Unit.

Control and Monitoring System

The control and monitoring system has four major functions. It controls the hydraulic drive and hence the control rod's position. Analog signals describing the condition of the experiment are derived from this unit and presented to the data acquisition system. Visual indication of the status of the experiment is provided. Finally, the experiment is interlocked with the reactor. The heart of this system is a control box having four sets of input/output lines. A block diagram is shown in Figure 13. A more detailed description follows.

The control functions involve the motor for the hydraulic pump, the four-way directional control valve and associated solenoid valves on the hydraulic system, and the rotary solenoid in the remote gripper. Five lines from the control box feed into a junction box on the hydraulic drive unit. This junction box contains a solenoid-operated relay to control the motor, a voltmeter and an ammeter to measure the motor's performance, an external power lead, and the leads from all the solenoid valves. The solenoid-operated relay and all solenoid valves are energized by 110 vac from the control box. The motor is driven by the 110 vac external power lead and is controlled by the solenoid-operated relay. The five leads from the control box are ground, common, a withdraw line, an insert line, and a motor on/off line. The stop position is derived by default, that is, a stop is the absence of either a withdrawal or an insertion signal.

A single-pole, single-throw switch in the control box places either zero or 110 vac on the motor on/off line, thus opening or closing the solenoid-operated relay and turning the motor on or off. A five-pole,

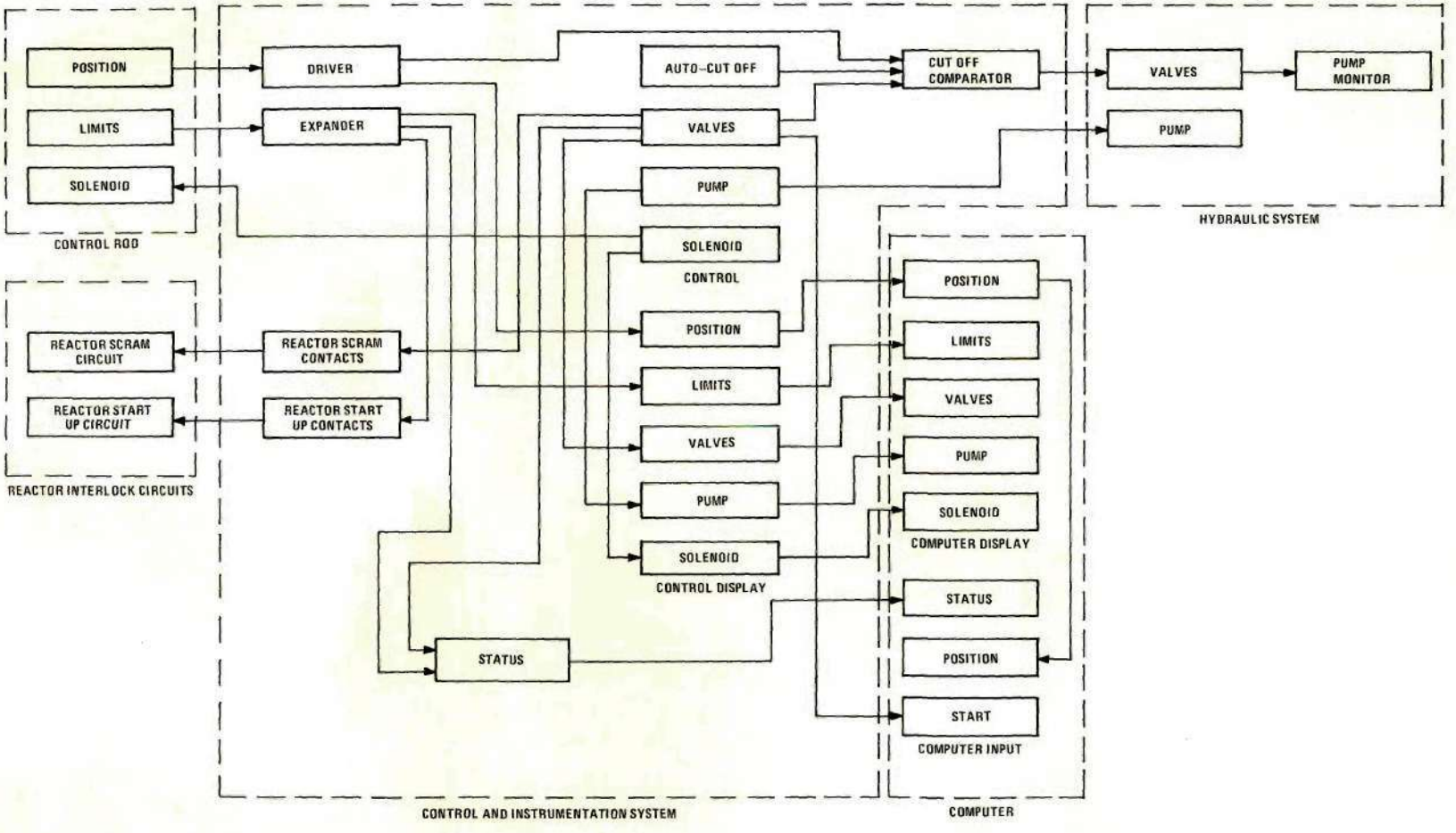

Figure 13. Block Diagram of the Control and Monitoring System.

triple-throw switch having positions for withdraw, stop, and insert is used to control the motion of the hydraulic rod. In the stop position, no current is fed to any of the solenoid valves. This blocks the four-way valve and stops all motion. In the withdraw position, 110 vac is placed on the withdraw line, while zero is on the insert line. This activates solenoid B, forcing the hydraulic drive to withdraw. In the insert position, 110 vac is placed on the insert line, while zero is on the withdraw line. This activates solenoids A, A', and A", forcing the hydraulic drive to insert.

Provision was made for removing the pressure near the end of the control rod travel in order to increase the cushioning. This is accomplished by a circuit which automatically puts the system in a stop condition at some preset depth of insertion. An evaluation component compares the depth of the control rod insertion with a preset cut-off value. Whenever the two are equal, the voltage on the down line is set to zero. In addition, the down line is held at zero volts with a latching relay until either a reset switch is thrown or the three-position control switch is turned to withdraw.

An on/off switch in the control box sends either zero or 12 vdc to the rotary solenoid in the gripper. Twelve volts is sufficient to hold the solenoid in the latched position and is small enough to keep the solenoid's heating to a safe level; however, it is not enough to cause the solenoid to latch. A momentary pushbutton switch, which applies 30 vdc to the latching solenoid, latches it, but does not damage the solenoid since the 30 vdc is applied only briefly.

Two analog signals give the condition of the experiment and they are sent to the data acquisition system. The first of these is a voltage proportional to the depth of insertion of the control rod. This varies from zero to minus five vdc and is obtained from the voltage drop across the potentiometer described in the link and instrumentation unit. The regulated power supply and line drivers for this position measurement are in the control box. The second signal contains the status of the experiment. This signal uniquely indicates the condition of six contacts. It functions by assigning a binary weighting to each of the contacts and adding these weights for each of the closed contacts. Table 1 gives the six contacts and their weighting values.

Table 1. Weighting Values for the Experimental Status

Contact	Value when closed	Value when open
Gripper engaged	-5.000	0.0
Full in	-2.500	0.0
Full out	-1.250	0.0
Hydraulic system inserting	-0.062	0.0
Hydraulic system withdrawing	-0.031	0.0
Hydraulic system stopped	-0.016	0.0

The status signal uses one of the five poles on the hydraulic control for the last three contacts. Each of the limit switches in the link and instrumentation unit triggers a three-pole relay in the control box to

achieve additional contacts. One set of these contacts is used for the first three entries in Table 1. A fixed voltage is sent through each of these contacts and through binary resistors to achieve a current proportional to the weighting value. The currents are added with an integrated circuit to produce a voltage proportional to the sum of the weighted values. As an example, suppose the status has a voltage of -6.266. This uniquely implies that the condition of the experiment is full out with the hydraulic drive in stop and the gripper engaged.

A visual indication on the status of the experiment is also obtained with this system. Neon lights on the control box indicate the condition of each of the six contacts in Table 1. In addition, neon lights indicate whether the pump motor is on and whether the control box is interlocked or off. The position of the control rod is monitored by a voltmeter, which can be used with a bypass switch to set the automatic cutoff point. Another meter monitors the voltage on the gripper's rotary solenoid. The control box sends all these visual indicators to the data acquisition system.

The final function of the control and monitoring system is to interlock the experiment. This interlock, as required by the Atomic Energy Commission, must insert the GTRR's shim-safety blades whenever the hydraulic drive is in the withdraw position. It must also disable the GTRR's ability to raise its shim-safety blades unless the control rod is fully withdrawn. These interlock features can be disabled with a key switch; however, such action turns off the pump motor and switches the hydraulic drive to the stop position. The first interlock function is achieved by opening the circuit to the magnetic clutches on the shim-

safety blades whenever the hydraulic drive is being withdrawn. With no current on the clutches, the shim-safety blades automatically insert. The GTRR's shim-safety blades are driven out by a circuit independent of that used to insert them. The second interlock function is performed by opening those drive-out circuits unless the full-out limit switch is closed.

The leads to the data acquisition system are terminated in a box similar to the control box. This box has all the visual indicators present in the control box, but has no control capability. In addition this box has two BNC jacks on which the voltages from the position and status are applied.

Nuclear Instrumentation

This experiment monitored the flux at six different positions while the control rod was inserted. Four boron miniature ionization chambers and one miniature fission chamber were placed in the reactor's core and moderator. Additionally, a gamma-compensated fission chamber was positioned in the graphite reflector. The boron and fission chambers are similar. They were both manufactured by Reactor Controls, Inc. of Oak Ridge, Tennessee. They are 3/16 inch in diameter and 2 inches long. The boron chambers are connected to a 1/8 inch, replaceable, polyvinyl co-axial cable and the assembly is sealed with heat-shrinkable tubing. The fission chamber is connected to an integral co-axial cable with alumina insulation. Figure 14 is a photograph of the boron ionization chambers.

Each of these detectors was connected to a Reactor Controls, Inc. model E-908 electrometer. These electrometers can either measure the current output from a detector or the deviation between the "average"

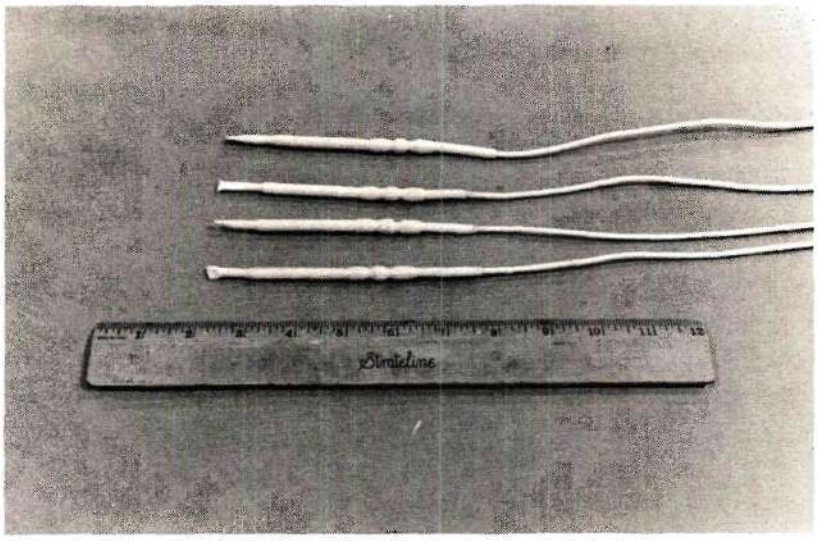

Figure 14. Boron Miniature Ionization Chambers.

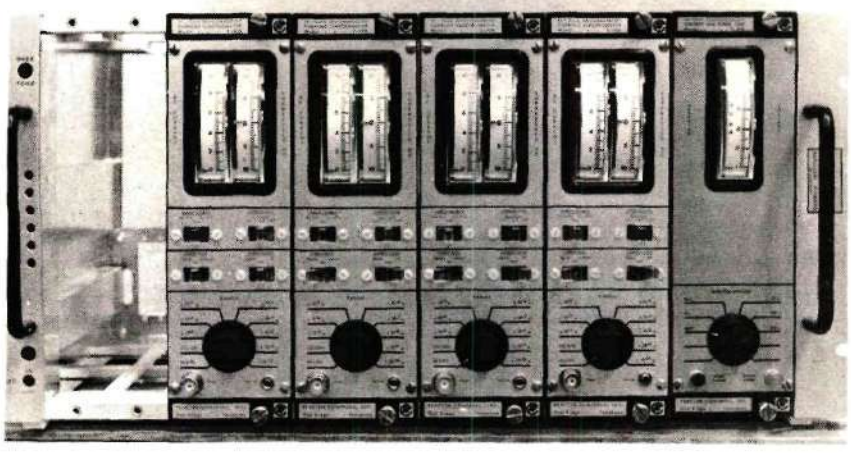

Figure 15. Electrometers and Power Supply Mounted in a NIM Bin.

current and the current. The second mode is used in noise analysis and is not of interest in this experiment. When measuring the current from a detector, the electrometers output a voltage either linearly proportional to the current or logarithmically proportional to the current. In the linear mode, the electrometer has full scale ranges varying from 10×10^{-10} to 10×10^{-3} amperes. In any range the output varies from zero to ten vdc. There are two logarithmic ranges on each electrometer. The gain of each range is two volts per decade; thus five decades of power can be monitored with any setting. The high-log range outputs eight volts for a current input of 300 microamps. The low-log range outputs eight volts for a current input of three microamps. Figure 15 is a photograph of these electrometers and their power supply. The performance of the electrometers was measured by supplying a known current from a precision current source and measuring the response with a digital voltmeter. The electrometers give a response linear within 0.1 percent throughout their current measuring range.

The compensated fission chamber is part of the GTRR's linear power measuring equipment. This detector is a General Electric Model 5467870G11. The output of this chamber was connected to a General Electric Model 534E7452G3 picoammeter. The signal from this unit ranges from zero to ten vdc and is sent over co-axial cables to the data acquisition equipment.

A detector channel consists of a detector connected to an electrometer. The output from the gamma uncompensated channels, operated in the

logarithmic mode, was compared to that of the gamma-compensated reactor channel, operated in its linear mode. This was accomplished by digitizing and recording the outputs of all channels as the reactor power level was changed. Figure 16 is a plot of these results for a typical channel. This graph indicates a logarithmic response over power levels from 100 watts to 100 kilowatts. Below 100 watts, the gamma background caused a deviation from the logarithmic response.

Detector Holders

As described before, the control rod assembly has two tubes into which miniature ionization chambers can be placed. In order to obtain flux measurements at other positions, two detector holders were made, one for insertion into fuel element positions and another for insertion into lattice extension sites. The holders are very similar, each consists of an aluminum tube, sealed at the bottom and open at the top. The detector holder for the fuel element position has a plenum plug attached to the closed end and a shield plug around the open end. When inserted into a fuel element position, detectors are easily lowered through the open end to any depth in the tube. The detector holder for the lattice extension site has no plenum plug since this is unnecessary in these core positions. It should be noted that the aluminum tube must be water-tight and that the shield plugs have to form a helium seal with the aluminum tubes and the reactor's lower shield.

Data Acquisition Equipment

Eight analog voltages from the experiment were measured as a function of time. These included the position and status, which varied from

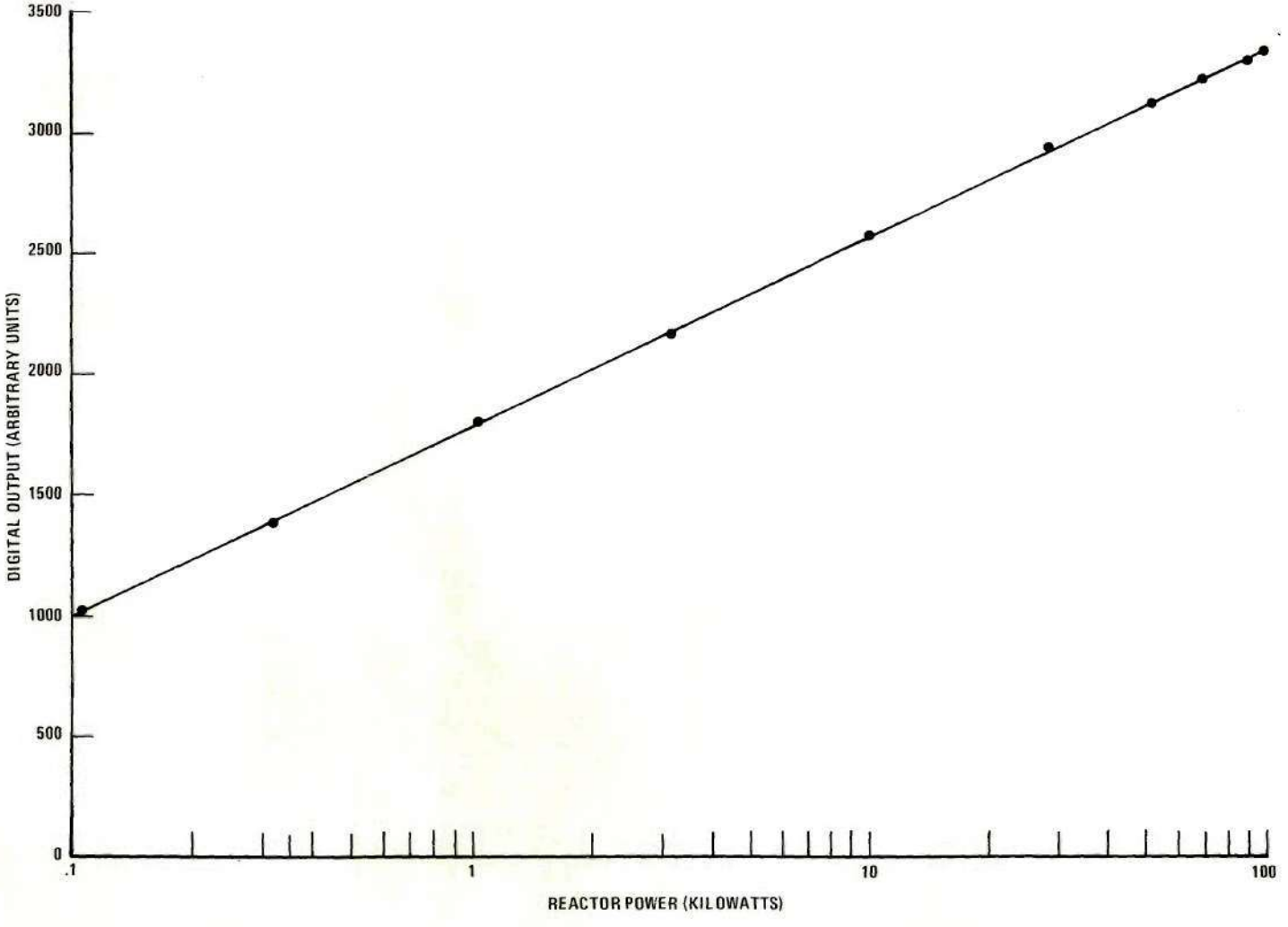

Figure 16. A Calibration of the No. 2 Detector, Electrometer, and Analog-to-Digital Channel.

zero to minus ten vdc, and the six detector signals which varied from zero to plus ten vdc. The data acquisition system to be described can sample and record these eight voltages at rates from 1000 times per second to once every 100 seconds. This system consists of two specially programmed computers, standard peripherals, an experimental interface, a multiplexing sample-and-hold device, and an analog-to-digital converter. Figure 17 is a block diagram of the data acquisition system.

The experiment ran under the supervision and control of a PDP-8 computer located near the GTRR. This computer will be referred to as the MASTER since it controls both the experiment and the PDP-8I computer, referred to as the SLAVE.

Connected to the MASTER computer is a specially designed interface which can be used to link this computer to various nuclear experiments. Though this interface can perform many functions, its primary use in this experiment was as a very accurate computer-controlled clock. This clock is made from an accurate one-megahertz quartz-crystal oscillator, an eight-digit buffer, and a comparator. This clock can produce cyclic signals, at computer selected intervals, ranging from one microsecond to 100 seconds in steps of one microsecond. These clock signals can be recognized by the computer and are used to determine the times at which the eight voltages are to be "read." In addition, these clock signals instruct the multiplexing sample-and-hold device that voltages are to be sampled.

The MASTER computer contains an analog-to-digital converter (ADC). This ADC uses a 12-bit successive approximation technique to accurately digitize a voltage to one part in 4096.

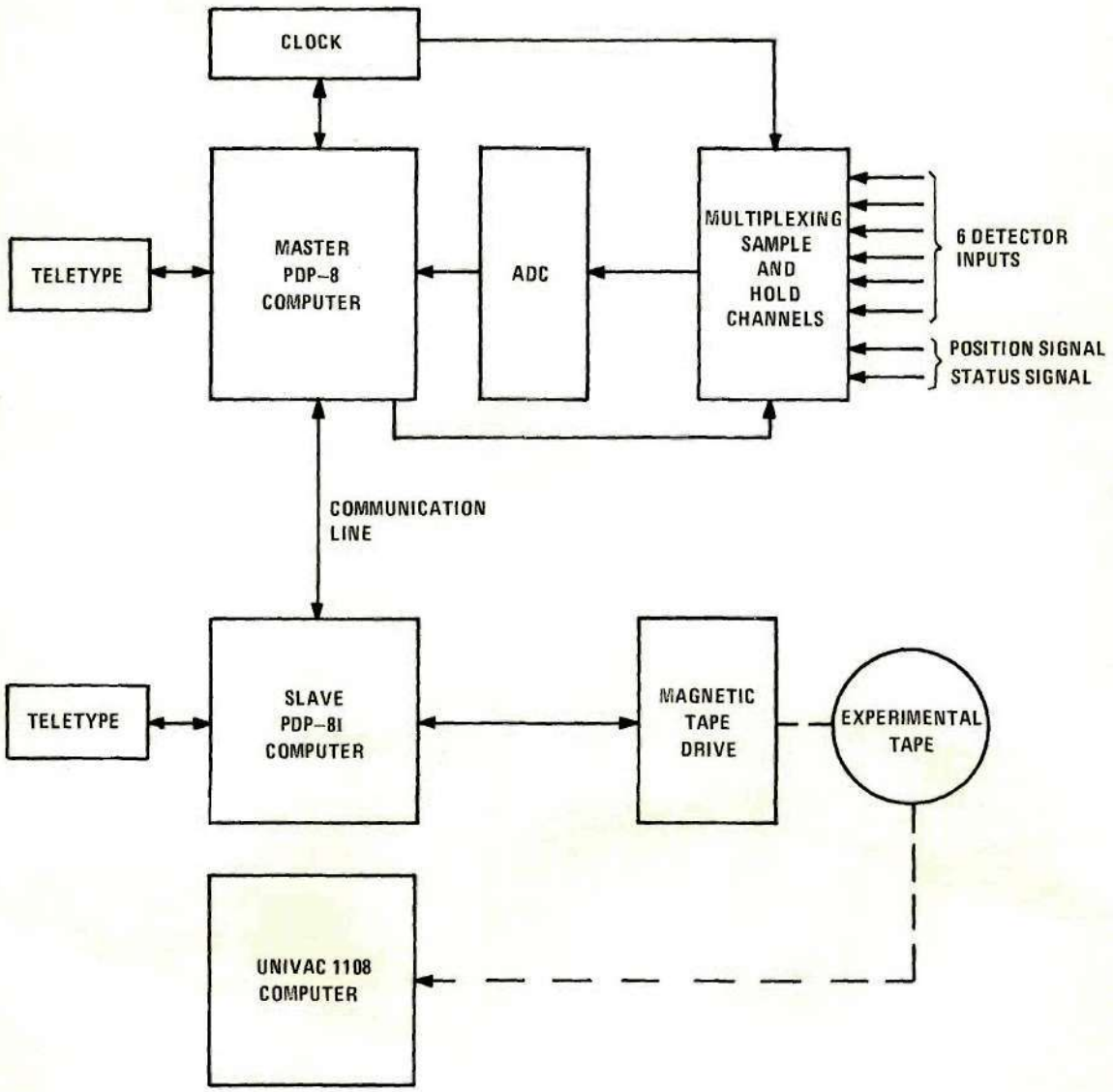

Figure 17. Block Diagram of the Data Acquisition System.

Since there is only one ADC and eight voltages to be digitized, an electronic switching network is used to selectively connect the different inputs to the ADC. This is the purpose of the multiplexing sample-and-hold. This device has eight outputs, any of which can be connected to the ADC under computer control. Associated with each output of the sample-and-hold is an input. The inputs are of three types. The first two types are very similar and are used for the six detector channels. The voltages at these inputs are inverted, biased, and amplified. (For this experiment, the bias was zero and the amplification was one.) Four of these inputs are sampled-and-held when a clock signal arrives, i.e. the outputs have a voltage representative of the input voltage at the time the last clock signal arrived. The other two detector inputs are not sampled-and-held but have their outputs continuously representative of the input voltage. The third type of input takes an input voltage and attenuates it. (For this experiment, there was no attenuation.) These two inputs were used for the status and position voltages. Figure 18 is a photograph of the MASTER computer system.

A high speed communications line connects the MASTER computer with the SLAVE. Data and commands are buffered in the MASTER computer and transferred to the SLAVE computer. The SLAVE computer places incoming data and commands in a buffer and block transfers the data to the magnetic tape drive. The SLAVE computer operates the magnetic tape drive only on command from the MASTER.

The magnetic tape produced by an experiment can be previewed on the SLAVE computer or transferred to a Univac 1108 for detailed analysis. A partial test of the data acquisition equipment was made with a simple

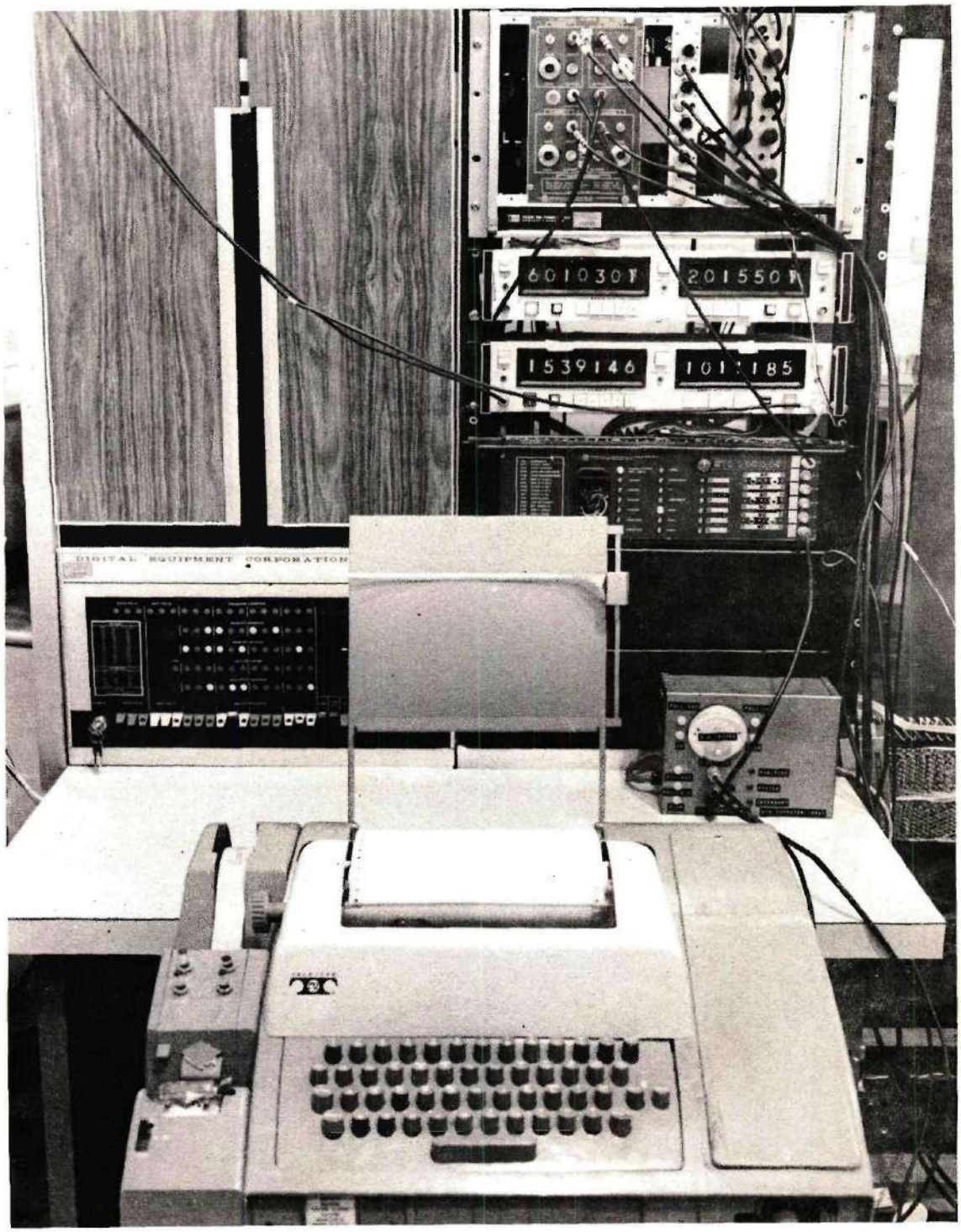

Figure 18. The MASTER PDP-8 Computer System.

current device and a special test program. The current device used capacitors and resistors to generate an exponentially-decaying current. This current was input into the electrometers, operating in the logarithmic mode. The output of these electrometers was fed into the data acquisition system.

The data acquisition equipment accurately measured currents with periods as short as 0.01 second. Such periods are much shorter than any produced during the experiments.

Data Tape Format

The data acquisition system has the capability of recording many experiments on a single magnetic tape. There are four elements which compose such a tape: the directory, the file structure, the records within a file, and the words which compose a record. These will be described briefly.

At the beginning of the tape is a directory to the rest of the tape. This directory contains, for each experiment on the tape, the experiment's number, record length, rate of sampling, number of detectors, the number of records for the experiment, the number of data points taken for the experiment, and the number of files on the tape preceeding this experiment. Clearly, this directory must be updated for each experiment. Since magnetic tape cannot be randomly accessed, special techniques are required to maintain the directory. The first step is to initialize the tape before putting any experiments on it. This is automatically done by the data acquisition system and consists of writing 4096 12-bit zeroes as a record at the beginning of the tape. Following this an extended record

gap and an end-of-file are written. In order to update the directory, the tape is rewound and 4096 words are read. This is the directory and can be updated in core by searching for the first string of all zeroes and replacing them with experimental information. After the tape is rewound, the directory is written back onto it and then it is positioned to the end of the first file. Note that no end-of-file is written on an update. This means that the updated directory is totally within the first file, since the extended record gap is longer than the tape positioning error. Thus, the directory is easily bypassed by positioning to the end of the first file. Incidentally, because of tape positioning error, the updated directory does not exactly overlay the original, but this is unimportant.

The next significant facet of the tape is its file structure. A file is simply a segment of tape between the beginning of the tape and a file mark, or between two file marks. The important considerations are that the tape unit can position itself to the beginning of any file and that every file either contains the directory or a complete experiment.

Each file of a tape is made up of a variable number of records. A record is a section of tape which can be read from the tape as a block of data. In addition, records, like files, may be skipped. Each experiment consists of one or more records in a file. The directory tells the number of files to skip to obtain any experiment and also the number of records in any experiment.

The final division on the tape is a word. A word is simply a 12-bit piece of data. Words must be read in blocks equal to the record

length. Since the experimental tape is to be read on the Univac 1108, a 36-bit word machine, all record lengths are required to be evenly divisible by three so that a whole number of Univac words can be read from each record block. All experiments used a block length of 1200 words.

Data Acquisition Software

An important part of the data acquisition system is the programming to control it, the software. There were four overriding considerations involved in the development of the software. These were:

1. High data rates were required.
2. Experimental documentation was a necessity.
3. Asynchronous devices had to be coordinated.
4. Data transmission had to be checked for errors.

Two programs were required, one for the MASTER computer and one for the SLAVE. High data rates require asynchronous operation of all devices, that is, each device must have access to the computer when needed, and as a corollary, no device must tie up the computer so as to prevent access by another device. Programs of this type are generally designed around interrupts. Initially the two programs were written in this manner; however, it was found that the overhead processor time associated with the PDP-8's single level interrupt would not yield rates commensurate with the speeds of all available devices. In order to overcome this problem, interrupt-like programs were written which took full advantage of all available busy flags without necessitating an interrupt overhead. A flow chart of the MASTER program is given in Figure 19. Figure 20 is a flow chart of the SLAVE program.

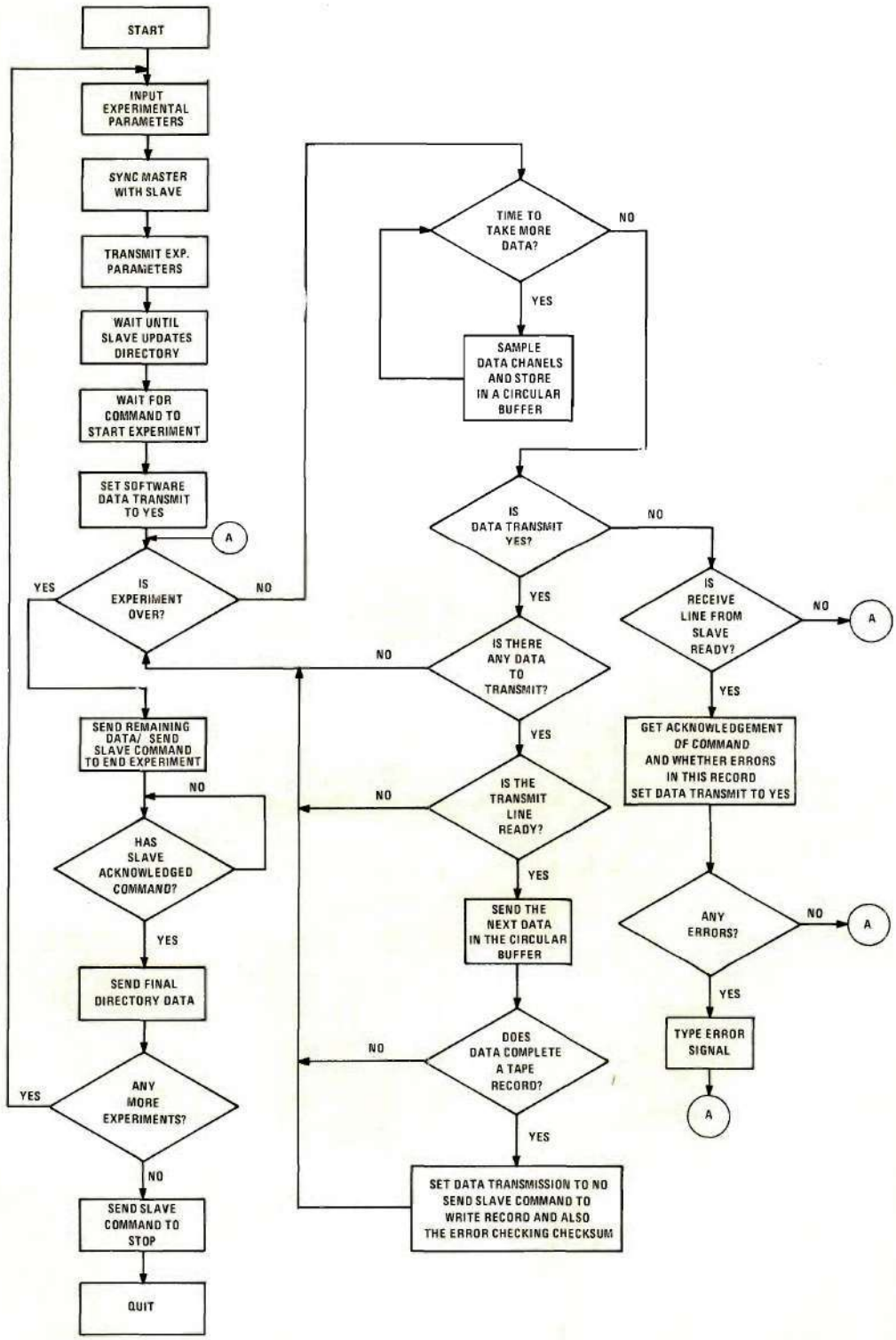

Figure 19. Flow Chart of the MASTER Program.

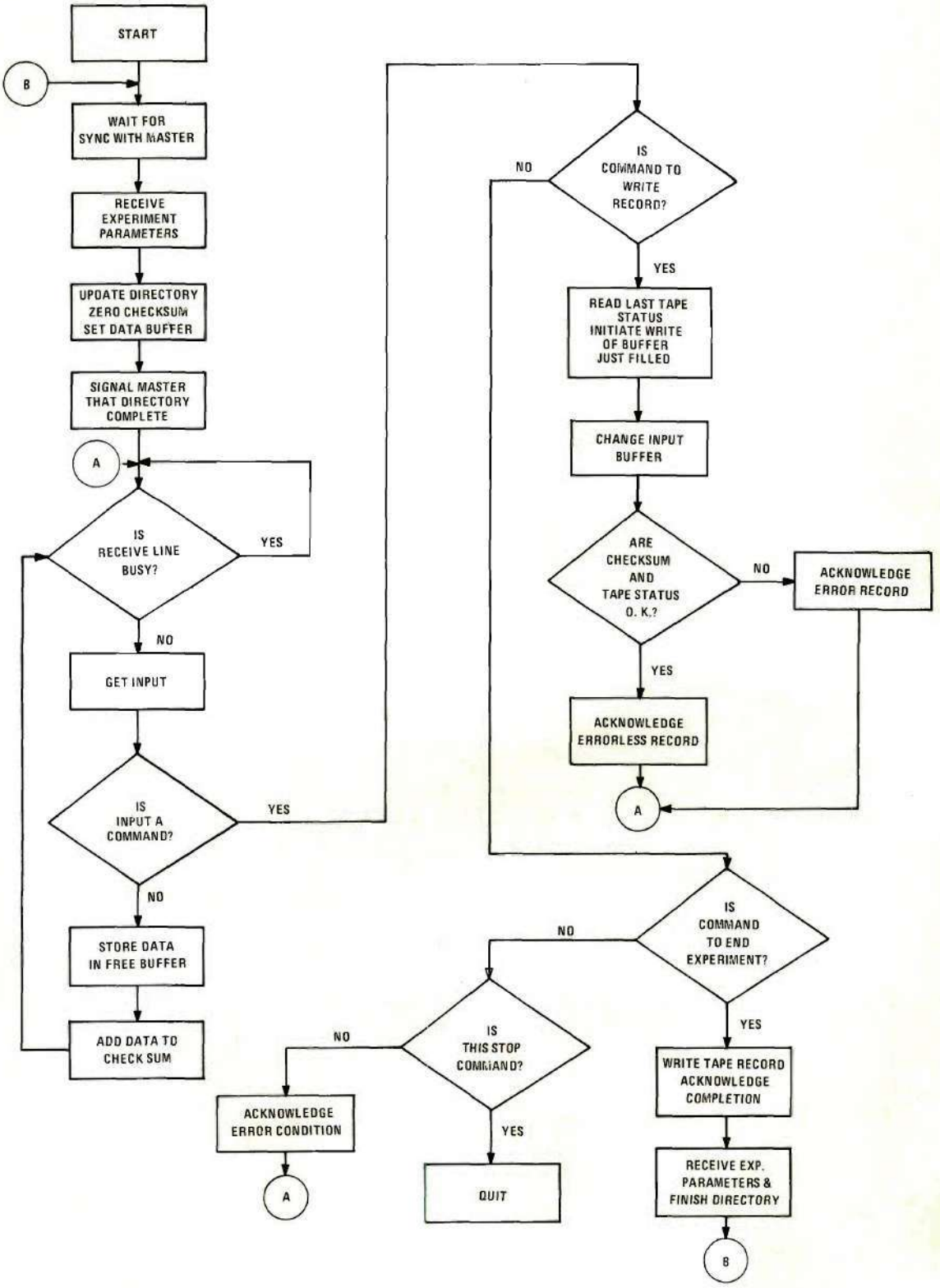

Figure 20. Flow Chart of the SLAVE Program.

The MASTER program obtains from the user via the teletype the experiment number, its description, the number of data channels, and, for each channel, the instrument's description, position, and initial reading. In addition, the rate of sampling and the record length for the magnetic tape are user-supplied. A determination of whether to add this experiment to the existing magnetic tape or to initialize another tape is then made by the experimenter.

After this information is input on the teletype, thereby obtaining a written record of the experiment, the MASTER transmits these data to the SLAVE. The SLAVE adds this experimental description to the directory, which is maintained on each tape, and positions the tape to the correct starting file. The SLAVE then signals the MASTER of the completion of the experiment's initialization.

The MASTER starts taking data on command by the operator. It simply collects the data, at the specified rate, and transmits them to the SLAVE. It buffers the input and output so that they may be overlapped. The MASTER determines when a new block of data is finished and should be transferred from the SLAVE to the magnetic tape. It then sends a command signal to the SLAVE instructing it to start writing the last data block on magnetic tape. With each such instruction it also transmits a data-block check-sum so that any transmission errors can be detected. The MASTER buffers all experimental data until a reply from the SLAVE indicates the acceptability of the last record and that it is ready to receive more data or instructions.

The operator signals the end of the experiment to the MASTER by changing a sense switch. The MASTER stops the clock and finishes trans-

mitting all data. It then commands the SLAVE to terminate this experiment. The SLAVE does so by writing an end-of-file mark on the tape and updating its directory. It then signals the MASTER that it is finished.

Chapter III contains experimental procedures and data reduction techniques used in the kinetics experiments. Experimental results are presented in Chapter III and Appendix B.

CHAPTER III

EXPERIMENTAL PROCEDURES AND RESULTS

Kinetics experiments were performed with an aluminum control rod and with a stainless steel control rod. For each of these control rods, several rates of insertion were monitored. In addition, the flux distributions for the full-out and full-in states were measured. This chapter reports the experimental procedure used and gives the results of the experiments.

Core Configuration and Flux Distributions

The GTRR and other experimental equipment were described in Chapter II. In order that the results of these experiments could be compared with calculations from a two-dimensional code, the control rod assembly was placed in V-10, the central vertical fuel element position. A detector holder was placed in vertical penetration V-18. The remaining 17 fuel element positions were filled with fuel elements. Another detector holder was placed in V-23, a lattice extension location. The reactor was made critical, with the control rod full out, by withdrawing the reactor's shim-safety blades. Criticality was reached for both the aluminum and stainless steel control rods when the shim-safety blades were withdrawn approximately 25.5 degrees. This amount of withdrawal represents more than 90 percent removal of the total worth of the shim-safety blades.

The geometry of this experiment is complicated by the triangular

lattice of the fuel elements, the uneven burnup in the fuel, the presence of the shim-safety blades, and the detector holders in V-18 and V-23. Chapter V contains a discussion on these effects and the analytical methods that were used.

The miniature detectors were used to obtain flux traversals in vertical penetrations V-10 and V-18. In addition, the radial flux at the core mid-plane was obtained in V-10, V-18, and V-23. In order to do this, the reactor was made critical with the experimental control rod full out. The ratio of the current of a detector at the mid-plane to that of a detector moved axially was used to obtain the axial traversals. The control rod was then inserted and the procedure repeated after the reactor power had decayed to a low level. The flux shapes for the fully inserted control rods were more difficult to obtain since the reactor power was continually decreasing. The radial measurements were obtained by placing all the detectors at the core mid-plane. While doing these measurements, the detectors were often moved; however, their spatial perturbations were small as evidenced by the nearly constant reading in one detector as another was passed within 1/2 inch of it.

The axial flux distributions are given in Figures 21-24. Table 2 gives the radial measurements. These measurements indicate that the axial distributions are not very dependent on whether the control rod is inserted or withdrawn. On the other hand, the radial measurements demonstrate a significant difference between the stainless steel control rod's being withdrawn or inserted. These flux distributions and radial measurements were of great value in formulating an analytical reactor model and are further discussed in Chapters V and VI.

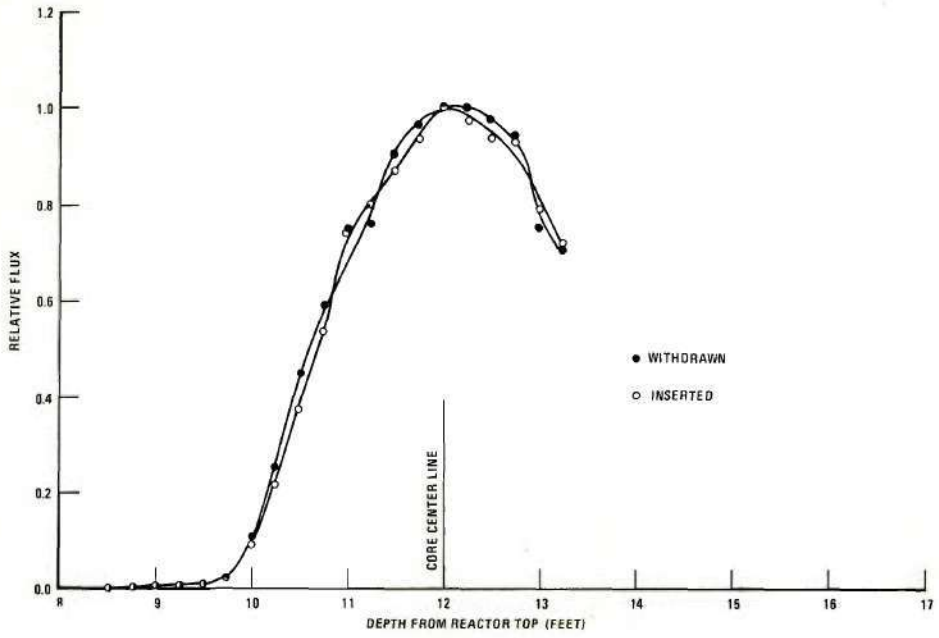

Figure 21. Experimental Flux Distributions in V-10 for the Aluminum Control Rod Withdrawn and Inserted.

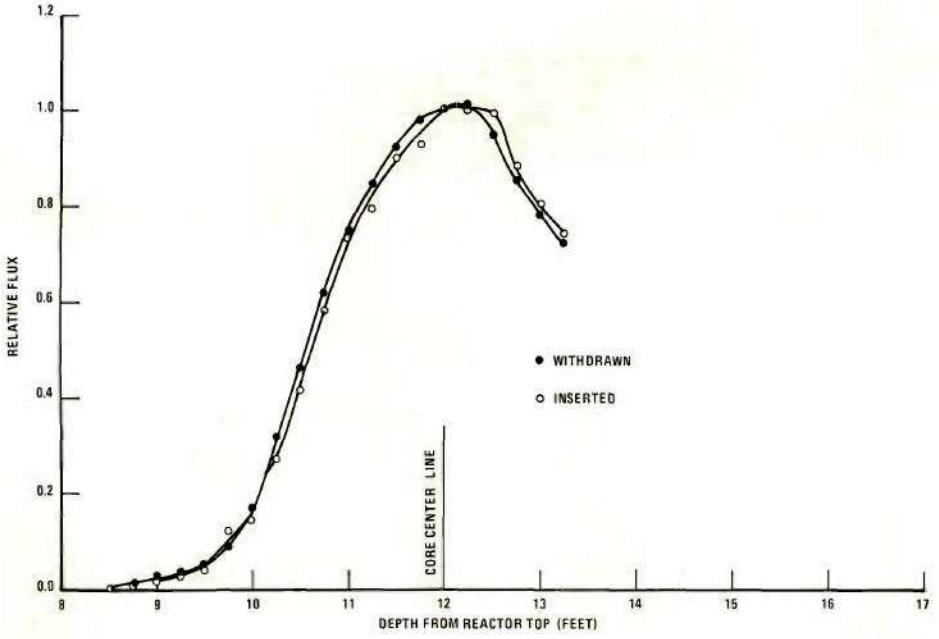

Figure 22. Experimental Flux Distributions in V-18 for the Aluminum Control Rod Withdrawn and Inserted.

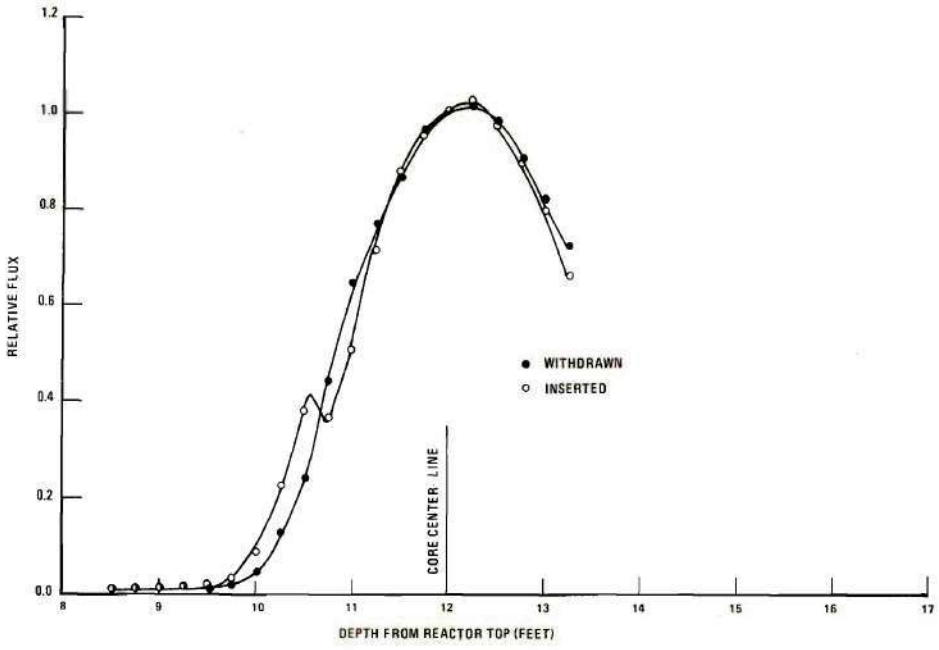

Figure 23. Experimental Flux Distributions in V-10 for the Stainless Steel Control Rod Withdrawn and Inserted.

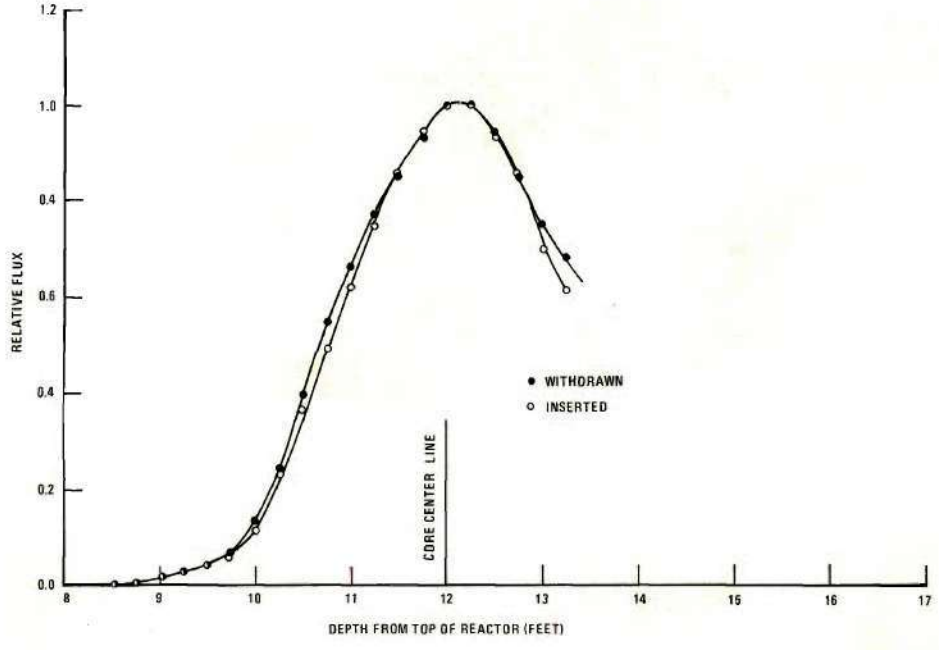

Figure 24. Experimental Flux Distributions in V-18 for the Stainless Steel Control Rod Withdrawn and Inserted.

Table 2. Radial Flux Measurements at the Core Mid-Plane

Configuration	Flux Relative to That in V-10		
	V-10	V-18	V-23
Aluminum Control Rod Withdrawn	1.000	0.824	0.672
Aluminum Control Rod Inserted	1.000	0.907*	0.733*
Stainless Steel Control Rod Withdrawn	1.000	0.789	0.564
Stainless Steel Control Rod Inserted	1.000	1.070	1.275

*Derived from other data rather than resulting from direct measurement.

Experimental Set-Up

The kinetics experiments for the aluminum rod were run for one week. One week later the kinetics experiments for the stainless steel rod were run for a week. In both cases the insertion of the experiment into the GTRR required one day. The fuel elements were first arranged to fill all available positions except V-10 and V-18. The detector holders were then placed in positions V-18 and V-23. The control rod assembly was inserted into position V-10. Prior to this the hydraulic drive had been attached to the link and instrumentation unit. These were then bolted to the face of the GTRR. As a precaution against oil leaks contaminating the reactor coolant, two separate layers of clear, heavy-gauge polyethylene were placed over the face of the reactor. This was a difficult task since penetrations for the experimental assembly had to be joined in a leak tight manner to the hydraulic drive. The penetrations for the detector leads presented similar problems.

The detectors were connected to the current electrometers which were located near the face of the reactor. Co-axial leads from the electrometers carried the outputs to the data-acquisition system. In addition a nine-twisted-pair cable connected the control rod's instrumentation to the control box, located on the reactor operator's console in the GTRR control room. Connections from this control box were also made with the hydraulic drive, the data acquisition system, and the reactor interlock system. As is common with electrical systems spread over many feet, ground loops and radiated interference had to be controlled. To handle the ground loops, all electrical systems, except the reactor's detector

channel, were powered from the same supply as the computer. To control radiated interference, all detector leads were over co-axial cable. The lead from the reactor channel also had an a-c filter at the data acquisition end. In addition, the signals from the potentiometer and the experimental status were carried over twisted pairs and had their ac shorted out with capacitor circuits at the data acquisition end. Even though these precautions greatly reduced the problems of signal transmission, the data were taken at such a rate that averaging techniques could be used to strip away any interference radiated at 60 Hertz.

The linking of the hydraulic drive with the control rod through the remote latching device was the next step. This phase of the operation was completely blind and had to be guided by instrumentation alone. The rotary solenoid was de-energized and the hydraulic piston rod extended until fully inserted. On full insertion the two parts of the remote latch engaged, as indicated by the instrumentation circuitry, i.e., the engaged limit switch was closed. The rotary solenoid was then turned on and the momentary push button depressed to cause the latch to close. The hydraulic drive was withdrawn and if the engaged condition persisted, latching had been accomplished. If not, the latching cycle was repeated.

After the experimental equipment was assembled, the control rod was withdrawn and the reactor made critical. The static flux shapes, already mentioned, were then experimentally determined.

Kinetics Experimental Procedures

Prior to any day's experiments, the system was checked out and a data acquisition calibration was made. These calibrations simply related,

for each detector, the digital output to be expected for a given power level. To do this, all channels, except the reactor's, were placed on the high-range logarithmic settings and the detector voltages set at 200 volts. The detectors were then placed at the GTRR's mid-plane. Using a special calibration program, the digital values of all detectors were obtained at different power levels, as measured with the reactor's detector channel. The inverse of this calibration was used in later programs to convert digital readings to power levels. Figure 16 shows a typical calibration for a detector. After the calibrations the detectors were positioned for the kinetics experiments. Table 3 gives the location of the detectors and defines the detector numbers.

The execution of the kinetics experiments was straightforward. The control rod was withdrawn by turning the control selector to withdraw. The reactor was made critical, brought to 100 kw and placed on automatic control. While the reactor was maintained at 100 kw to saturate the delayed neutron precursors, the valves of the hydraulic system were adjusted to give the desired insertion rate. In addition, any desired automatic cut-off point was set. Finally the data acquisition system was made ready to do the experiment, and put in a "wait" condition.

After the precursor saturation period, typically 1,800 seconds or more, the data acquisition system was instructed to monitor the experiment at a rate of 100 samples (800 data values) per second. The reactor was taken out of automatic control and the control rod inserted at the preset rate. After the control rod was fully in and the power level reduced to below 100 watts, the experiment was terminated by manually changing the state of one of the computer's sense switches.

Table 3. Positions of the Detectors for the Kinetics Experiments

Number	Detector Description	Position	Height
1	Miniature Boron Ion Chamber	V-18	24" above Core Mid-Plane
2	"	V-18	12" below Core Mid-Plane
3	"	V-10	9" above Core Mid-Plane
4	"	V-10	9" below Core Mid-Plane
5	Miniature Fission Chamber	V-23	Core Mid-Plane
6	Reactor Fission Chamber	3 1/2 feet from core centerline	24" below Core Mid-Plane

Data Reduction

Three data reduction programs were written. One of these operated on the SLAVE PDP-8I. This program was written in FOCAL, an interpretive, interrupt-driven language. It reads a segment of an experiment and displays a sampling of these data on a storage scope. This was quite valuable since it enabled an experiment to be checked for errors at any time and to be rerun if necessary.

Two data reduction programs were written for the Univac 1108. Both used FORTRAN and were run in a batch mode. These programs used the Univac-furnished subroutine NTRAN which permits the transfer of binary data, without special FORTRAN formating, from magnetic tape. The simplest of these two programs takes any number of experimental tapes and transfers them to a single tape. The directories are combined in this process to produce a tape that appears to have come from a single series of experiments. This program was used to transfer all the experiments to a single tape.

The final data reduction program reads the data for an experiment from magnetic tape, and uses calibration data to produce fluxes, position, and status versus time. It analyzes the data over any specified time step, and also averages the data over any desired period of time. In addition to providing this analysis, this program also provides the fractional change in the fluxes and the ratio of all fractional changes to all others.

Results

The record of any experiment consisted of the reactor's power

history previous to the experiment, the initial flux values, the fractional changes of the flux values at each detector with time, and the depth of insertion of the control rod versus time. Four experiments for the aluminum control rod and six experiments for the stainless steel control rod are reported here. Appendix B contains the reports, in tabular form for these ten experiments. Table 4 summarizes these experiments and defines the experiment numbers. As an aid in visualizing these results, two experiments are graphically displayed in Figures 25 and 26. Figure 25 demonstrates the lack of spatial flux distribution change in the aluminum control rod experiment, while Figure 26 shows a definite spatial flux distribution change for the stainless steel rod. The data for the other experiments, as well as the analysis in Chapter V and VI, indicate that the spatial distribution changes are almost entirely the result of adiabatic effects. However, Chapter VI points out the overall significance of even small non-adiabatic changes.

Table 4. Summary of the Kinetics Experiments

Experiment No.	Control Rod	Time Required for 50% Insertion (Seconds)	Fractional Change at Detector 5 at 50% Insertion	Ratio of Fractional Changes of Detector 3 to Detector 5 at 50% Insertion	Time Required for 100% Insertion (Seconds)	Fractional Change at Detector 5 at 100% Insertion	Ratio of Fractional Changes of Detector 3 to Detector 5 at 100% Insertion
1	Aluminum	0.95	.5568	0.916	2.2	.3101	.900
2	"	2.1	.5255	0.910	4.8	.2652	.891
3	"	5.8	.4745	0.900	11.6	.2090	.890
4	"	240	.0452	0.931	525	.0039	.851
5	Stainless	1.1	.1720	0.641	2.6	.0742	.640
6	"	2.6	.1531	0.620	6.2	.0539	.616
7	"	5.7	.1307	0.611	11.3	.0431	.601
8	"	20	.0716	0.647	43	.0147	.671
9	"	80	.0208	0.644	166	.0028	.607
10	"	152	.0093	0.645	312	.0014	.571

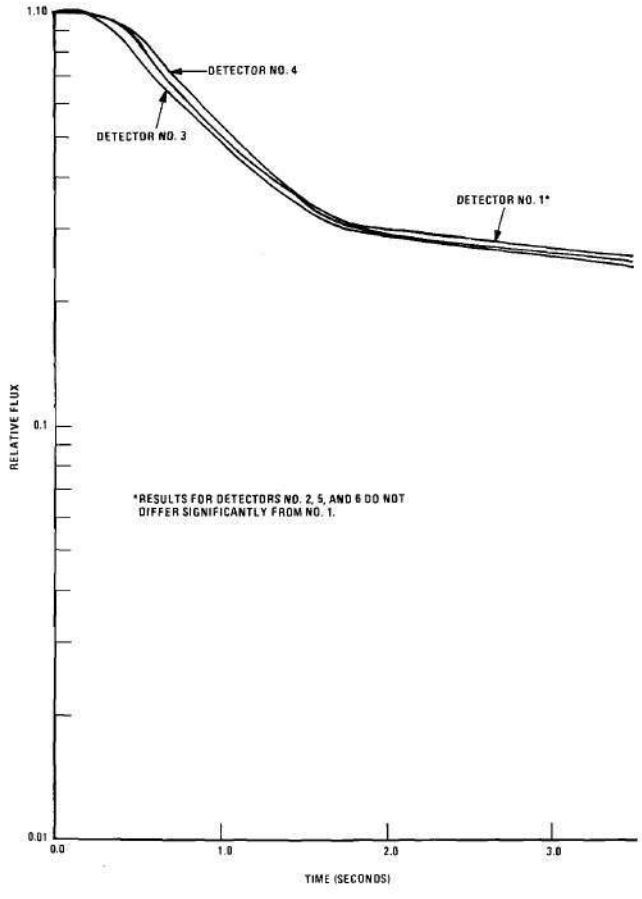

Figure 25. Graphic Results of the 2.2 Second Aluminum Control Rod Experiment.

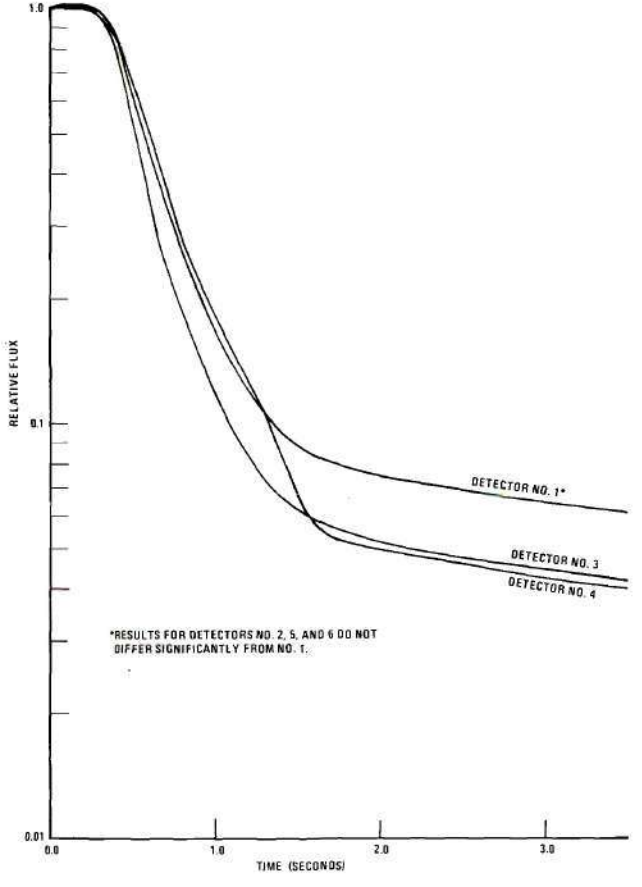

Figure 26. Graphic Results of the 2.6 Second Stainless Steel Control Rod Experiment.

CHAPTER IV

ANALYTICAL METHODS

This chapter assumes multigroup diffusion theory and proceeds to develop the theta-weighted, finite-differenced kinetics method. The numerical techniques used to obtain solutions, based on this theory, are also presented. Following this is a brief description of the computer codes written to implement these methods. Chapter V reports the calculations for a model of the experiments described in Chapters II and III. The comparison of these results with theory is given in Chapter VI.

Multigroup Kinetics Theory

The kinetics theory developed proceeds from an assumption of multigroup diffusion theory. The development is similar to that of reference 14. Multigroup diffusion theory represents a time, energy, and spatial balance of neutrons. The governing equation for the g^{th} energy group is

$$\frac{1}{V_g}\frac{\partial \phi_g(\vec{r},t)}{\partial t} = \nabla\cdot D_g(\vec{r},t)\,\nabla\phi_g(\vec{r},t) + \chi_g\,(1-\beta)\sum_{g'=1}^{G}\nu\,\Sigma_{fg'}(\vec{r},t)\cdot\phi_{g'}(\vec{r},t) - \left(\Sigma_{ag}(\vec{r},t) + \sum_{g'=1}^{G}\Sigma_{g\to g'}(\vec{r},t)\right)\phi_g(\vec{r},t) + \sum_{g'=1}^{G}\Sigma_{g'\to g}(\vec{r},t)\,\phi_{g'}(\vec{r},t) + \sum_{\ell=1}^{L} f_{\ell\to g}\,\lambda_\ell\,P_\ell(\vec{r},t), \quad (1)$$

where the following definitions apply:

V_g is the group neutron velocity,

$\vec{r}$ is a position vector,

t is the time,

$\phi_{g'}(\vec{r},t)$ is the neutron flux, at a position $\vec{r}$ and time t, for group g',

$D_{g'}(\vec{r},t)$ is the diffusion coefficient, at position $\vec{r}$ and time t, for group g',

χ_g is the fraction of fission neutrons produced in energy group g,

β is the fraction of fission neutrons which are delayed,

G is the number of neutron energy groups,

$\nu \Sigma_{fg'}(\vec{r},t)$ is the fission cross section, at position $\vec{r}$ and time t for neutrons of energy group g',

$\Sigma_{ag}(\vec{r},t)$ is the absorption cross section at position $\vec{r}$ and time t for neutrons of energy group g,

$\Sigma_{g'\to g}(\vec{r},t)$ is the removal cross section, at position $\vec{r}$ and time t, for neutrons scattering from energy g' to energy g,

L is the number of delayed neutron precursors,

$f_{\ell\to g}$ is the fraction of delayed neutrons from the ℓ^{th} type precursor, which go to neutron energy group g,

λ_ℓ is the decay constant for neutron precursors of type ℓ,

$P_\ell(\vec{r},t)$ is the number of neutron precursors of type ℓ at position $\vec{r}$ and time t.

There are G sets of these neutron balance equations. In addition, there are balance equations for the neutron precursors. The governing

equation for the ℓ^{th} type of precursor is

$$\frac{\partial P_\ell (\vec{r},t)}{\partial t} = - \lambda_\ell P_\ell(\vec{r},t) + \sum_{g'=1}^{G} \beta_\ell \nu \Sigma_{fg'} (\vec{r},t) \phi_{g'} (\vec{r},t), \qquad (2)$$

where β_ℓ is the fraction of all fission neutrons produced by the ℓ^{th} precursor type.

This method has all the assumptions of diffusion theory. It has also been assumed that there are no external sources, that the β_ℓ's and λ_ℓ's are independent of position, time, and neutron energy group, and that the fission fraction χ_g is independent of the energy of the neutron causing the fission.

The delayed neutron precursors are treated as being produced at the instant of fission. Additionally, it is assumed that each group of the precursors decays with a single decay constant, and that the delayed neutron is produced at the same spatial position as its precursor. These assumptions are discussed further in Chapter V.

This theory has G + L sets of spatially-dependent, coupled differential equations which must be solved with time. Solution of these equations for multiregion problems is not feasible, so the first step will be to replace a continuous geometrical and nuclear model of a reactor with a discontinuous one. Only two-dimensional cylindrical or cartesian theory will be considered. The basic approaches are similar; in particular, consider cylindrical geometry. Suppose the reactor extends from a radius of zero to R. A discontinuous model will distribute some number of points, say I, at radii r_i; where r_1 equals zero and r_I equals R. In a similar fashion, J points will be distributed along the z axis, where z_1 equals

zero and z_J equals Z; Z being the height of the reactor. In order that any cylindrical shell region can be described, the r and z positions of the limits of a region must be contained in the set of numbers (r_i, z_j). The geometrically continuous reactor has then been replaced by an orthogonal set of points (r_i, z_j). Any point will then be totally within a region, on a boundary, or on an interface between several regions. The group flux and each precursor are replaced by a set of values existing only at the grid points. Equations for the new set of quantities are obtained by integrating equations 1 and 2 over a volume associated with each mesh point. The volume is that cylindrical section defined by the midpoints of lines extending from a mesh point to the four adjacent mesh points. Figure 27 shows a cross section for such a volume for mesh point (r_i, z_j).

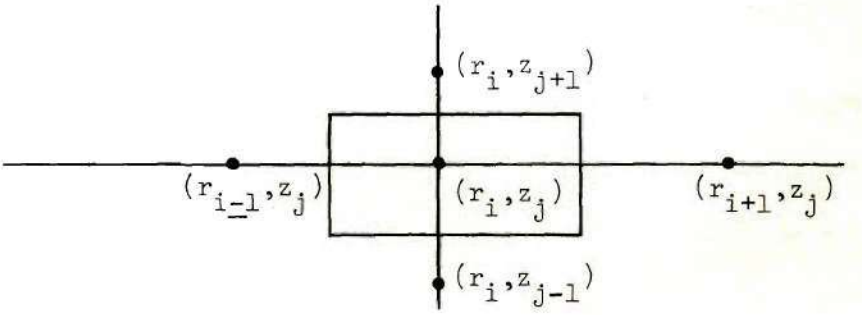

Figure 27. Volume of Integration for Mesh Point (r_i, z_j)

For mesh points on a boundary, the volume extends only to the boundary. Each term of equations (1) and (2) is to be integrated. Consider all terms of the form $a(\vec{r},t)\ \phi_g(\vec{r},t)$ and $bP_\ell(\vec{r},t)$. The approximate forms of integration used are:

$$\int_{\text{volume ij}} a\,(\vec{r},t)\,\phi_g\,(\vec{r},t)\,dV \approx \phi_g\,(r_i,z_j,t) \int_{\text{volume ij}} a\,(\vec{r},t)\,dV$$

and

$$\int_{\text{volume ij}} bP_\ell\,(\vec{r},t)\,dV \approx bP_\ell\,(r_i,z_j,t) \int_{\text{volume ij}} dV\ .$$

That is, the integral of a term is the value of the flux or precursor at the mesh point (r_i,z_j), times the integral over the volume of the multiplier. Since the multipliers are all region-dependent, the integration is at most a sum of four products of volume and region constants. The neutron leakage term, $\nabla\cdot D_g\,(\vec{r},t)\,\nabla\phi_g\,(\vec{r},t)$, cannot be handled in the preceding manner; however, by using Gauss's theorem,[28] this volume integral can be converted to a surface integral of $D_g\,(\vec{r},t)\,\nabla\phi_g\,(\vec{r},t)$. This surface integral was evaluated as outlined in reference 29. Use is made of a Taylor series expansion of the leakage, continuity of leakage, and continuity of flux to evaluate this term as a combination of the flux at the mesh point and four adjacent points, and terms involving the values of $D_g\,(\vec{r},t)$. Defining

$\phi_g^{ij}(t)$ as $\phi_g\,(\vec{r},t)$; $\vec{r} = (r_i,z_j)$,

W^{ij} as the volume associated with mesh point (r_i,z_j),

${}_1D_g^{ij}(t)$ as $D_g\,(\vec{r},t)$; $\vec{r} = (r_i + \Delta,\ z_j + \Delta)$; Δ small and positive,

${}_2D_g^{ij}(t)$ as $D_g\,(\vec{r},t)$; $\vec{r} = (r_i - \Delta,\ z_j + \Delta)$,

${}_3D_g^{ij}(t)$ as $D_g\,(\vec{r},t)$; $\vec{r} = (r_i - \Delta,\ z_j - \Delta)$,

${}_4D_g^{ij}(t)$ as $D_g\,(\vec{r},t)$; $\vec{r} = (r_i + \Delta,\ z_j - \Delta)$,

h_R^i as $r_{i+1} - r_i$,

h_L^i as $r_i - r_{i-1}$,

h_T^j as $z_{j+1} - z_j$,

h_B^j as $z_j - z_{j-1}$, and

$L_g^{ij}(t)$ as the approximation of the integral leakage over the volume associated with (r_i, z_j), one obtains:

$$L_g^{ij}(t) = \pi \left\{ \left(\phi_g^{i\ j+1}(t) - \phi_g^{ij}(t) \right) \left[\left(r_i h_R^i + \frac{h_R^{i\,2}}{4} \right) \frac{{}_1D_g^{ij}(t)}{h_T^j} \right. \right. \tag{3}$$

$$+ \left(r_i h_L^i - \frac{h_L^{i\,2}}{4} \right) \frac{{}_2D_g^{ij}(t)}{h_T^j} \Big] + \left(\phi_g^{i\ j-1}(t) - \phi_g^{ij}(t) \right) \left[\left(r_i h_R^i + \frac{h_R^{i\,2}}{4} \right) \frac{{}_4D_g^{ij}(t)}{h_B^j} \right.$$

$$+ \left(r_i h_L^i - \frac{h_L^{i\,2}}{4} \right) \frac{{}_3D_g^{ij}(t)}{h_B^j} \Big] + \left(\phi_g^{i+1\ j}(t) - \phi_g^{ij}(t) \right) \left[\left(\frac{r_i}{h_R^i} + \frac{1}{2} \right) \left(h_T^j\ {}_1D_g^{ij}(t) \right. \right.$$

$$\left. \left. + h_B^j\ {}_4D_g^{ij}(t) \right) \right] + \left(\phi_g^{i-1\ j}(t) - \phi_g^{ij}(t) \right) \left[\left(\frac{r_i}{h_L^i} - \frac{1}{2} \right) \left(h_T^j\ {}_2D_g^{ij}(t) + h_B^j\ {}_3D_g^{ij}(t) \right) \right] \Big\} .$$

Approximations of this type are discussed in reference 30. This reference contains a discussion on the modification of the terms of $L_g^{ij}(t)$ to obtain any desired boundary conditions. It should be noted that all terms of $L_g^{ij}(t)$ which would involve division by zero will be assigned special values to force the solution to fit the various boundary conditions. The definition of $L_g^{ij}(t)$ for Cartesian co-ordinates can be found in the preceding reference.

Using a superscript to denote the volume integrated value of all spatially dependent reactor parameters, equations (1) and (2) can be reformulated as below to give kinetics theory for a discontinuous reactor

model.

$$\frac{W^{ij}}{V_g}\frac{d\phi_g^{ij}(t)}{dt} = L_g^{ij}(t) + \chi_g\,(1-\beta)\sum_{g'=1}^{G}\nu\,\Sigma_{fg'}^{ij}(t)\,\phi_{g'}^{ij}(t) - \left(\Sigma_{ag}^{ij}(t) + \sum_{g'=1}^{G}\Sigma_{g\to g'}^{ij}(t)\right)\phi_g^{ij}(t) + \sum_{g'=1}^{G}\Sigma_{g'\to g}^{ij}(t)\,\phi_{g'}^{ij}(t) + W^{ij}\sum_{\ell=1}^{L} f_{\ell\to g}\,\lambda_\ell P_\ell^{ij}(t) \tag{4}$$

$$W^{ij}\frac{dP_\ell^{ij}(t)}{dt} = \sum_{g=1}^{G}\beta_\ell\,\nu\,\Sigma_{fg}^{ij}(t)\,\phi_g^{ij}(t) - \lambda_\ell W^{ij}\,P_\ell^{ij}(t) \tag{5}$$

Equation (4) can be further simplified by lumping together all the terms multiplied by $\phi_g^{ij}(t)$ and $\phi_{g'}^{ij}(t)$. Defining

$$\tau_{g'\to g}^{ij}(t) \quad \text{as} \quad \Sigma_{g'\to g}^{ij} + \chi_g\,(1-\beta)\,\nu\,\Sigma_{fg'}^{ij}(t)\,, \quad g' \text{ unequal to } g, \qquad \text{and}$$

$$\tau_{g'\to g}^{ij}(t) \quad \text{as} \quad \chi_g\,(1-\beta)\,\nu\,\Sigma_{fg}^{ij}(t) - \sum_{\substack{g''=1\\ g''\neq g}}^{G}\Sigma_{g\to g''}^{ij}(t) - \Sigma_{ag}^{ij}(t), \quad g' \text{ equal to } g,$$

equation (4) can be rewritten as

$$\frac{W^{ij}}{V_g}\frac{d\phi_g^{ij}(t)}{dt} = L_g^{ij}(t) + \sum_{g'=1}^{G}\tau_{g'\to g}^{ij}(t)\,\phi_{g'}^{ij}(t) + W^{ij}\sum_{\ell=1}^{L} f_{\ell\to g}\,\lambda_\ell P_\ell^{ij}(t) \tag{6}$$

A review of this brief development is in order. Initially, kinetics theory was expressed as a series of G + L coupled, time and spatially de-

pendent differential equations. These equations are too complicated to be solved for realistic two-dimensional problems, so approximations were made to develop a theory which, though less valid, could be solved. To do so involved converting the spatially continuous reactor into a finite, two-dimensional mesh, and associating with each mesh a volume of the original space. The kinetics equations were then integrated, by making simplifying assumptions, over each of these volumes to produce, at each mesh point, relationships involving the group fluxes and precursors at that point and also the group fluxes at the adjacent mesh points. The result is that, instead of having G + L coupled, spatially continuous, differential equations to solve, one has (G + L) × (I × J) coupled, but not spatially continuous, differential equations to solve.

The equations derived from kinetics theory must have boundary conditions and initial values. The spatial boundary conditions are concerned with the values of the flux and current along the geometrical edges of the problem. These may be specified as a linear relationship between the two. Reference 30 demonstrates a way of imposing boundary conditions on a mesh which in some way approximates those on the spatially continuous model. In this study, either the flux or the current was set to zero along the edge. This is simply accomplished by setting all terms except $L_g^{ij}(t)$ of equation (4) to zero. Then the separate terms of $L_g^{ij}(t)$ can be adjusted to achieve these simpler boundary conditions.

The initial flux conditions for this study are always the equilibrium flux for a just-critical reactor. This solution is obtained by setting all time derivatives to zero and adjusting the cross sections

until criticality is obtained. The initialization of the precursors is discussed later.

Analytical Techniques

The solution of the (G + L) × (I × J) set of coupled differential equations just derived can be solved only approximately for the values of G, L, I, and J normally encountered in reactor analysis.

The basic approach is to separate the precursor solution process from the flux solution and then to solve some energy groups with a spatial scheme, while solving others with an adiabatic scheme.

Without loss of generality, suppose that the values of all quantities are known at time zero, and that the values are desired for some future time h. Denote the first with a time of zero and the latter with a time of h. Consider the precursor equations for some point (r_i, z_j), ignoring for the present the ij superscript. Since the precursors are continuous with time, there exists some time t_1 for which

$$\left.\frac{dP_\ell(t)}{dt}\right|_{t_1} = \frac{P_\ell(h) - P_\ell(0)}{h} \qquad 0 < t_1 < h \ .$$

Suppose that at this time t_1, $P_\ell(t_1) = \frac{1}{2} P_\ell(0) + \frac{1}{2} P_\ell(h)$

and that $\nu \Sigma_{fg'}(t_1) \phi_{g'}(t_1) = \frac{1}{2} (\nu \Sigma_{fg'}(0) \phi_{g'}(0) + \nu \Sigma_{fg'}(h) \phi_{g'}(h))$.

Then $\frac{W}{h} (P_\ell(h) - P_\ell(0)) = \frac{1}{2} \beta_\ell \sum_{g'=1}^{G} (\nu \Sigma_{fg'}(0) \phi_{g'}(0) + \nu \Sigma_{fg'}(h) \phi_{g'}(h))$

$- \frac{1}{2} W \lambda_\ell [P_\ell(h) + P_\ell(0)]$. Solving for $P_\ell(h)$ gives

$$P_\ell(h) = \frac{2 - h\lambda_\ell}{2 + h\lambda_\ell} P_\ell(0) + \frac{h\beta_\ell}{W(2 + h\lambda_\ell)} \sum_{g'=1}^{G} (\nu \Sigma_{fg'}(0)\, \phi_{g'}(0) \tag{7}$$

$$+ \nu \Sigma_{fg'}(h)\, \phi_{g'}(h)) .$$

This means that the precursors at any point at time h may be easily found, given the precursors and flux at this point for time zero and the values of the neutron flux at this point for time h.

The precursors will now be eliminated from the equations for the flux at time h. As before, there is some other time t_2 between zero and h for which $\left.\frac{d\phi_g(t)}{dt}\right|_{t_2} = \frac{\phi_g(h) - \phi_g(0)}{h}$. Eventually, this approximation will be used as the time derivative, but for the moment assume that at this time $P_\ell(t_2) = \frac{1}{2}(P_\ell(0) + P_\ell(h))$. Thus,

$W \sum_{\ell=1}^{L} f_{\ell\to g} \lambda_\ell P_\ell(t_2)$ can be replaced by $\frac{W}{2} \sum_{\ell=1}^{L} f_{\ell\to g} \lambda_\ell (P_\ell(0) + P_\ell(h))$.

Substituting for $P_\ell(h)$ from equation (7) gives

$$W \sum_{\ell=1}^{L} f_{\ell\to g} \lambda_\ell P_\ell(t_2) = W \sum_{\ell=1}^{L} \frac{2\lambda_\ell f_{\ell\to g}}{2 + h\lambda_\ell} P_\ell(0) \tag{8}$$

$$+ \sum_{g'=1}^{G} \frac{1}{2} h \left[(\nu \Sigma_{fg'}(0)\, \phi_{g'}(0) + \nu \Sigma_{fg'}(h)\, \phi_{g'}(h)) \sum_{\ell=1}^{L} \frac{\beta_\ell \lambda_\ell f_{\ell\to g}}{2 + h\lambda_\ell} \right].$$

Defining

$$R_{g'\to g}(0) = \frac{1}{2} h \nu \Sigma_{fg'}(0) \sum_{\ell=1}^{L} \frac{\beta_\ell \lambda_\ell f_{\ell\to g}}{2 + h\lambda_\ell} \qquad \text{and}$$

$$R_{g'\to g}(h) = \frac{1}{2}\, h\, \nu\, \Sigma_{fg'}(h) \sum_{\ell=1}^{L} \frac{\beta_\ell \lambda_\ell f_{\ell\to g}}{2 + h\lambda_\ell}, \qquad \text{then}$$

$$W \sum_{\ell=1}^{L} \lambda_\ell f_{\ell\to g}\, P_\ell(t_2) = \sum_{g'=1}^{G} \left(R_{g'\to g}(0)\, \phi_{g'}(0) + R_{g'\to g}(h)\, \phi_{g'}(h)\right) \qquad (9)$$

$$+ W \sum_{\ell=1}^{L} \frac{2\lambda_\ell f_{\ell\to g}}{2 + h\lambda_\ell} P_\ell(0).$$

Note that $R_{g'\to g}(0)$ and $R_{g'\to g}(h)$ depend on h, but have the same dimensions as a macroscopic cross section, i.e., cm^{-1}. It is clear that the substitution of $R_{g'\to g}$ into the neutron equations will eliminate all dependence on the precursors at time h. Substituting t_2 for t into equation (6), the result is

$$\frac{W}{V_g} \frac{\phi_g(h) - \phi_g(0)}{h} = L_g(t_2) + \sum_{g'=1}^{G} \tau_{g'\to g}(t_2)\, \phi_{g'}(t_2) \qquad (10)$$

$$+ W \sum_{\ell=1}^{L} \frac{2\lambda_\ell f_{\ell\to g}}{2 + h\lambda_\ell} P_\ell(0) + \sum_{g'=1}^{G} R_{g'\to g}(0)\, \phi_{g'}(0) + \sum_{g'=1}^{G} R_{g'\to g}(h)\, \phi_{g'}(h).$$

Only the terms evaluated at time t_2 remain to be approximated. The following approximations enable these terms to be calculated:

$$L_g(t_2) \approx (1 - \theta)\, L_g(0) + \theta\, L_g(h); \qquad 0 \leqq \theta \leqq 1$$

$$\tau_{g'\to g}(t_2)\phi_{g'}(t_2) \approx (1 - \theta)\, \tau_{g'\to g}(0)\, \phi_{g'}(0) + \theta\, \tau_{g'\to g}(h)\, \phi_{g'}(h);$$

$$0 \leqq \theta \leqq 1 .$$

Substitution of these approximations into equation (10) gives

$$\frac{\phi_g(h) - \phi_g(0)}{h} = (1 - \theta) \frac{V_g}{W} \left[L_g(0) + \sum_{g'=1}^{G} \tau_{g' \to g}(0)\ \phi_{g'}(0) \right] \tag{11}$$

$$+ \theta \frac{V_g}{W} \left[L_g(h) + \sum_{g'=1}^{G} \tau_{g' \to g}(h)\ \phi_{g'}(h) \right] + V_g \sum_{\ell=1}^{L} \frac{2\lambda_\ell f_{\ell \to g}}{2 + h\lambda_\ell} P_\ell(0)$$

$$+ \frac{V_g}{W} \sum_{g'=1}^{G} R_{g' \to g}(0)\ \phi_{g'}(0) + \frac{V_g}{W} \sum_{g'=1}^{G} R_{g' \to g}(h)\ \phi_{g'}(h) .$$

By grouping terms and replacing the superscripts, one obtains

$$- \phi_g^{ij}(h) + \frac{\theta h V_g}{W^{ij}} \left[L_g^{ij}(h) + \sum_{g'=1}^{G} \tau_{g' \to g}^{ij}(h)\ \phi_{g'}^{ij}(h) \right] \tag{12}$$

$$+ \frac{hV_g}{W^{ij}} \sum_{g'=1}^{G} R_{g' \to g}^{ij}(h)\ \phi_{g'}(h) = - \phi_g^{ij}(0) - \frac{(1-\theta)\ hV_g}{W^{ij}} \left[L_g^{ij}(0) \right.$$

$$\left. + \sum_{g'=1}^{G} \tau_{g' \to g}^{ij}(0)\ \phi_{g'}^{ij}(0) \right] - \frac{hV_g}{W^{ij}} \sum_{g'=1}^{G} R_{g' \to g}^{ij}(0)\ \phi_{g'}^{ij}(0)$$

$$- hV_g \sum_{\ell=1}^{L} \frac{2\lambda_\ell f_{\ell \to g}}{2 + h\lambda_\ell} P_\ell^{ij}(0) .$$

Recall that equation (12) holds for each mesh point and that L_g^{ij} involves a combination of the fluxes at a mesh point and the adjacent points. The result is a very large set of simultaneous equations, $G \times I \times J$, whose solution is the flux at time h. Also note that a θ of one results in an implicit scheme while a θ of zero, and an approximation of $R_{g' \to g}^{ij}(h)\ \phi_{g'}^{ij}(h)$ results in an explicit scheme.

The manner in which boundary conditions are handled can now be

readily explained. If ij represents a boundary point, then the equations are represented as $- \phi_g^{ij}(h) + L_g^{ij}(h) = 0$. At those boundaries requiring zero flux, set $L_g^{ij}(h) = 0$. This will force the flux on the boundary to zero. A boundary condition of zero slope requires further approximations. It is necessary to set the flux at a boundary point and its normal adjacent point equal. This will give a first-order zero slope. In order to do this, one sets all terms of $L_g^{ij} = 0$, except for the one modifying the normal flux, which is set to one. This forces the two fluxes to be identical. At a point where zero slope and zero flux are both required, the zero flux boundary condition is established.

A system of G X I X J simultaneous equations whose solution is an approximation of the neutron flux at time h has been developed. As shown before, the precursors at time h are simply obtained, given the flux values at time h. This is a point solution scheme for all groups. The quality of the solution depends on the θ and h used. A θ of zero leads to a rapid solution of the system of equations, but these solutions are only stable for step sizes less than some problem-dependent value, usually one which is comparable to the average prompt neutron lifetime. A θ greater than or equal to 1/2 leads to a stable solution process for any step size h. A θ of one is the most stable, while a θ of 1/2 has a solution with the least error. For subcritical problems, a θ of one should be used; for supercritical problems, a θ of 1/2 should be used.[31]

The theory developed will allow the solution of the above equations as they are, or permit a simple, less precise, solution to be found. The development of an adiabatic solution for all groups follows. The key to

this process is to assume only the shape of the neutron fluxes, and from this to adjust the relative magnitudes of the group fluxes so that the equations are solved in an integral, or weighted sense instead of point-wise.

Assume $\phi_g^{ij}(h) = A_g^h \psi_g^{ij}(h)$ and $\phi_g^{ij}(0) = A_g^0 \psi_g^{ij}(0)$, where A_g^0, $\psi_g^{ij}(0)$, and $\psi_g^{ij}(h)$ are known. Substituting these values into equation (12) and defining $\mathcal{L}_g^{ij}$ as L_g^{ij} was defined, except using the functions ψ instead of ϕ, one obtains:

$$A_g^h \left[- \psi_g^{ij}(h) + \frac{\theta h V_g}{W^{ij}} \mathcal{L}_g^{ij}(h) \right] + \frac{\theta h V_g}{W^{ij}} \sum_{g'=1}^{G} \tau_{g' \to g}^{ij}(h) \, A_{g'}^h \, \psi_{g'}^{ij}(h) \tag{13}$$

$$+ \frac{h V_g}{W^{ij}} \sum_{g'=1}^{G} R_{g' \to g}^{ij}(h) \, A_{g'}^h \, \psi_{g'}^{ij}(h) = A_g^0 \left[- \psi_g^{ij}(0) - (1 - \theta) \frac{h V_g}{W^{ij}} \mathcal{L}_g^{ij}(0) \right]$$

$$- (1 - \theta) \frac{h V_g}{W^{ij}} \sum_{g'=1}^{G} \tau_{g' \to g}^{ij}(0) \, A_{g'}^0 \, \psi_{g'}^{ij}(0) - \frac{h V_g}{W^{ij}} \sum_{g'=1}^{G}$$

$$R_{g' \to g}^{ij}(0) \, A_{g'}^0 \, \psi_{g'}^{ij}(0) - h V_g \sum_{\ell=1}^{L} \frac{2 \lambda_\ell f_{\ell \to g}}{2 + h \lambda_\ell} P_\ell^{ij}(0) \, .$$

For each group, take the indicated sum of equation (13) multiplied by W^{ij} over the entire mesh. After rearranging terms the result is:

$$A_g^h \sum_{\text{mesh}} \left[- W^{ij} \psi_g^{ij}(h) + \theta h V_g \mathcal{L}_g^{ij}(h) \right] \tag{14}$$

$$+ \theta h V_g \sum_{g'=1}^{G} A_{g'}^h \sum_{\text{mesh}} \tau_{g' \to g}^{ij}(h) \psi_{g'}^{ij}(h) + h V_g \sum_{g'=1}^{G} A_{g'}^h \sum_{\text{mesh}} R_{g' \to g}^{ij}(h) \, \psi_{g'}^{ij}(h)$$

(Continued)

$$= A_g^0 \sum_{mesh} \left[- W^{ij} \psi_g^{ij}(0) - (1 - \theta)\, hV_g \mathcal{L}_g^{ij}(0) \right]$$

$$- (1 - \theta)\, hV_g \sum_{g'=1}^{G} A_{g'}^0 \sum_{mesh} \tau_{g' \to g}^{ij}(0)\, \psi_{g'}^{ij}(0)$$

$$- hV_g \sum_{g'=1}^{G} A_{g'}^0 \sum_{mesh} R_{g' \to g}^{ij}(0)\, \psi_{g'}^{ij}(0)$$

$$- hV_g \sum_{\ell=1}^{L} \frac{2\lambda_\ell f_{\ell \to g}}{2 + h\lambda_\ell} \sum_{mesh} W^{ij}\, P_\ell^{ij}(0) \; .$$

The result is G equations in G unknowns. Define

$$\alpha(g,g') = \theta hV_g \sum_{mesh} \tau_{g' \to g}^{ij}(h)\, \psi_{g'}^{ij}(h) + hV_g \sum_{mesh} R_{g' \to g}^{ij}(h)\, \psi_{g'}^{ij}(h)$$

where g is unequal to g'. When g is equal to g', define

$$\alpha(g,g) = \sum_{mesh} \left[- W^{ij}\, \psi_g^{ij}(h) + \theta hV_g \mathcal{L}_g^{ij}(h) \right] + \theta hV_g \sum_{mesh} \tau_{g \to g}^{ij}(h)\, \psi_g^{ij}$$

$$+ hV_g \sum_{mesh} R_{g \to g}^{ij}(h)\, \psi_g^{ij}(h) \; .$$

Also define B(g) as the right-hand side of equation (14). Then the solution of $\alpha A = B$ is the array A_g^h. Although this scheme appears more complex, the solution of A_g^h involves a system of only G simultaneous equations instead of G × I × J equations. The disadvantage is in the loss of detail, since the answers are averages which depend on the accuracy of ψ_g.

The proposed method of solution utilizes a combination of these two methods. It takes advantage of the fact that the only practical way of solving the point system of equations is to use an iterative technique.

Typically, such schemes use outer and inner iterations. For each inner iteration, the assumption is made that all group fluxes other than the one being considered are known. This permits the terms involving them to be moved to the right-hand side of equation (12). The result is the simpler task of solving the spatial one-group problems. The outer iteration consists of cycling repeatedly through the groups until the difference between the current iteration and the previous one satisfies some convergence criterion. To combine the two schemes already discussed, modify the outer iteration to skip over any inner iterations on those groups being treated adiabatically, and to use $A_g \psi_g$ as the off-group flux approximations for these adiabatic groups. At the end of this outer iteration, an adiabatic solution is sought which utilizes given flux shapes for the adiabatic groups, the t = 0 flux shapes for the initial non-adiabatic flux shapes, and the present iterative solution for the t = h non-adiabatic flux shapes. In this case, only the values of A_g^h pertaining to the adiabatic group will have meaning.

A kinetics code built on this theory has the advantages of speed and versatility. Since those groups being treated adiabatically may be changed during the course of a calculation, the more precise point systems can be used only when necessary. Such a code also contains the means for determining self-consistency, since the same problem can be done several ways and the differences in answers compared. An additional advantage when doing a purely space-time solution is that an adiabatic step, using the t = 0 space-time flux values, is used to obtain the initial guess of the flux at t = h.

Code Development

The kinetics method just developed was implemented on a Univac 1108 having two arithmetic units, 192,000 36-bit words, tape units, and FASTRAN storage, operating under an EXECUTIVE VIII monitor. FORTRAN IV was used as the programming language because of its compatibility with other computer systems. Three computer programs using common subroutines were written. The three programs were a two-dimensional, multigroup statics code; a similar code generating a series of static solutions for different reactor configurations and saving these solutions on magnetic tape as adiabatic flux shapes; and a two-dimensional, multigroup kinetics code.

Statics

The statics code solved the statics equations associated with the kinetics equations. For point (ij) the statics equation is as follows, where k is the reactor multiplication and the other symbols are as previously defined:

$$0 = L_g^{ij}(0) + \frac{1}{k}\chi_g \sum_{g'=1}^{G} \nu \Sigma_{fg'}^{ij}(0)\, \phi_{g'}^{ij}(0) \qquad (15)$$

$$- \left(\Sigma_{ag}^{ij}(0) + \sum_{g'=1}^{G} \Sigma_{g\to g'}^{ij}(0)\right) \phi_g^{ij}(0) + \sum_{g'=1}^{G} \Sigma_{g'\to g}^{ij}(0)\, \phi_{g'}^{ij}(0).$$

It has been assumed that $f_{\ell\to g} = \chi_g$ for all precursors. If not, then the χ_g's must be compensated in a straightforward manner. These equations were solved by using an outer and inner iteration. The outer iteration assumes that all group fluxes except one, as well as k, are

known and proceeds to solve for the unknown group flux by using an inner iteration. The inner iteration uses a group-wise overrelaxed Gauss-Seidell method[32] to obtain new fluxes for a particular group. The ratio between the average flux after an outer iteration to that before that outer iteration is the factor which, when multiplied by the assumed k, will give a new estimate of k. In addition, the ratio between the different fluxes at a point permits a point-dependent k to be calculated. This program collects after each outer iteration the new fluxes and k as well as the largest and smallest values of the point-dependent k's. The outer iteration is stopped when the difference between the largest and smallest point k's is less than some input parameter or when the number of outer iterations exceeds some input parameter.

Parameters for a critical reactor may be obtained by dividing the fission cross sections by the resulting k, or reactor multiplication. Options are also provided so that the code can be used to do a poison search in any number of regions.

The statics code was tested by comparing its solutions to those produced by sample runs on EXTERMINATOR.[33] There was no appreciable difference between runs on the two codes. In addition, simple point problems having their buckling replaced by spatial dimensions were run for different geometric meshes. The statics code produced solutions which agreed with the point solutions.

Kinetics

A kinetics code, using the kinetics method just developed, was written to simulate the experiments described in Chapters II and III.

As such, this code had to be special-purpose; however, the only parts of the code that are not general purpose are the evaluation, with time, of region cross sections and boundaries. Since this evaluation is done in special subroutines, the code is readily adaptable to other problems by changing only these parts. This section is only concerned with the general part of the code; the evaluation of regions and boundaries is described in Chapter V.

A discussion of the inputs to this kinetics code helps to describe its operation. The major inputs are from a magnetic tape prepared by the adiabatic shapes code. This tape contains all information needed to specify, for a particular control rod, the non-kinetics data. These data contain the mesh, region descriptions, cross sections, the initial reactor multiplication, and the initial flux values. In addition, this tape contains a set of flux shapes for various depths of insertion of the control rod.

There are two types of card input. The first describes the kinetics parameters for a particular simulation. These include the β_ℓ's and the λ_ℓ's, the power history, as a histogram, and the time dependence of the control rod position in table form. This serves to define the desired simulation. The power history is used in the initialization of the precursor concentrations. These times, as well as the β_ℓ's and λ_ℓ's, are sufficient to calculate the precursor fractional saturation. The precursor concentrations are set equal to the product of their equilibrium values and calculated fractional saturations.

The second type of card input controls the mathematics of the

simulation solution. The code is written so that multiple sets of controls can be input, thus using different parameters over the course of the solution. The controls specify the θ to be used, the groups to be treated adiabatically, the maximum permitted average fractional change per time step, the minimum time step, the maximum time step, the time step to be used in calculating the over-relaxation constants, the print time step, the number of prints, and the average outer iteration error. The average inner error is taken to be one-fifth the outer iteration error. These parameters are used by the code to select its own time step and to control the number of outer iterations. The minimum time step is suspended whenever a smaller time step must be taken to reach a print time. Results are output only at the print times.

The solution process for the non-adiabatic groups is the same as that described for the statics equations, while the solution for the adiabatic groups is like that described in the analytical method. The flux shapes for the adiabatic calculations are taken from linear interpolation of the data on the adiabatic tape.

The testing of this code was more difficult than the testing of the statics, since no comparable codes existed. For testing purposes the kinetics code was modified to run homogeneous, multigroup problems. A special multigroup point-reactor kinetics code was written so that some checks on the kinetics code could be obtained. Tests over different geometries, meshes, time scales, and severity of perturbations demonstrated excellent agreement between the two codes.

Final tests on the kinetics code were performed by running identical

problems with different mathematical controls. The results were consistent, adding further credence to the predictions of the code.

Adiabatic Shapes

The code to make the magnetic tape of adiabatic shapes is simple, given the kinetics and statics codes. This code uses the special subroutines in the kinetics code to find the state of the reactor for any depth of insertion of the control rod. The subroutines of the statics code are then used to find the statics solution. Card input determines the number of such shapes to be calculated

CHAPTER V

ANALYTICAL MODEL AND CALCULATIONS

The analytical model used to simulate the experiments described in Chapters II and III is presented in this Chapter. The numerical results obtained with the computer codes described in Chapter IV are contained in this Chapter and Appendix C.

Reactor Models

The experiment was simulated with a twelve region, rz, cylindrical model. The basic model is similar to the eight region statics model discussed in reference 34. The central core of this model has been replaced with a four region control rod representation. Figure 28 is a cross section of the model with the control rod partially inserted. Two versions of this model, each containing two sets of region descriptions were used. In the first version, the radius of the core is varied to increase the reactor fuel loading. One of the two models represents a ten-element core configuration, without an experimental assembly. This ten-element core is known to be just critical from the initial startup experiments on the GTRR. The model is described in Table 5. The dimensions and all non-fission cross sections are those given in reference 34. The fission cross sections are those of reference 34 divided by 1.030 to force criticality agreement with a physically critical assembly. The other model represents a 17-element core configuration with an experimental assembly in the cen-

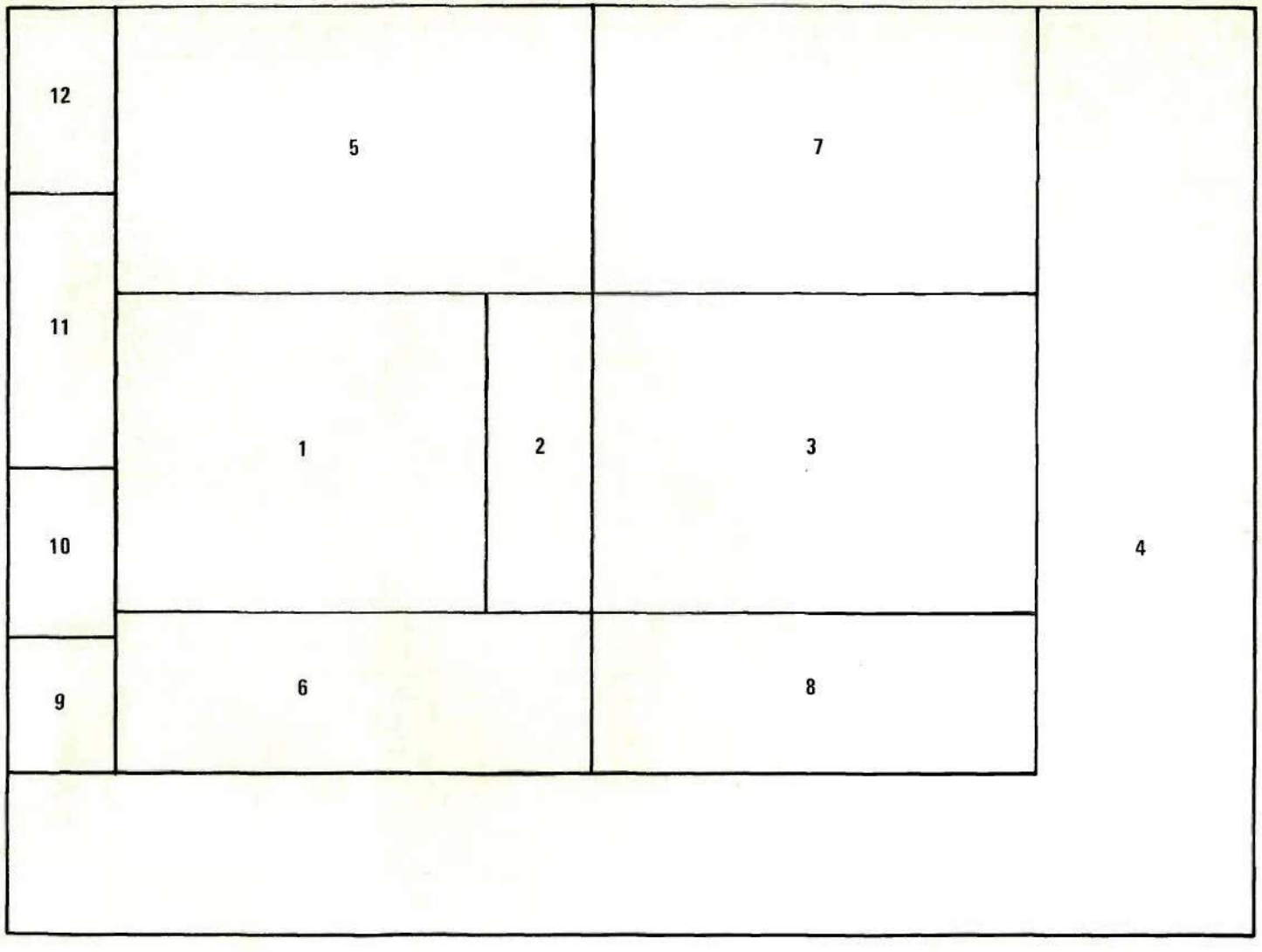

Figure 28. Cross Section of the Geometrical Model with the Control Rod Partially Inserted.

Table 5. Region Parameters for the Ten-Fuel-Element Variable-Radius Model

Region No.	Inner Radius (cm)	Outer Radius (cm)	Lower Height (cm)	Upper Height (cm)	No. of Mesh Pts. (r x z)	D_1 (cm)	D_2 (cm)	Σ_{a1} (cm^{-1})	Σ_{a2} (cm^{-1})	$\Sigma_{1\to2}$ (cm^{-1})	$\nu\Sigma_{f1}$ (cm^{-1})	$\nu\Sigma_{f2}$ (cm^{-1})
1	0.00	25.31	102.31	163.27	9 x 9	1.3821	0.8934	7.551×10^{-4}	1.188×10^{-2}	7.934×10^{-3}	8.738×10^{-4}	2.209×10^{-2}
2	25.31	34.89	102.31	163.27	3 x 9	1.3135	0.8260	1.56×10^{-4}	8.160×10^{-5}	9.517×10^{-3}	---	---
3	34.89	82.00	94.69	170.89	8 x 11	1.3187	0.8657	1.61×10^{-4}	7.855×10^{-4}	8.334×10^{-3}	---	---
4	0.00	152.40	0.00	60.96	23 x 4	1.1113	0.8620	0.00	2.587×10^{-4}	2.338×10^{-3}	---	---
4	82.00	152.40	60.96	240.82	6 x 22	1.1113	0.8620	0.00	2.587×10^{-4}	2.338×10^{-3}	---	---
5	0.00	34.89	163.27	240.82	11 x 9	1.3244	0.8389	1.62×10^{-4}	3.210×10^{-4}	9.282×10^{-3}	---	---
6	0.00	34.89	60.96	102.31	11 x 6	1.3389	0.8563	1.70×10^{-4}	6.348×10^{-4}	8.974×10^{-3}	---	---
7	34.89	82.00	170.89	240.82	8 x 8	1.3365	0.8534	1.69×10^{-4}	5.849×10^{-4}	9.023×10^{-3}	---	---
8	34.89	82.00	0.00	94.69	8 x 5	1.3449	0.8635	1.74×10^{-4}	7.599×10^{-4}	8.849×10^{-3}	---	---

tral fuel element position. Table 6 contains the specifications of this model. Regions three through eight are the same as in the ten-element model. The cross sections for regions nine through 12 were obtained from cross-section programs TEMPEST[35] and FORM.[36] Region nine represents the plenum plug on the experimental assembly; region ten represents the aluminum shroud and moderator; region 11 represents the aluminum shroud, moderator, and a control rod; region 12 represents the aluminum shroud, moderator, and the one-inch diameter stainless steel drive rod. The region one cross sections are more involved. They were obtained through a two step process. The first step was to simulate the 17-element core and one detector holder by weighting the cross sections from regions one and two of Table 5 with factors of 17 and one respectively. Such cross sections produce, with the control rod in its full out position, a multiplication greater than one. This is to be expected since the 17 fuel elements are required because of burnup in the fuel. In addition the reactor in this configuration has approximately 3.2 percent of its reactivity held by the shim-safety blades. To correct for these factors, a poison search on region one was performed. This search produced the absorption cross sections for region one given in Table 6.

When the control rod is fully inserted, it centers on the core and extends three inches beyond each end of it. The motion of the control rod is controlled by parameters input into the kinetics or adiabatic shapes programs. For these codes to work all the volume between four adjacent mesh points must be of the same composition. These codes determine, for the experimental assembly with a partially extended control rod, which volumes are totally of one region and assign this region to those volumes. The only such volumes that are not completely of one region are

Table 6. Region Parameters for the 17-Fuel-Element Varisble-Radius Model

Region No.	Inner Radius (cm)	Outer Radius (cm)	Lower Height (cm)	Upper Height (cm)	No. of Mesh Pts. (r x z)	D_1 (cm)	D_2 (cm)	Σ_{a1} (cm^{-1})	Σ_{a2} (cm^{-1})	$\Sigma_{1\to2}$ (cm^{-1})	$\nu\Sigma_{f1}$ (cm^{-1})	$\nu\Sigma_{f2}$ (cm^{-1})
1(Al.rod)	8.00	34.89	102.31	163.27	7 x 9	1.3783	0.8897	8.145×10^{-4}	1.2695×10^{-2}	8.022×10^{-3}	8.253×10^{-4}	2.0866×10^{-2}
1(S.S.rod)	8.00	34.89	102.31	163.27	7 x 9	1.3783	0.8897	8.074×10^{-4}	1.2584×10^{-2}	8.022×10^{-3}	8.253×10^{-4}	2.0866×10^{-2}
2	---	---	---	---	---	---	---	---	---	---	---	---
3	34.89	82.00	94.69	170.89	8 x 11	1.3187	0.8657	1.61×10^{-4}	7.855×10^{-4}	8.334×10^{-3}	---	---
4	0.00	152.40	0.00	60.96	23 x 4	1.1113	0.8620	0.00	2.587×10^{-4}	2.338×10^{-3}	---	---
4	82.00	152.40	60.96	240.82	6 x 22	1.1113	0.8620	0.00	2.587×10^{-4}	2.338×10^{-3}	---	---
5	8.00	34.89	163.27	240.82	7 x 9	1.3244	0.8389	1.62×10^{-4}	3.210×10^{-4}	9.282×10^{-3}	---	---
6	8.00	34.89	60.96	102.31	7 x 6	1.3389	0.8563	1.70×10^{-4}	6.348×10^{-4}	8.974×10^{-3}	---	---
7	34.89	82.00	170.89	240.82	8 x 8	1.3365	0.8534	1.69×10^{-4}	5.849×10^{-4}	9.023×10^{-3}	---	---
8	34.89	82.00	0.00	94.69	8 x 5	1.3449	0.8635	1.74×10^{-4}	7.599×10^{-4}	8.849×10^{-3}	---	---
9	0.00	8.00	60.96	94.69	5 x 5	1.4820	1.0340	2.33×10^{-4}	3.140×10^{-3}	6.406×10^{-3}	---	---
10	0.00	8.00	94.69	94.69-170.89	varies	1.3200	0.8335	1.60×10^{-4}	2.260×10^{-4}	9.375×10^{-3}	---	---
11(Al.rod)	0.00	8.00	94.69-170.89	170.89-240.82	varies	1.3887	0.9162	1.95×10^{-4}	1.606×10^{-3}	7.996×10^{-3}	---	---
11(S.S.rod)	0.00	8.00	94.69-170.89	170.89-240.82	varies	1.1490	0.7345	1.303×10^{-3}	2.179×10^{-2}	8.061×10^{-3}	---	---
12	0.00	8.00	170.89-240.82	240.82	varies	1.2684	0.8070	4.49×10^{-4}	6.072×10^{-3}	9.064×10^{-3}	---	---

the interface volumes between regions 10 and 11 and between regions 11 and 12; these occur when the partial insertion does not exactly place the control rod region on the model's mesh. The codes generate artificial regions for these interfaces which have cross sections equal to the volume-weighted averages of the adjacent regions. Figure 29 gives the predicted thermal flux shapes in V-18 for the aluminum control rod. Comparison with the experimental values shows a large discrepancy between the theoretical and experimental axial flux shapes. The thermal peaks predicted by theory were not experimentally found. Since the radial position of V-18 places it within the core of this model, strong thermal poisons which are present within the axial extent of the core cause the peaking. Examination of the experiment shows that V-18 is six inches from the nearest fuel even though it may be within an equivalent homogeneous core. Since axial flux shapes just outside the core region of this model agree much better with experiment, it was concluded that position V-18 is more nearly akin to the reflector than to the core.

It was this conclusion which led to the development of the second version, one of fixed core radius and variable fuel concentrations. The dimensions of this version were chosen to produce a compromise between the distance of V-18 from the center of the core, while maintaining it outside the homogenous core. In other words, the radius of the 17-element core was reduced while the radius at which V-18 would be simulated was increased. The result was a core radius of 26.2 cm and a radial positioning of V-18 at 34.2 cm instead of at its physical position of 26.4 cm.

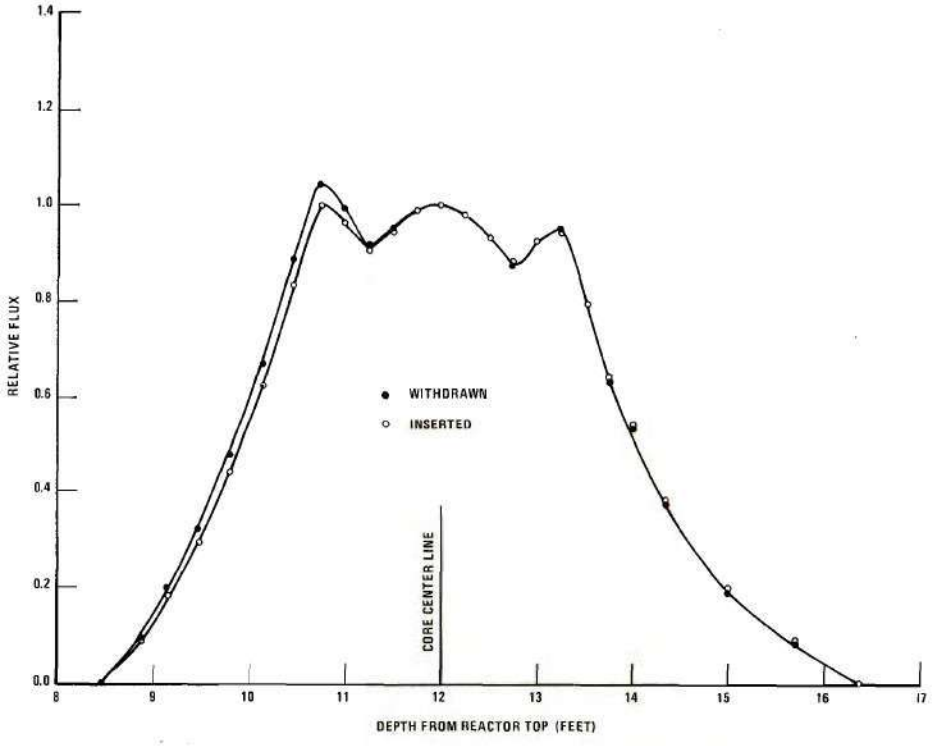

Figure 29. Analytical Flux Distributions in V-18 for the Aluminum Control Rod Withdrawn and Inserted as Calculated with the Variable Radius Model

The complete model for the fixed-radius, variable-composition model was obtained in a manner similar to that of the variable-radius model. The first step was to run a ten-fuel-element mock-up and adjust the fission cross sections so as to predict criticality for the physically critical ten-element GTRR startup. Table 7 defines this ten-element model. Only regions one and six have compositions different from those in Table 5. Region six cross sections were obtained from TEMPEST and FORM for revised atom densities. Region one cross sections were obtained from the same codes for a fuel density equal to ten fuel elements in a 26.2 cm-radius core. To force criticality the fission cross sections had to be divided by 1.080.

Table 8 describes the 17-element fixed-radius model. Attention is called to regions one and five. The 3.2 percent worth of the shim-safety blades at the time of the experiment was added as poison to region five, the region physically containing the shim-safety blades during the experiment. New cross sections, based on the appropriate fuel loading, were calculated for region one. The resulting fission cross-sections were "corrected" by dividing the cross section code values by the same amount used in the ten element core i.e. 1.080. These cross sections still produced a multiplication greater than one for the same reasons given in the variable radius version. The absorption cross sections for region one reported in Table 8 reflect a poison search of region one to account for burnup.

Figures 30 through 33 show the resulting static flux shapes. The agreement with experiment (shown in Figs. 22 and 24) is seen to be much

Table 7. Region Parameters for the Ten-Fuel-Element Fixed-Radius Model

Region No.	Inner Radius (cm)	Outer Radius (cm)	Lower Height (cm)	Upper Height (cm)	No. of Mesh Pts. (r x z)	D_1 (cm)	D_2 (cm)	Σ_{a1} (cm^{-1})	Σ_{a2} (cm^{-1})	$\Sigma_{1\to 2}$ (cm^{-1})	$\nu\Sigma_{f1}$ (cm^{-1})	$\nu\Sigma_{f2}$ (cm^{-1})
1	0.00	26.20	102.31	163.27	10 x 9	1.3672	0.8907	7.84×10^{-4}	1.589×10^{-2}	7.996×10^{-3}	8.553×10^{-4}	1.471×10^{-2}
2	---	---	---	---	---	---	---	---	---	---	---	---
3	26.20	82.00	94.69	170.89	10 x 11	1.3187	0.8657	1.61×10^{-4}	7.855×10^{-4}	8.334×10^{-3}	---	---
4	0.00	152.40	0.00	60.96	24 x 4	1.1113	0.8620	0.00	2.587×10^{-4}	2.338×10^{-3}	---	---
4	82.00	152.40	60.96	240.82	6 x 22	1.1113	0.8620	0.00	2.587×10^{-4}	2.338×10^{-3}	---	---
5	0.00	26.20	163.27	240.82	10 x 9	1.3244	0.8389	1.62×10^{-4}	3.210×10^{-4}	9.282×10^{-3}	---	---
6	0.00	26.20	60.96	102.31	10 x 6	1.3636	0.8859	1.83×10^{-4}	1.142×10^{-3}	8.474×10^{-3}	---	---
7	26.20	82.00	170.89	240.82	10 x 8	1.3365	0.8534	1.69×10^{-4}	5.849×10^{-4}	9.023×10^{-3}	---	---
8	26.20	82.00	60.96	94.69	10 x 5	1.3449	0.8635	1.74×10^{-4}	7.599×10^{-4}	8.849×10^{-3}	---	---

Table 8. Region Parameters for the 17-Fuel-Element Fixed-Radius Model

Region No.	Inner Radius (cm)	Outer Radius (cm)	Lower Height (cm)	Upper Height (cm)	No. of Mesh Pts. (r x z)	D_1 (cm)	D_2 (cm)	Σ_{a1} (cm^{-1})	Σ_{a2} (cm^{-1})	$\Sigma_{1\to2}$ (cm^{-1})	$\nu\Sigma_{f1}$ (cm^{-1})	$\nu\Sigma_{f2}$ (cm^{-1})
1(Al.rod)	8.00	26.20	102.31	163.27	6 x 9	1.4195	0.9529	1.296×10^{-3}	2.8043×10^{-2}	6.716×10^{-3}	1.528×10^{-3}	4.896×10^{-2}
1(S.S.rod)	8.00	26.20	102.31	163.27	6 x 9	1.4195	0.9529	1.293×10^{-3}	2.7984×10^{-2}	6.716×10^{-3}	1.528×10^{-3}	4.896×10^{-2}
2	---	---	---	---	---	---	---	---	---	---	---	---
3	26.20	82.00	94.69	170.89	10 x 11	1.3187	0.8657	1.61×10^{-4}	7.855×10^{-4}	8.334×10^{-3}	---	---
4	0.00	152.40	0.00	60.96	24 x 4	1.1113	0.8620	0.00	2.587×10^{-4}	2.338×1^{-3}	---	---
4	82.00	152.40	60.96	240.82	6 x 22	1.1113	0.8620	0.00	2.587×10^{-4}	2.338×10^{-3}	---	---
5	8.00	26.20	163.27	240.82	6 x 9	1.3244	0.8389	2.867×10^{-3}	5.681×10^{-3}	9.282×10^{-3}	---	---
6	0.00	26.20	60.96	102.31	10 x 6	1.3636	0.8859	1.83×10^{-4}	1.142×10^{-3}	8.474×10^{-3}	---	---
7	26.20	82.00	170.89	240.82	10 x 8	1.3365	0.8534	1.69×10^{-4}	5.849×10^{-4}	9.023×10^{-3}	---	---
8	26.20	82.00	60.96	94.69	10 x 5	1.3449	0.8635	1.74×10^{-4}	7.599×10^{-4}	8.849×10^{-3}	---	---
9	0.00	8.00	60.96	94.69	5 x 5	1.4820	1.0340	2.33×10^{-4}	3.140×10^{-3}	6.406×10^{-3}	---	---
10	0.00	8.00	94.69	94.69-170.89	varies	1.3200	0.8335	1.60×10^{-4}	2.260×10^{-4}	9.375×10^{-3}	---	---
11(Al.rod)	0.00	8.00	94.69-170.89	170.89-240.82	varies	1.3887	0.9162	1.95×10^{-4}	1.606×10^{-3}	7.996×10^{-3}	---	---
11(S.S.rod)	0.00	8.00	94.69-170.89	170.89-240.82	varies	1.1490	0.7345	1.303×10^{-3}	2.179×10^{-2}	8.061×10^{-3}	---	---
12	0.00	8.00	170.89-240.82	240.82	varies	1.2684	0.8070	4.49×10^{-4}	6.072×10^{-3}	9.064×10^{-3}	---	---

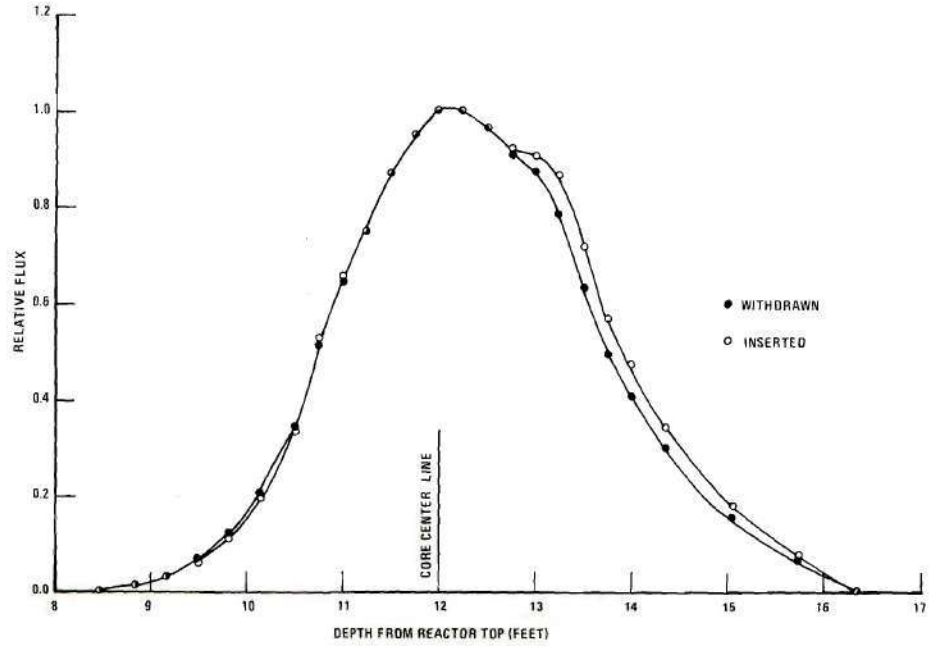

Figure 30. Analytical Flux Distributions in V-10 for the Aluminum Control Rod Withdrawn and Inserted.

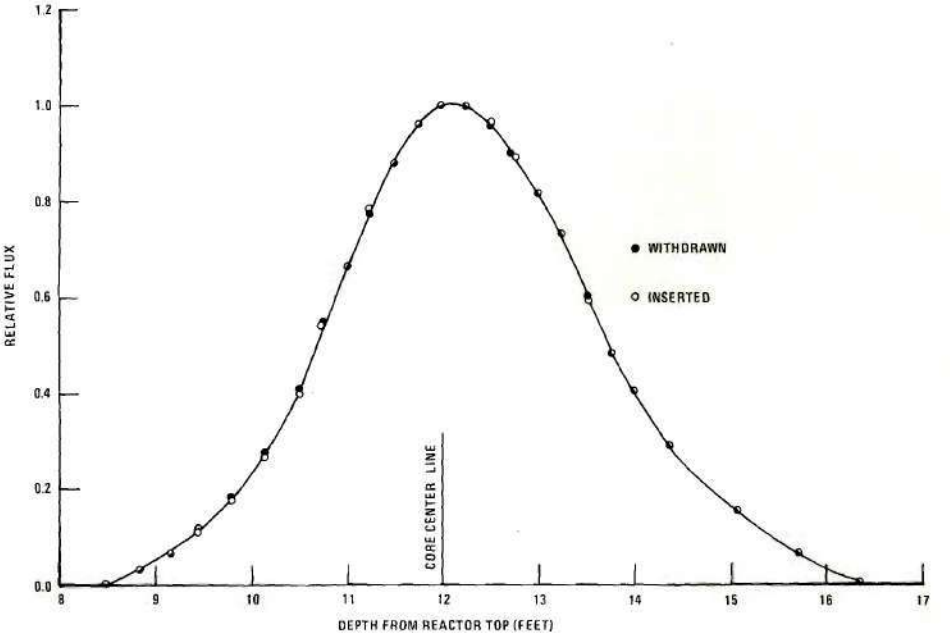

Figure 31. Analytical Flux Distributions in V-18 for the Aluminum Control Rod Withdrawn and Inserted.

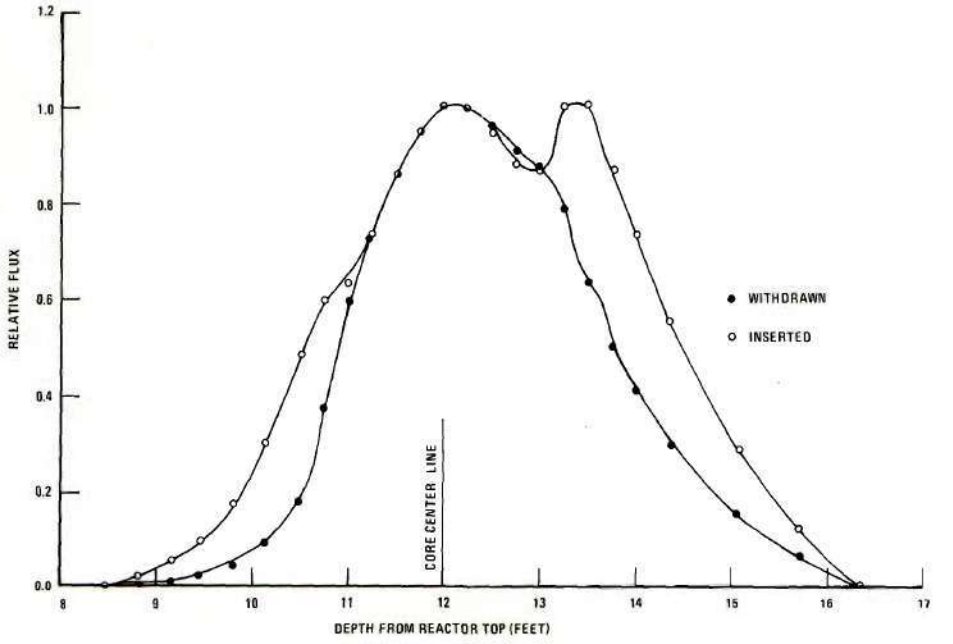

Figure 32. Analytical Flux Distributions in V-10 for the Stainless Steel Control Rod Withdrawn and Inserted.

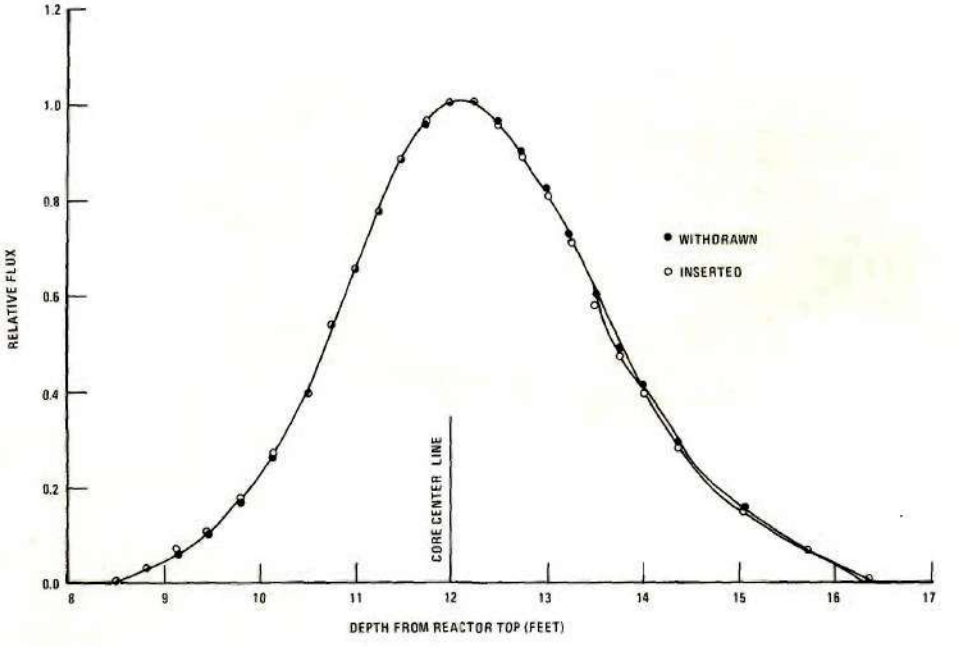

Figure 33. Analytical Flux Distributions in V-18 for the Stainless Steel Control Rod Withdrawn and Inserted.

improved. Figures 34 and 35 give the analytical radial flux shapes through the core mid-plane. These can be compared with the tabular radial measurements in Table 2.

All kinetics predictions were made with the 17-fuel-element, fixed-radius model. The mathematical controls were varied from run to run, but were held constant for each run. These parameters are tabulated in Appendix C.

Some of the kinetics parameters were different for each simulation while others were uniform for all runs. The velocity of the thermal group was taken as 2.2×10^5 cm/sec while that of the fast group was set at 2.08×10^8 cm/sec.

The delayed neutron parameters which were taken from the work of Graham[37] on the GTRR are given in Table 9. Graham's work discussed in detail the difficulties of obtaining sets of precursor constants applicable to the GTRR. Since the GTRR is a heavy-water moderated reactor, one has both delayed neutrons produced directly from fission product decay and photoneutrons produced indirectly through gamma-neutron reactions in deuterium. Approximately 15 percent of the delayed neutrons are photoneutrons. The photoneutron groups are indicated in Table 9. The theory, given in Chapter IV, states three assumptions made concerning the precursors. It was assumed that the delayed neutron precursors are produced at the instant of fission. Actually the precursors, whether photoneutron or other, may be the result of complicated disintegration chains. Typically, the decay producing the delayed neutron is characterized by a time

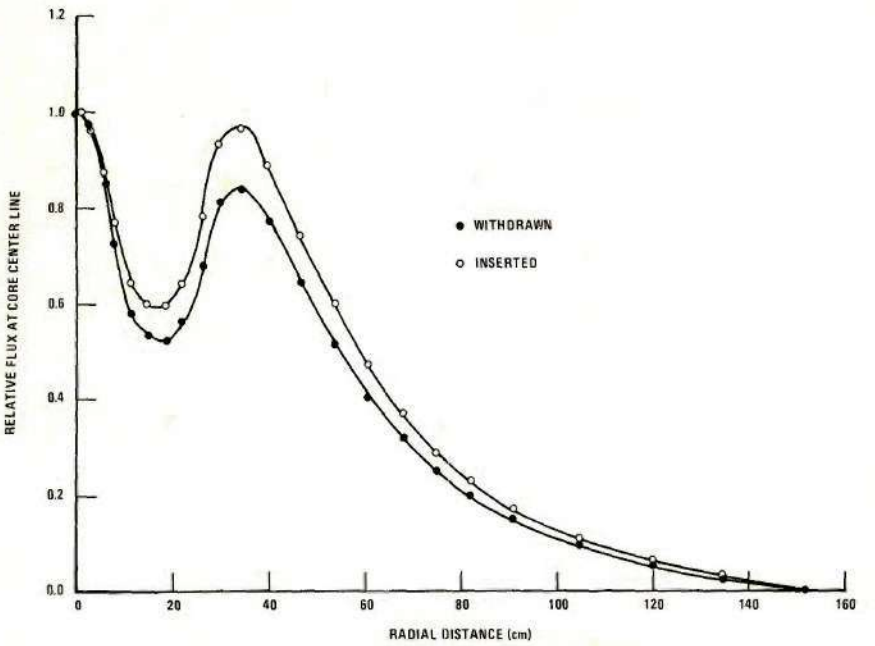

Figure 34. Analytical Radial-Flux Distributions for the Aluminum Control Rod Withdrawn and Inserted.

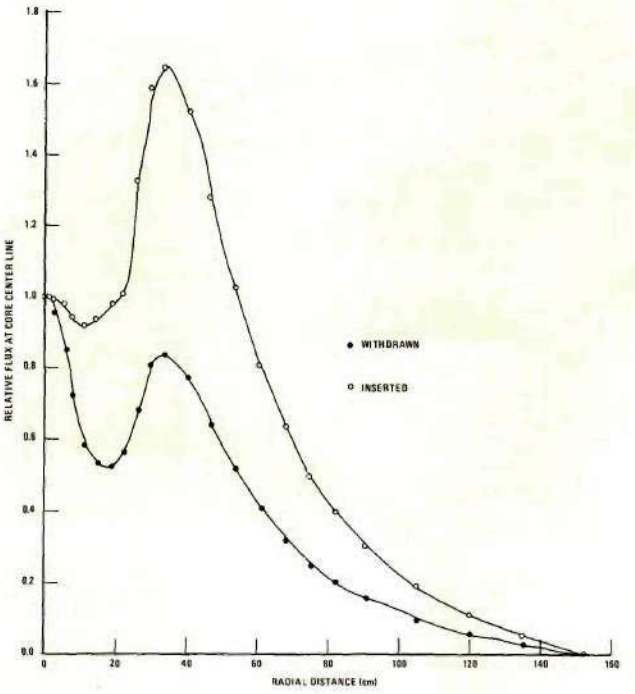

Figure 35. Analytical Radial-Flux Distributions for the Stainless Steel Control Rod Withdrawn and Inserted.

Table 9. Delayed Neutron Parameters--GTRR Eight-Group Set

Group	β_ℓ	λ_ℓ
1	4.741×10^{-3}	2.37×10^{-1}
2**	2.356×10^{-3}	3.33×10^{-2}
3	3.692×10^{-4}	8.33×10^{-3}
4	2.628×10^{-5}	8.89×10^{-4}
5	1.676×10^{-5}	3.03×10^{-4}
6	2.418×10^{-5}	1.09×10^{-4}
7*	3.010×10^{-6}	4.54×10^{-5}
8*	1.140×10^{-5}	5.94×10^{-7}

*Photoneutron parameters

**Mixed group, approximately 30% photoneutron

constant much longer than that leading to the production of the precursor and thus this assumption is generally valid. The assumption that the delayed neutron precursors of a single group decay with a single decay constant is valid for any single precursor, but the groups as given in Table 9 lump together precursors of approximately the same decay constants. This is necessary since the individual precursors are not always known and since experimental resolution of these constants is not sufficient to separate the data into the parameters of the individual precursors. The final assumption was that the delayed neutron is produced at the same spatial location that the precursor was produced. This assumption involves little approximation for the non-photoneutrons. The photoneutrons, however, are produced by gamma emission, and thus are created at some location distant to the production of the precursor. The mean free path of 3 MeV gamma rays in D_2O is approximately 25 cm; therefore, this assumption loses validity. Fortunately, the abundance of photoneutrons is small compared to that of the other delayed neutrons. Additionally, the model developed in this Chapter distributes the fuel over an 8 cm radius so that this weakness is less pronounced for this model than for more spatially-detailed ones.

These assumptions often complicate the choice of a single set of space-independent delayed neutron parameters to use in a simulation. Fortunately the parameters used in Table 9 are obtained from measurements on a 13-fuel-element GTRR core which is similar to the actual experimental configuration. The choice of the delayed neutron parameters to use in simulations for which there are no experimentally measured β's and λ's is discussed in reference 37.

Calculations

Each of the ten experiments were simulated with space-time and adiabatic calculations. Appendix C reports these results in tabular form. Figures 36 and 37 are plots of the simulations of the experiments shown in Figures 25 and 26. Comparisons between the figures shows reasonable agreement. Chapter VI contains more comparisons between analysis and experiment.

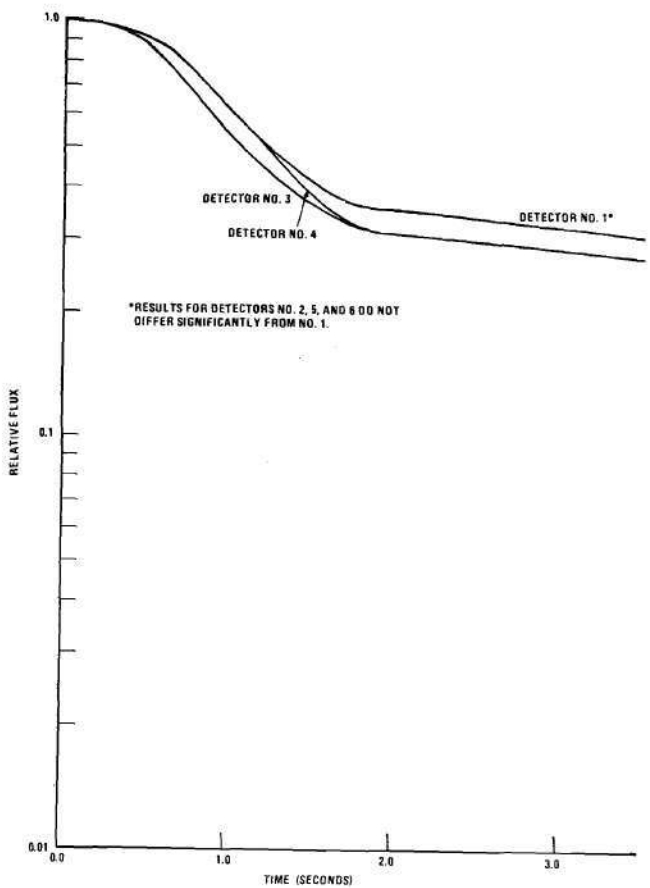

Figure 36. Graphic Results of the 2.2 Second Aluminum Control Rod Experiment Simulation.

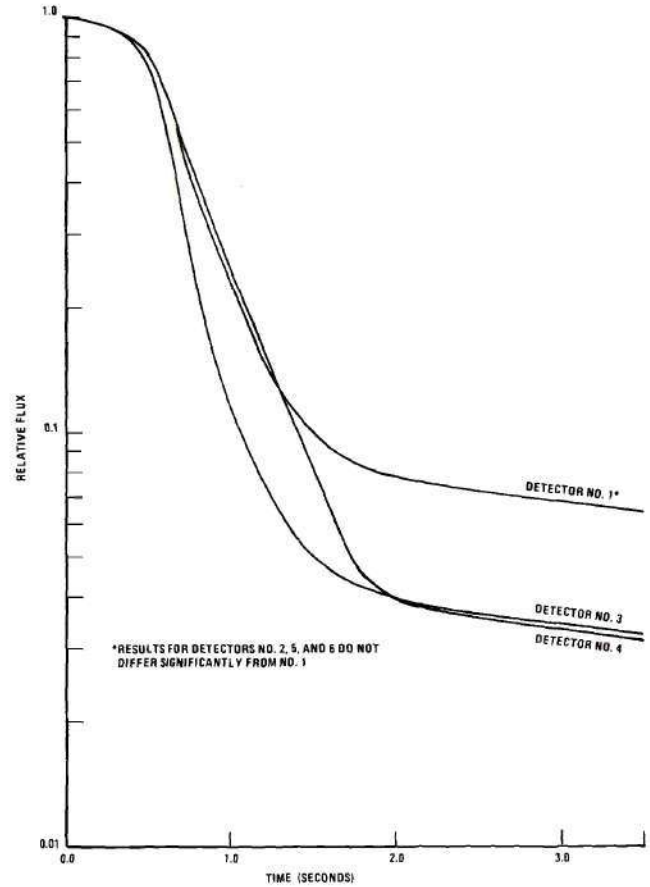

Figure 37. Graphic Results of the 2.2 Second Stainless Steel Control Rod Experiment Simulation.

CHAPTER VI

CONCLUSIONS AND RECOMMENDATIONS

Experimental measurements and analytical calculations were presented in earlier chapters. This chapter compares theory with experiment, draws conclusions, and makes recommendations.

Kinetics calculations can only be as good as the statics model permits. The statics model can be broken down into its ability to predict (1) flux distributions and (2) reactor multiplications. The previous chapter examined the differences between the calculated and measured static flux traversals. A simple comparison of the spatial differences between the kinetics calculations and the experiment is shown in Figure 38. This figure graphically displays the analytical and experimental ratios of the fractional changes of detectors three and four to detector five for experiment five. The other stainless steel experiments give similar results, leading one to conclude that the dominant effect demonstrated here is due to changes in the equilibrium flux distribution at any depth of rod insertion. Hence, these curves have their shape derived more from the statics model than from the kinetics. Discrepancies in the spatial distributions produced by the kinetics code can thus be traced to the inability of the homogeneous statics model to accurately simulate the heterogeneous GTRR.

Another test of a statics model is its ability to predict reactor multiplication. Unlike flux distributions, reactor multiplication, k_{eff},

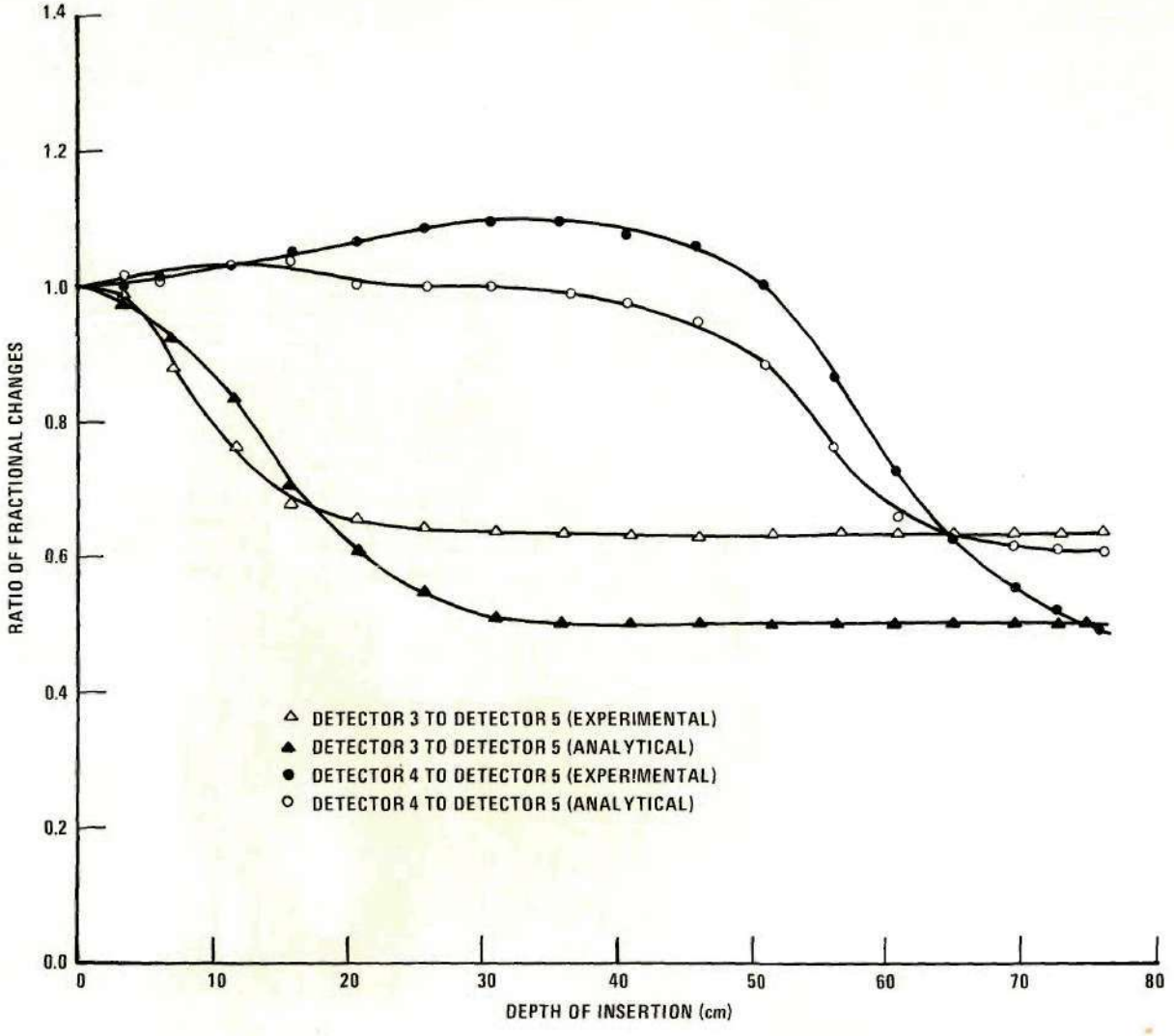

Figure 38. Ratio of Fractional Flux Changes Versus the Depth of Insertion for Experiment 5.

cannot be measured directly but must be inferred from kinetics measurements. By assuming point reactor kinetics and that the flux between any two points in time is described by a single exponential function, rod worths can be calculated from measurements of flux versus time. The experimental worths, $(k_{eff}-1)/k_{eff}$, of the two control rods were obtained from inverse kinetics calculations based on a program similar to RE-129.[38] This program was written in FOCAL and run on a PDP-8I computer. The flux at detector five was used for the inverse kinetics calculations because analysis indicated that, of all the detectors, detector five most closely followed the reactor's volume-averaged flux. Figures 39 and 40 show both the results of the inverse kinetics calculations and the theoretical worths for the aluminum and stainless steel control rods. It can be seen that the experimental (inverse kinetics) worth of the aluminum rod is generally greater than that predicted, while that of the stainless steel rod is initially greater and eventually less.

Figures 41 and 42 show the ratio of space-time analysis to experiment results at detector five for various experiments. The simulations for the aluminum control rod indicate that less change is predicted than was measured. Since the amount of change is dependent on the worth of the control rod, these curves demonstrate, in a qualitative way, that the theoretical worth of the aluminum control rod is too low. This conclusion is consistent with that drawn through inverse kinetics arguments without making the simplifying assumptions of an inverse kinetics model. Figure 42 shows that analysis of a stainless steel control rod experiment initially predicts too large a change, then not enough, and finally too much.

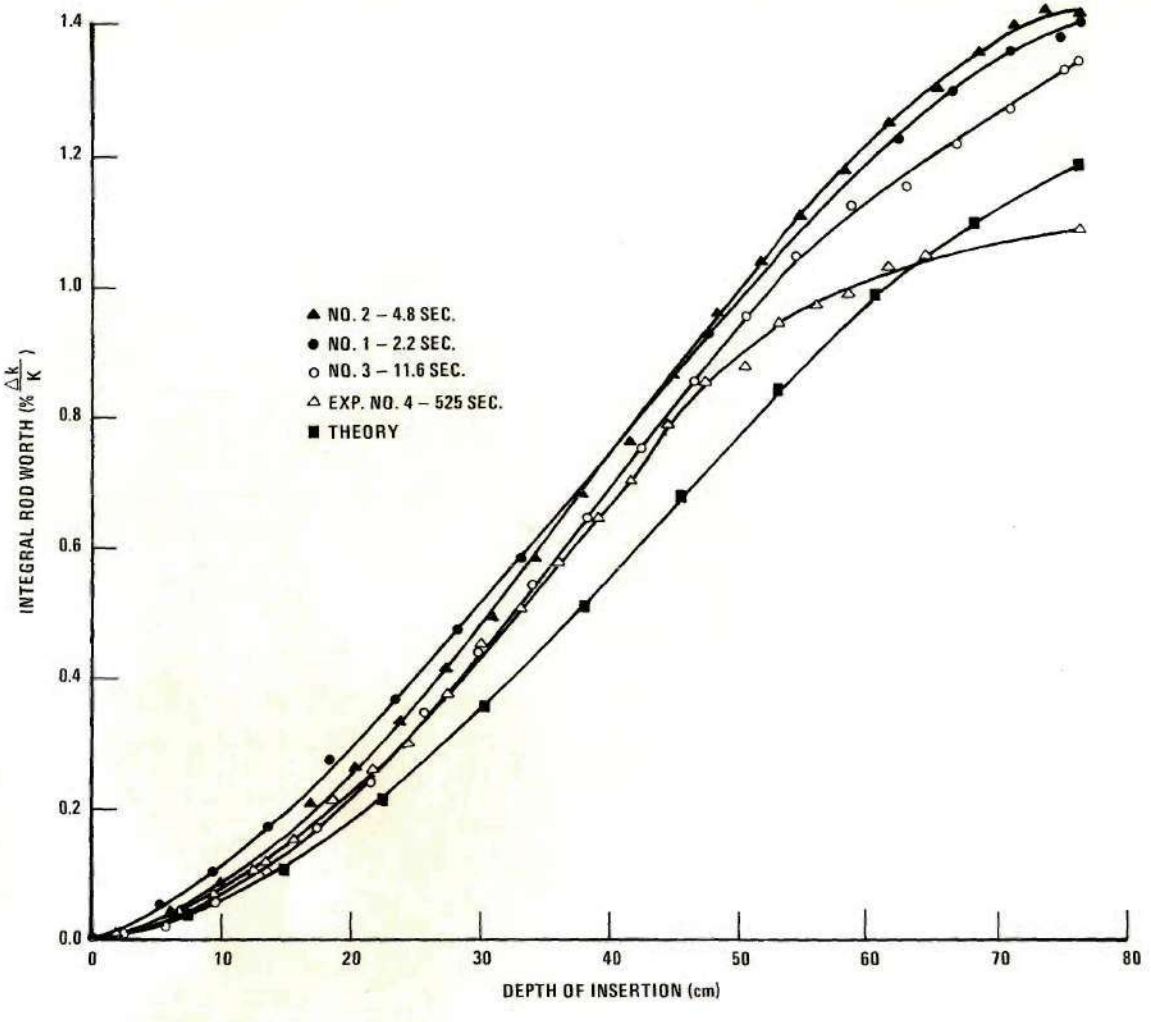

Figure 39. Experimental and Theoretical Worths of the Aluminum Control Rod.

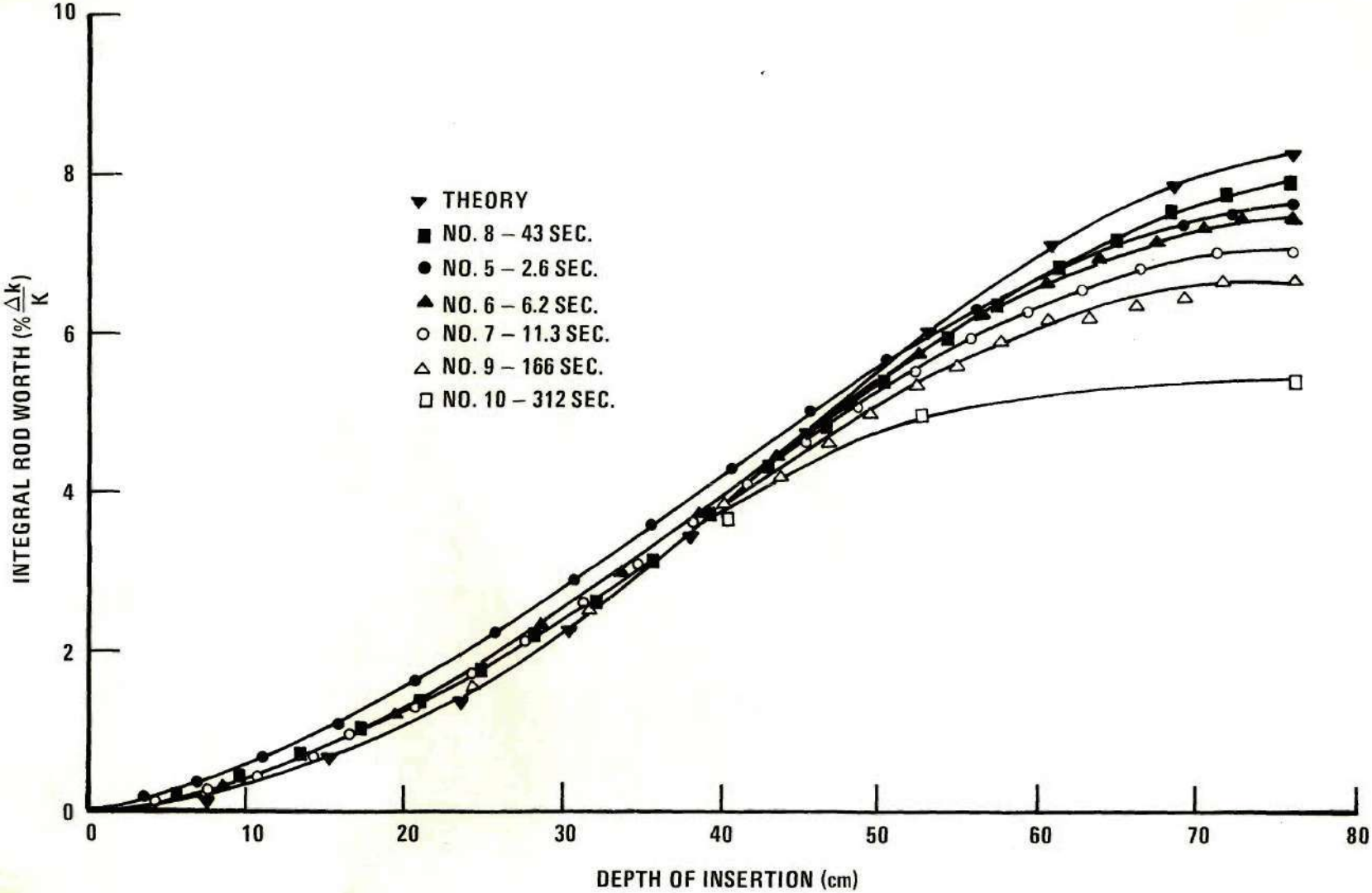

Figure 40. Experimental and Theoretical Worths of the Stainless Steel Control Rod.

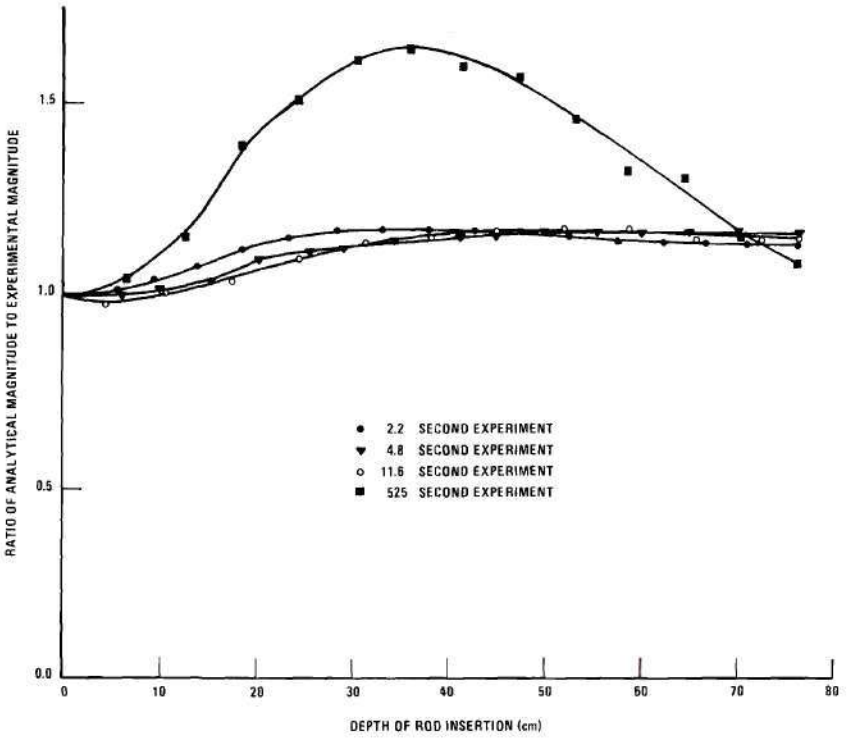

Figure 41. Ratio of Analytical Calculations to Experimental Results for the Aluminum Control Rod.

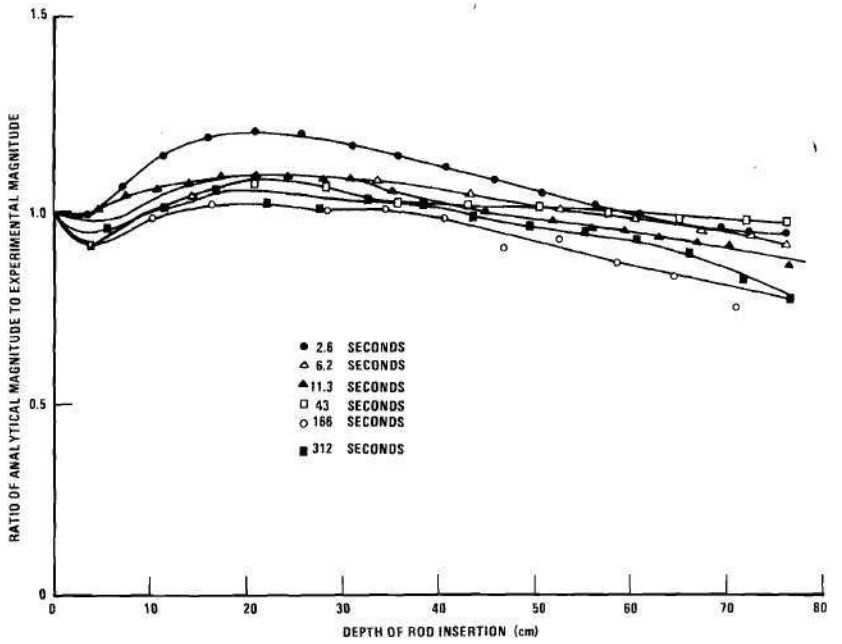

Figure 42. Ratio of Analytical Calculations to Experimental Results for the Stainless Steel Control Rod.

As with the aluminum control rod, this indicates that the analytical worth of the stainless steel control rod is initially too large, then too small and finally too large. The worths shown in Figure 40 support the last two conclusions, but not the initial effect of too large a reactivity worth. Examination of Figure 42 suggests that the initial over-approximation of the worth occurs only over the first five cm of control rod. This is explained by the way in which the kinetics model simulates the movement of the control rod between grid points, the first of which is located at a depth of insertion of 7.6 cm. Whenever the bottom of the control rod is between grid points, an artificial region is created which consists of a volume-weighted average of the control rod region and the moderator and shroud region. When the bottom of the control rod is above the core mid-plane, this results in an artificially increased rod effect because homogenization reduces self-shielding and also places some control material in regions of higher importance. These effects are not as significant for aluminum and were therefore present to a lesser extent.

Since the discrepancies between analysis and experiment are explained by the inability of the statics model to predict very accurate reactor multiplications, more accurate kinetics predictions would result from a better statics model, and a more accurate weighting scheme for the "between grid" control rod positions. It should be noted that a simple change in the absorption cross section for the aluminum control rod would likely produce good agreement between analysis and experiment, but that such a simple correction would not likely produce the more complicated correction required for the stainless steel control rod.

An objective of this thesis was to compare adiabatic and space-time methods. Chapter V reported calculations based on space-time and adiabatic models for the six detector locations. By examining the ratios of these six results to each other for the adiabatic and space-time calculations, it can be determined that the spatial shape, as represented by these six points, differs little between the two methods. Nevertheless, values of the fractional changes as given in Appendix C differ surprisingly for the two methods. Figure 43 is a graph of the maximum ratio of the adiabatic predictions of the flux at detector five to the space-time ones versus the time required for insertion. There are significant differences for faster insertions; however, these differences diminish for longer insertions. This underscores the conclusion that small spatial differences can lead to large disagreements in adiabatic calculations. Additionally, the space-time calculations agree better with experiment than the adiabatic calculations. The kinetics code was subsequently run treating the fast group adiabatically and the thermal group with space-time approximations. There were no significant differences between these runs and the purely space-time runs. This suggests the feasibility of performing many-group, two-dimensional calculations economically. It is recommended that this experimental and analytical work be extended to faster reactivity-insertion rates in order to produce more dramatic magnitude and spatial effects.

In addition to these general conclusions there are a number of specific observations which can be made.

The inverse kinetics results shown in Figures 38 and 39 demonstrate

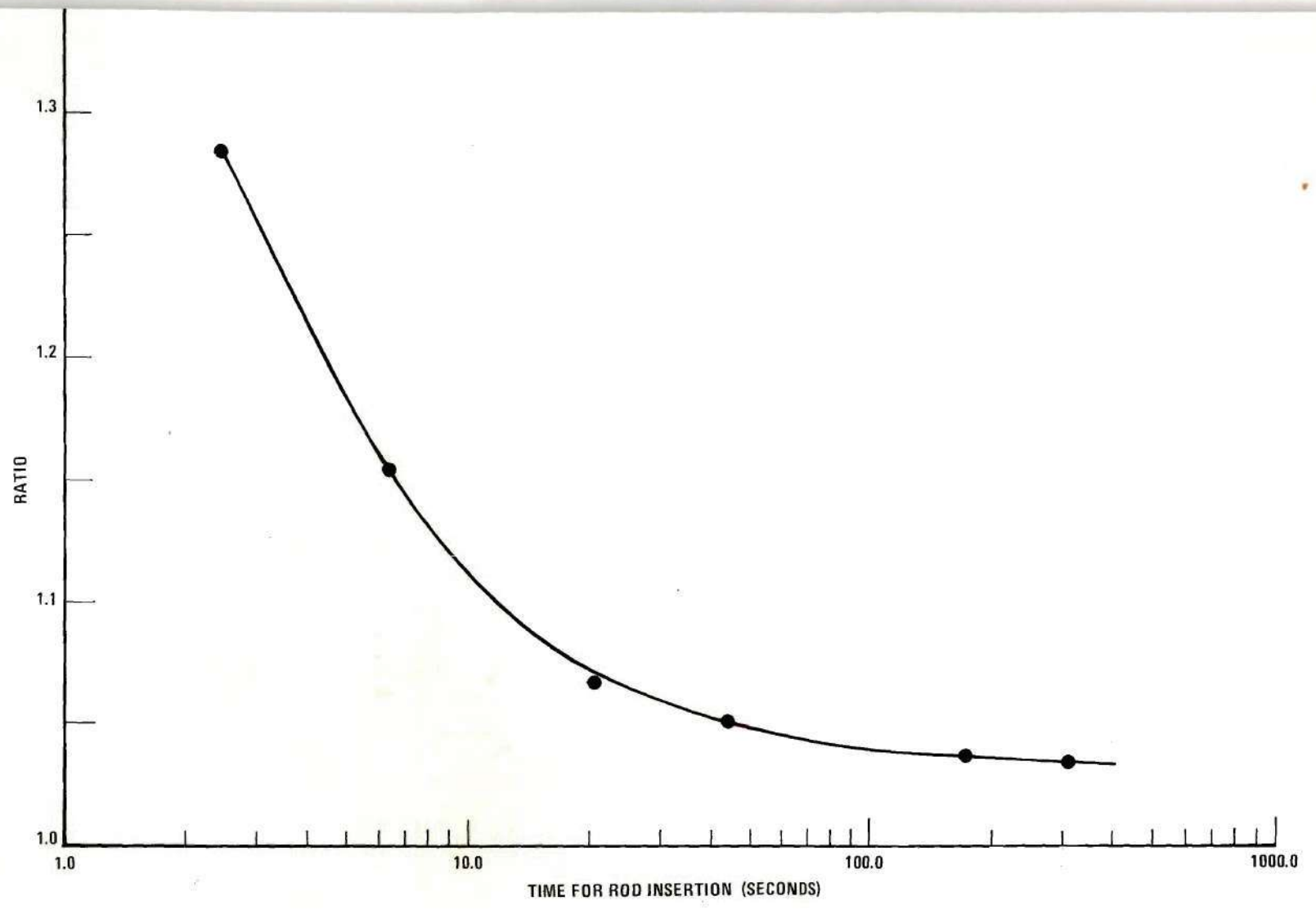

Figure 43. Maximum Ratio of the Space-Time Solution to the Adiabatic Solution at Detector 5 for Different Times of Rod Insertion.

that this control rod calibration technique works fairly well over different worths and rates of insertion.

Several observations on the experimental system are relevant. In general, the automated data acquisition worked so smoothly that encouragement would be given to expanded interaction between computerized systems and reactor operation. Additionally, the control rod and hydraulic drive performed flawlessly throughout the experiment. It is recommended that future work incorporate control rod operation under computer control for the production of predetermined power vs. time profiles.

Other observations are concerned with the detector system. The power calibrations of the non-gamma compensated chambers with the gamma-compensated reactor detector illustrate that in-core detectors without gamma-compensation are useful at power levels as low as 100 watts. It is recommended that gamma detectors be obtained to investigate the applicable power range in greater detail. The response of the detectors and comparison with theory conclusively demonstrate that the power monitors more accurately measure the power when they are in reflector regions. Finally, the experiments with the six detectors gave an indication of the distances a local perturbation will be propagated. Figure 38 demonstrates that local perturbations propagate only within about 10 cm in the GTRR. This distance is approximately 10 diffusion lengths.

The following underscore the four major conclusions of this research:

1. The use of homogeneous statics models to predict the flux distributions in heterogeneous reactors requires the consideration of not

only the physical dimensions but also of the reactor material in which the measurements are performed; thus models such as the fixed-radius, variable-composition one discussed in Chapter V may be necessary for reasonable prediction of the experimental situation.

2. The kinetics analyses produced results generally agreeing with experiment over wide ranges of perturbation magnitude and rate; however, very accurate predictions of experiment would require a geometrical model having a reactor multiplication, for all configurations, very close to that of the experimental assembly.

3. For high rates of insertion, the adiabatic results differ significantly from the space-time ones, even though the adiabatic spatial assumption is reasonably accurate.

4. The treatment of the thermal group with space-time methods and the fast group with adiabatic methods produces results in agreement with those obtained using the more costly space-time calculations for both groups. Thus, mixed methods may increase the number of energy groups which can be economically represented while retaining the superior accuracy of the space-time method in critical energy groups.

APPENDICES

APPENDIX A

DESCRIPTION OF THE HYDRAULIC DRIVE

The hydraulic drive provides the motive force for the control rod. A schematic of the system is shown in Figure 10. The symbols are defined in reference 27. Photographs of the system are shown in Figures 11 and 12. For reasons of safety, the primary requirement of the system is to maintain the rate of withdrawal of the control rod to less than 0.03 inch per second. In addition, the failure of any single component, the failure of any combination of hydraulic lines leading to the hydraulic piston, or pressure changes in the system must not increase the rate of withdrawal. Capability for providing various rates of insertion is the main experimental consideration. The system developed provides this capability. The individual components will be described and then the various operational states of the system will be discussed.

The key to the hydraulic system is the four-way valve. It has four ports; one port is connected to a supply of oil and another is connected to the system reservoir. The oil supply comes from a fixed displacement pump driven by a 110v, two horsepower motor. The pump forces oil through a check valve to prevent damage to the pump from feedback of a system overload into the pump. The oil then flows through a pressure relief valve which can be adjusted for a system pressure up to 800 psi. The pressure relief valve supplies enough oil to the system to maintain the set pressure and dumps the remainder to the reservoir. Gauge G1 measures

the system pressure. That oil directed through the four-way valve is sent through a full-flow high-pressure filter in order to prevent clogging in the very small withdrawal orifices. Whenever solenoid A is energized, the oil supply is connected to line L2 and the reservoir is connected to line L1. Whenever solenoid B is energized, the oil supply is connected to line L1 and the reservoir is connected to line L2. When neither is energized the ports from the oil supply and reservoir as well as L1 and L2 are blocked shut.

Attached to the hydraulic unit on line L1 are two flow control valves and guage G2. The flow control valves are each free-flow in one direction and regulate flow in the other direction. Flow control valve V1 is free-flow out of the four-way valve and regulated into it. Flow control valve V2 is free-flow into the four-way valve and regulated out of it.

Valve V2 is pressure compensated and used to regulate the withdrawal rates. It is adjusted to the correct value and locked in position. When solenoid B is energized the difference between the pressure indicated by G1 and G2 is the pressure drop across V2. When solenoid A is energized gauge G2 reads the pressure drop across valve V1. A hose H1 leads from G2 to the bottom of the hydraulic cylinder.

Line L2 branches into two paths. The simplest one contains a manually operated valve V3, a guage G3, and a flow control valve V4. Valves V3 and V7 will isolate the hydraulic cylinder from the hydraulic pump unit when closed. Valve V4 is constructed like valve V1, is free-flow toward the four-way valve, and is regulated in the other direction. When solenoid

A is energized, G3 indicates the system pressure; when solenoid B is is energized, it reads the pressure drop across V3. A hose H2 extends from V4 to the top of the hydraulic cylinder.

The other branch for L2 controls the pilot operated check valve. This valve is opened when pressure is allowed in hose H3, and closed when this pressure is removed. The check valve in this line forces any drainage to flow into the reservoir. The manual valve V5, when closed, maintains the pilot operated check valve in its last state. The normally open solenoid valve A' is closed only when solenoid A is energized. This valve allows H3 to drain to the reservoir. When valve V5 is open and solenoid A is energized, valve A' closes and forces pressure to be diverted through hose H3 to open the pilot-operated check valve. Any other combination drains H3 to close the pilot-operated check valve. Hose H4 serves as a leak drain from the pilot operated check valve to the reservoir.

The only additional equipment on the hydraulic pump unit is the accumulator, solenoid valve A'', a check valve, and manual valve V7. The accumulator is simply a cylinder with an enclosed free piston. Nitrogen gas is trapped on one end and oil forced into the other end. The oil, under pressure, compresses the gas. Whenever the system pressure decreases, the gas forces oil into the system. For a system pressure of 500 psi the one gallon accumulator is about half full of oil. Normally-closed solenoid valve A'' opens when A is energized, permitting the accumulator to dump its oil into manual valve V7. If V7 is open, oil flows through hose H5 to the top of the hydraulic cylinder. If valve V7 is closed, no oil from the accumulator can flow through H5, but it can feed back through the four-way valve. The check valve prevents flow bypassing valve V8 on

withdrawal. This equipment, located on the hydraulic pump unit is connected to the hydraulic cylinder by five hoses 40 feet long.

The hydraulic cylinder has a 3 1/4 inch bore, a one-inch-diameter piston rod, a 30-inch stroke, and is slightly cushioned on the bottom end. At the bottom end there is the hose H1 and a 1/2 inch regenerative tube leading through manual valve V6 and the pilot-operated check valve to the head of the cylinder. The manual valve can be used to block the regenerative flow. The pilot-operated check valve is free-flow from the head of the cylinder to the bottom and blocked in the reverse direction. Whenever pressure is applied to the pilot line H3 a piston in the valve is forced up, opening the valve to flow in either direction. The drain line H4 from this valve simply collects any leakage from the pilot line H3 past the opening piston. The valve opens quickly, but requires about 1/4 second to close.

Gauge G4 and hose H5 from the accumulator enter at the top of the cylinder. Immediately above this point flow control valve V8, identical to valve V2, regulates the oil flow out of the cylinder, but is free flow into the cylinder. Valve V8 must be adjusted and locked like valve V2. Hose H2 is connected to this valve. When solenoid B is energized, the difference in pressure between G3 and G4 is the drop across valve V8. Valves V8 and V2 are adjusted so that the required withdrawal rate is obtained and so that the pressure drop across each of them is the same.

There are four modes of operation of the hydraulic system. Withdrawal of the hydraulic rod is straightforward. Solenoid B is energized, sending oil through L1. Valve V1 is free-flow for oil in this direction

and V2 regulates the rate of oil going into H1. The pilot-operated check is closed, forcing the oil into the bottom of the cylinder and consequently withdrawing the piston rod. Withdrawal of the piston rod forces oil through V8 which also regulates the rate of flow. The oil returns to the reservoir through H5, since V4 is free-flow in this direction. Note that the flow of oil is doubly regulated and that, since the regulating valves are pressure compensated, the failure of either will not change the rate of withdrawing the piston rod.

The simplest method of inserting the rod is to use the non-regenerative cycle. Valves V6 and V7 are closed, and valves V3 and V4 are opened. Valve V1 is set to give the desired rate of insertion. Solenoids A, A', and A" are energized. This causes oil to flow freely through L2, V3, V4, H2, and V8 into the top of the hydraulic cylinder. The cylinder moves down, forcing oil through H1 and V2. The oil's only non-friction restriction is encountered in V1 which has been adjusted to give the desired rate. In this mode the system inserts the rod from a rate of 0.03 inch per minute to 2 1/2 inches per minute.

Another mode of operation of the system is the controlled regenerative cycle. Valve V6 is opened while valves V7 and V1 are closed. Valve V4 is adjusted to give the desired rate of insertion. Oil is forced into L2, restricted by V4 and sent through H2, bypassing V8, into the top of the cylinder. Pressure is also applied to H3 opening the pilot-operated check valve. Since valve V1 is closed, oil cannot flow into H1. The result is that oil flows from the bottom of the cylinder, through the regenerative line into the top of the cylinder. This is possible because

the piston rod extends, creating volume into which the oil can flow. In order to extend the rod, only a volume of oil equal to the volume of the piston rod needs to be pumped into the cylinder. In the non-regenerative cycle, the volume of oil needed for full extension is equal to the volume of the cylinder, thus faster insertions are possible with the regenerative cycle. The rates of insertion for the regenerative mode vary from three inches per second to 15 inches per second.

The final mode of operation is the uncontrolled regenerative cycle. The valve settings are as before except V4 is fully open, as is V7. In this mode, the accumulator dumps its oil directly into the head of the cylinder, without valving restrictions. This mode produces the fastest insertion; however, the increase in speed is too small to justify using this method.

APPENDIX B

RESULTS OF THE KINETICS EXPERIMENTS

This appendix contains the tabular presentation of the ten experiments discussed in Chapter III. The initial flux values can be obtained from the static flux distributions given in Chapter III; the reactor's power history can be represented as a histogram. Because of the short half-life of most of the delayed neutron precursors, only the power history on the day of the experiment was recorded. The reported experiments were performed on four different days. Figures 44 through 47 give the applicable power histories.

The output of the data analysis program described in Chapter III and run on the Univac 1108 is reported in Tables 10 through 19. The tables report the depth of the control rod and the ratios between the current from a detector to the current from that detector at the start of the control rod's insertion versus the time from the start of the insertion. The experiment numbers are defined in Table 4; the detector numbers are defined in Table 3.

The total error in the fractional changes tabulated in this appendix is the result of both systematic and random errors. Systematic errors include nonlinear detector response, non-logarithmic electrometer output and gamma background. The miniature ionization chambers produce a current which is linear with flux level up to 50 kW. Above this power level the detectors become nonlinear because recombination and space charge

effects prevent collection of all ion pairs produced by neutron reactions in the sensitive volume. Furthermore, in the low power region, response is nonlinear due to a low level gamma background. Also, the logarithmic element in the electrometers becomes non-logarithmic at currents corresponding to power levels higher than 50 kW. The errors in the detectors and the electrometers tend to off-set each other since, at high power levels, the detectors produce less current than they would if all ion pairs were collected, while the electrometers produce a voltage larger than they would if the amplifier circuit operated in a completely logarithmic fashion. These systematic errors imply an uncertainty in the actual neutron levels; however, discounting random errors, a given neutron level will result in a particular voltage output, i.e., the voltage output at any power level is reproducible. Thus, a calibration of voltage output versus power, as measured with a detector not having these stated systematic errors, can be used to compensate for the systematic errors.

The non-systematic errors include random fluctuations in the number of neutrons around a detector, noise in the electrometers, and variations in the sample-and-hold signal to the ADC of the computer.

The relative flux is determined by recording versus time the log response of the detectors as measured with the ADC. These numbers are converted to power levels by logarithmically interpolating between calibration points which tabulate for each detector the log response versus power level as determined with the GTRR's linear power monitor. The error in a flux measurement is then the result of an error in a log measurement as operated on by a calibration which may also be in error.

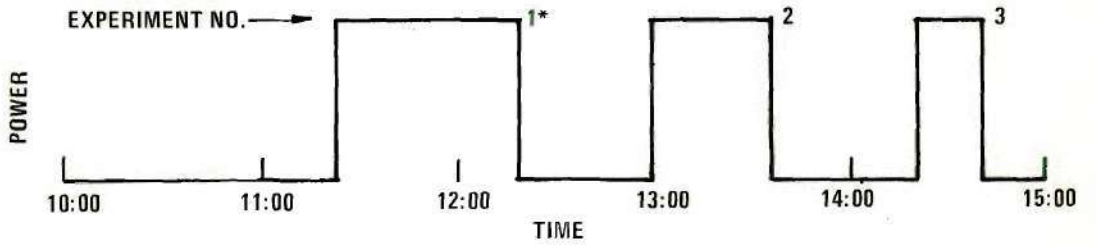

Figure 44. Power Histogram for July 1, 1971.

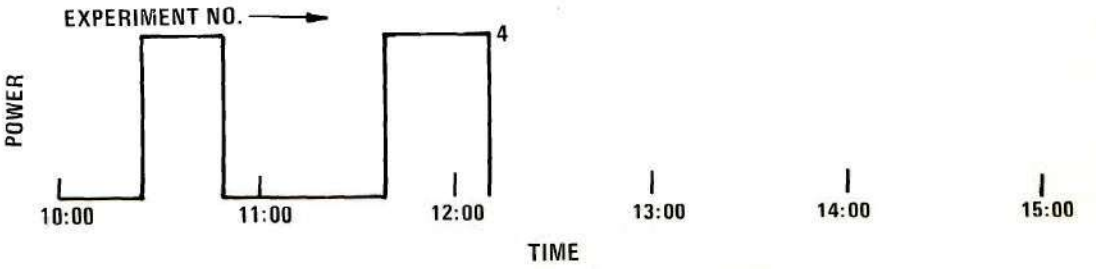

Figure 45. Power Histogram for July 2, 1971.

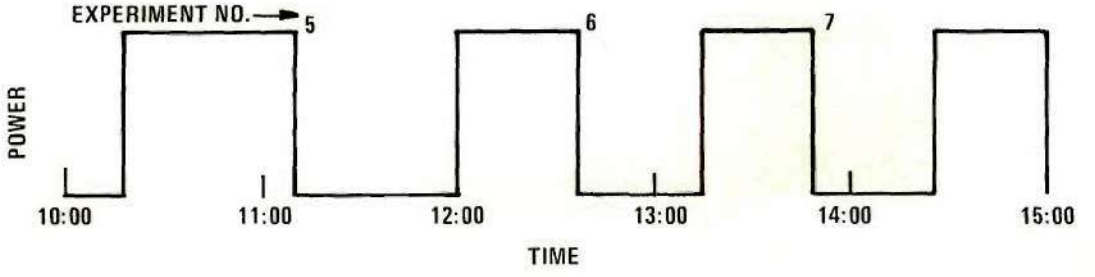

Figure 46. Power Histogram for July 15, 1971.

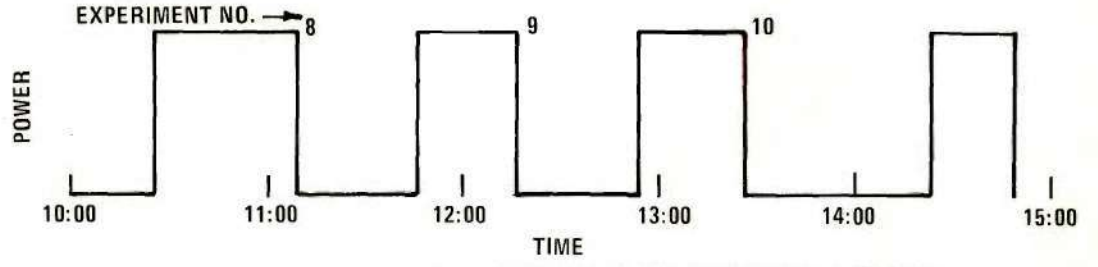

*THE POSITION OF THE EXPERIMENT NUMBER INDICATES THE TIME AT WHICH THE EXPERIMENT WAS STARTED.

Figure 47. Power Histogram for July 16, 1971.

The error in a relative flux measurement is that error in a flux measurement plus the error in determining the initial flux.

The error in determining a current from a detector which is operating in either the linear or log mode is the combination of the errors in neutron fluctuations, electrometer uncertainties, and sample-and-hold error. The first two of these errors are Gaussian, each with standard deviations less than 0.1 percent. The last error is not Gaussian; however, for a constant precise voltage input, 63 percent of the digital results are within four units of the average value irrespective of the level of the voltage. For these experiments, the digital results varied from 500 at 100 watts to 3500 at 100 kW; thus, the errors in the sample-and-hold ADC system are less than 0.8 percent. Combining this with the previously discussed neutron and electrometer standard deviations yields an error in determining a non-calibrated flux level of less than one percent.

The error in the flux level as determined with a linear scale depends on the digital output since it is the ratio of a fixed uncertainty to a decreasing average value, but it is also less than one percent.

The error in a calibration point, i.e., a simultaneous measurement of a log measurement from a detector and the measurement of power with the GTRR linear power channel is a combination of errors in the log and linear measurements.

Assuming an error in a log reading of one percent and a calibration reference standard with similar error, one obtains a flux in error by five percent. The factor of five is attributable to the decreased sensitivity of a five decade log scale over a linear scale. The relative

flux has an associated error of 10 percent since it is a ratio of two numbers, each having five percent error.

The relative flux distributions were measured by current meter observations and have an error of five percent as determined by the precision of visual data recording over the least sensitive portion of the scale.

Table 10. Representative Results of Experiment 1.
A 2.2 Second Aluminum Control Rod Insertion

Time (sec)	Depth (cm)	Fractional Changes for Detectors					
		1	2	3	4	5	6
.0	.0	1.0000	1.0000	1.0000	1.0000	1.0000	1.0000
.1	1.3	1.0196	1.0131	1.0013	1.0037	1.0000	.9980
.2	2.4	1.0063	.9955	.9815	.9887	.9856	.9917
.3	5.4	.9851	.9683	.9404	.9577	.9546	.9708
.4	9.3	.9348	.9340	.8786	.9203	.9112	.9370
.5	13.8	.8894	.8860	.7815	.8485	.8547	.8912
.6	18.5	.7477	.7871	.7083	.7881	.7760	.8350
.7	23.4	.6779	.7120	.6391	.7123	.7074	.7713
.8	28.3	.6109	.6421	.5867	.6437	.6424	.7061
.9	33.1	.5602	.5838	.5331	.5851	.5829	.6428
1.0	38.0	.5101	.5335	.4866	.5342	.5304	.5853
1.1	42.8	.4597	.4882	.4444	.4909	.4856	.5351
1.2	47.7	.4280	.4498	.4112	.4488	.4474	.4914
1.3	52.5	.3993	.4193	.3810	.4089	.4150	.4547
1.4	57.3	.3716	.3926	.3552	.3730	.3906	.4247
1.5	62.3	.3520	.3671	.3349	.3445	.3680	.3998
1.6	66.7	.3301	.3464	.3182	.3234	.3491	.3789
1.7	71.0	.3165	.3299	.3040	.3083	.3349	.3622
1.8	74.9	.3090	.3211	.2961	.2998	.3268	.3500
1.9	75.7	.3037	.3150	.2912	.2947	.3222	.3424
2.0	76.0	.3017	.3105	.2877	.2908	.3181	.3371
2.1	76.1	.2959	.3058	.2835	.2876	.3139	.3329
2.2	76.2	.2933	.3018	.2792	.2836	.3101	.3285
3.0	76.3	.2680	.2739	.2552	.2605	.2843	.3014
4.0	76.3	.2444	.2468	.2366	.2359	.2641	.2749
5.0	76.3	.2525	.2390	.2187	.2260	.2444	.2537
6.0	76.4	.2310	.2179	.2017	.2083	.2258	.2360
7.0	76.4	.2164	.2017	.1880	.1936	.2113	.2218
8.0	76.4	.2041	.1885	.1763	.1818	.1979	.2091
9.0	76.4	.1921	.1771	.1662	.1721	.1867	.1979
10.0	76.4	.1824	.1676	.1580	.1628	.1775	.1884
15.0	76.4	.1471	.1314	.1250	.1308	.1415	.1359
20.0	76.4	.1255	.1091	.1035	.1102	.1180	.1142
30.0	76.4	.0966	.0815	.0767	.0829	.0896	.0875
40.0	76.4	.0764	.0631	.0593	.0646	.0709	.0703
50.0	76.4	.0625	.0504	.0472	.0520	.0567	.0574
60.0	76.4	.0508	.0406	.0380	.0423	.0452	.0470
70.0	76.4	.0428	.0337	.0319	.0352	.0373	.0396
80.0	76.4	.0369	.0286	.0273	.0298	.0318	.0343
90.0	76.5	.0313	.0241	.0233	.0251	.0266	.0293
100.0	76.5	.0272	.0208	.0203	.0215	.0232	.0259

Table 11. Representative Results of Experiment 2.
A 4.8 Second Aluminum Control Rod Insertion

Time (sec)	Depth (cm)	Fractional Changes for Detectors					
		1	2	3	4	5	6
.0	.0	1.0000	1.0000	1.0000	1.0000	1.0000	1.0000
.2	2.0	1.0074	1.0016	.9862	.9907	1.0053	.9998
.4	6.1	.9625	.9643	.9371	.9504	.9635	.9671
.6	10.0	.9197	.9228	.8832	.9087	.9170	.9212
.8	13.5	.8843	.8938	.7967	.8692	.8758	.8766
1.0	17.0	.7835	.8412	.7317	.8016	.8026	.8303
1.2	20.4	.6951	.7344	.6707	.7438	.7458	.7781
1.4	23.9	.6478	.6802	.6214	.6863	.6929	.7261
1.6	27.4	.5983	.6287	.5778	.6346	.6427	.6747
1.8	30.9	.5510	.5822	.5372	.5885	.5947	.6242
2.0	34.4	.5084	.5390	.4976	.5455	.5479	.5772
2.2	37.9	.4702	.4997	.4593	.5056	.5046	.5333
2.4	41.4	.4446	.4664	.4266	.4736	.4693	.4936
2.6	44.9	.4074	.4346	.3962	.4399	.4346	.4578
2.8	48.3	.3810	.4045	.3701	.4060	.4034	.4258
3.0	51.7	.3569	.3799	.3454	.3781	.3790	.3986
3.2	55.0	.3338	.3550	.3253	.3516	.3577	.3757
3.4	58.4	.3231	.3349	.3077	.3260	.3396	.3555
3.6	61.8	.3039	.3150	.2918	.3040	.3220	.3379
3.8	65.1	.2885	.2991	.2776	.2866	.3074	.3222
4.0	68.4	.2781	.2849	.2661	.2719	.2947	.3089
4.2	71.6	.2628	.2718	.2544	.2599	.2831	.2963
4.4	74.4	.2546	.2621	.2462	.2507	.2747	.2874
4.6	75.3	.2506	.2571	.2410	.2464	.2693	.2807
4.8	76.3	.2481	.2529	.2364	.2425	.2652	.2772
5.0	76.2	.2457	.2477	.2319	.2380	.2606	.2725
6.0	76.2	.2519	.2437	.2195	.2181	.2498	.2571
7.0	76.2	.2368	.2254	.2028	.2141	.2318	.2400
8.0	76.2	.2215	.2094	.1899	.2001	.2155	.2225
9.0	76.2	.2056	.1933	.1772	.1861	.1986	.2039
10.0	76.2	.1969	.1834	.1678	.1777	.1882	.1917
15.0	76.2	.1568	.1416	.1319	.1399	.1497	.1565
20.0	76.2	.1345	.1190	.1095	.1192	.1277	.1397
30.0	76.2	.0994	.0853	.0792	.0867	.0930	.1020
40.0	76.2	.0787	.0661	.0611	.0678	.0722	.0806
50.0	76.3	.0644	.0525	.0485	.0543	.0572	.0666
60.0	76.3	.0533	.0426	.0393	.0444	.0469	.0595
70.0	76.5	.0446	.0351	.0325	.0369	.0391	.0410
80.0	76.3	.0377	.0295	.0277	.0309	.0318	.0338
90.0	76.2	.0321	.0251	.0237	.0262	.0271	.0291
100.0	75.9	.0284	.0217	.0206	.0226	.0235	.0252

Table 12. Representative Results of Experiment 3.
An 11.6 Second Aluminum Control Rod Insertion

Time (sec)	Depth (cm)	Fractional Changes for Detectors					
		1	2	3	4	5	6
.0	.0	1.0000	1.0000	1.0000	1.0000	1.0000	1.0000
.4	1.0	1.0383	1.0266	.9993	1.0035	1.0127	.9996
.8	3.2	1.0205	1.0137	.9795	.9868	.9975	.9825
1.2	5.7	.9877	.9884	.9490	.9607	.9717	.9580
1.6	8.3	.9655	.9642	.9143	.9349	.9422	.9279
2.0	10.9	.9438	.9329	.8710	.9014	.9041	.8937
2.4	13.6	.8941	.8981	.8086	.8680	.8650	.8551
2.8	16.3	.8447	.8546	.7556	.8285	.8208	.8122
3.2	19.0	.8029	.8118	.7051	.7520	.7777	.7679
3.6	21.7	.7183	.7624	.6567	.6969	.7268	.7211
4.0	24.4	.6275	.7106	.6086	.6499	.6633	.6768
4.4	27.2	.5822	.6045	.5549	.6057	.6185	.6319
4.8	29.9	.5420	.5613	.5165	.5617	.5749	.5887
5.2	32.6	.4986	.5213	.4787	.5223	.5319	.5479
5.6	35.4	.4691	.4844	.4461	.4892	.4938	.5096
6.0	38.2	.4273	.4499	.4099	.4542	.4570	.4728
6.4	41.0	.3986	.4192	.3812	.4214	.4235	.4398
6.8	43.6	.3695	.3902	.3525	.3912	.3941	.4091
7.2	46.4	.3454	.3622	.3283	.3628	.3675	.3819
7.6	49.2	.3225	.3351	.3056	.3373	.3425	.3568
8.0	51.9	.3000	.3106	.2845	.3128	.3218	.3344
8.4	54.7	.2847	.2903	.2670	.2907	.3018	.3145
8.8	57.5	.2696	.2727	.2531	.2706	.2847	.2967
9.2	60.2	.2582	.2566	.2460	.2508	.2692	.2809
9.6	63.0	.2419	.2410	.2329	.2349	.2619	.2670
10.0	65.7	.2588	.2302	.2225	.2216	.2496	.2540
10.4	68.4	.2516	.2388	.2128	.2103	.2381	.2422
10.8	71.2	.2414	.2294	.2031	.1997	.2277	.2309
11.2	73.9	.2283	.2152	.1931	.1891	.2166	.2215
11.6	76.3	.2214	.2079	.1860	.1938	.2090	.2135
12.0	76.2	.2157	.2013	.1804	.1898	.2030	.2080
15.0	76.2	.1817	.1678	.1521	.1605	.1714	.1766
20.0	76.2	.1498	.1352	.1229	.1318	.1383	.1418
30.0	76.2	.1106	.0957	.0869	.0952	.1034	.0969
40.0	76.3	.0871	.0733	.0662	.0734	.0773	.0751
50.0	76.3	.0705	.0581	.0522	.0584	.0629	.0616
60.0	76.3	.0594	.0472	.0423	.0477	.0503	.0504
70.0	76.3	.0479	.0380	.0343	.0389	.0412	.0422
80.0	76.3	.0413	.0325	.0293	.0332	.0342	.0355
90.0	76.3	.0351	.0274	.0250	.0280	.0292	.0311
100.0	76.3	.0302	.0233	.0216	.0238	.0248	.0266

Table 13. Representative Results of Experiment 4. A 525 Second Aluminum Control Rod Insertion

Time (sec)	Depth (cm)	Fractional Changes for Detectors					
		1	2	3	4	5	6
.0	.0	1.0000	1.0000	1.0000	1.0000	1.0000	1.0000
10.0	1.9	1.0186	1.0101	.9907	.9906	.9887	.9749
20.0	3.6	.9638	.9644	.9407	.9475	.9335	.9288
30.0	5.1	.9296	.9240	.8943	.9017	.9080	.8882
40.0	6.7	.8662	.8660	.8343	.8500	.8326	.8178
50.0	8.2	.7932	.8031	.7738	.7827	.7973	.7692
60.0	9.7	.7251	.7399	.7095	.7204	.7177	.6952
70.0	11.2	.6492	.6650	.6284	.6521	.6502	.6296
80.0	12.7	.5821	.5994	.5538	.5909	.5911	.5724
90.0	14.2	.5168	.5350	.4776	.5311	.5082	.4981
100.0	15.7	.4439	.4662	.4060	.4663	.4506	.4456
110.0	17.2	.3946	.4094	.3525	.4104	.3950	.3943
120.0	18.7	.3367	.3494	.3028	.3520	.3284	.3300
130.0	20.1	.2919	.3010	.2602	.3016	.2901	.2972
140.0	21.6	.2463	.2543	.2215	.2551	.2407	.2460
150.0	23.1	.2101	.2171	.1903	.2176	.2059	.2119
160.0	24.5	.1749	.1826	.1609	.1831	.1774	.1894
170.0	26.0	.1452	.1523	.1363	.1531	.1489	.1624
180.0	27.4	.1201	.1259	.1143	.1274	.1243	.1376
190.0	28.9	.0993	.1047	.0957	.1066	.1030	.1010
200.0	30.3	.0839	.0882	.0815	.0892	.0870	.0855
210.0	31.8	.0699	.0735	.0687	.0739	.0734	.0721
230.0	34.7	.0490	.0502	.0491	.0506	.0535	.0529
250.0	37.6	.0354	.0359	.0356	.0360	.0396	.0394
270.0	40.4	.0262	.0267	.0261	.0266	.0293	.0296
290.0	43.3	.0202	.0208	.0197	.0206	.0223	.0230
310.0	46.2	.0155	.0160	.0151	.0159	.0171	.0182
330.0	49.0	.0129	.0132	.0121	.0132	.0138	.0152
350.0	51.8	.0103	.0103	.0097	.0102	.0111	.0126
370.0	54.7	.0088	.0086	.0080	.0085	.0091	.0099
390.0	57.5	.0075	.0074	.0068	.0072	.0079	.0094
410.0	60.3	.0066	.0065	.0060	.0062	.0068	.0065
430.0	63.1	.0056	.0057	.0052	.0053	.0061	.0059
450.0	66.0	.0050	.0051	.0046	.0047	.0054	.0052
470.0	68.8	.0045	.0045	.0042	.0041	.0049	.0048
490.0	71.6	.0041	.0042	.0038	.0038	.0045	.0044
510.0	74.4	.0037	.0038	.0035	.0034	.0041	.0041
530.0	76.2	.0034	.0036	.0033	.0032	.0039	.0038
550.0	76.2	.0034	.0034	.0032	.0030	.0037	.0036
570.0	76.2	.0031	.0033	.0031	.0029	.0036	.0035
590.0	76.2	.0030	.0032	.0030	.0028	.0034	.0033

Table 14. Representative Results of Experiment 5.
A 2.6 Second Stainless Steel Control Rod Insertion

Time (sec)	Depth	Fractional Changes for Detectors					
		1	2	3	4	5	6
.0	.0	1.0000	1.0000	1.0000	1.0000	1.0000	1.0000
.1	.7	1.0182	1.0055	1.0138	1.0004	.9809	.9912
.2	.4	1.0182	1.0127	1.0116	1.0031	.9809	.9904
.3	1.9	1.0135	1.0073	.9939	.9887	.9692	.9853
.4	3.6	.9383	.9423	.8912	.9092	.8936	.9441
.5	7.0	.7253	.7843	.6629	.7510	.7495	.8454
.6	11.2	.5602	.6164	.4544	.6100	.5941	.7082
.7	15.9	.4228	.4590	.3059	.4635	.4509	.5645
.8	20.8	.3164	.3412	.2229	.3389	.3388	.4374
.9	25.8	.2450	.2672	.1694	.2607	.2610	.3377
1.0	30.7	.1921	.2142	.1345	.2082	.2087	.2649
1.1	35.7	.1568	.1763	.1102	.1704	.1720	.2132
1.2	40.7	.1332	.1489	.0927	.1425	.1457	.1756
1.3	45.7	.1147	.1281	.0801	.1196	.1263	.1485
1.4	50.6	.1028	.1128	.0711	.0992	.1121	.1286
1.5	56.3	.0924	.1005	.0644	.0772	.1011	.1135
1.6	60.9	.0862	.0919	.0599	.0619	.0940	.1025
1.7	65.2	.0821	.0856	.0569	.0557	.0885	.0946
1.8	69.3	.0780	.0815	.0546	.0525	.0852	.0891
1.9	72.4	.0777	.0793	.0533	.0511	.0831	.0848
2.0	74.5	.0754	.0777	.0524	.0500	.0817	.0825
2.1	75.5	.0744	.0765	.0516	.0492	.0802	.0799
2.2	75.9	.0724	.0750	.0506	.0483	.0789	.0785
2.3	76.0	.0720	.0737	.0499	.0476	.0777	.0770
2.4	76.1	.0708	.0727	.0490	.0468	.0765	.0755
2.5	76.2	.0697	.0714	.0483	.0459	.0753	.0742
3.0	76.2	.0643	.0663	.0448	.0427	.0701	.0685
4.0	76.2	.0580	.0590	.0396	.0379	.0629	.0610
5.0	76.2	.0512	.0526	.0359	.0339	.0565	.0472
6.0	76.2	.0521	.0501	.0328	.0308	.0529	.0488
10.0	76.2	.0388	.0372	.0241	.0236	.0399	.0362
15.0	76.3	.0300	.0280	.0184	.0181	.0308	.0276
20.0	76.3	.0257	.0234	.0152	.0152	.0257	.0224
30.0	76.3	.0178	.0163	.0111	.0109	.0188	.0158
40.0	76.3	.0138	.0126	.0087	.0085	.0151	.0129
50.0	76.3	.0108	.0102	.0070	.0068	.0120	.0099
60.0	76.3	.0089	.0086	.0057	.0056	.0098	.0081
70.0	76.3	.0073	.0070	.0047	.0046	.0081	.0067
80.0	76.3	.0061	.0060	.0040	.0039	.0067	.0055
90.0	76.3	.0053	.0051	.0033	.0033	.0058	.0048
100.0	76.3	.0045	.0043	.0028	.0028	.0048	.0040

Table 15. Representative Results of Experiment 6.
A 6.2 Second Stainless Steel Control Rod Insertion

Time (sec)	Depth (cm)	Fractional Changes for Detectors					
		1	2	3	4	5	6
.0	.0	1.0000	1.0000	1.0000	1.0000	1.0000	1.0000
.2	.4	1.0116	1.0075	1.0032	1.0040	1.0097	1.0024
.4	1.0	.9993	1.0045	1.0015	1.0036	1.0013	1.0030
.6	2.5	.9555	.9482	.9286	.9345	.9453	.9689
.8	6.5	.7192	.7764	.6819	.7539	.7731	.8310
1.0	10.5	.5730	.6332	.5129	.6224	.6289	.6821
1.2	14.1	.4679	.5066	.3649	.5062	.5078	.5583
1.4	17.6	.3807	.4054	.2776	.4085	.4133	.4582
1.6	20.9	.3124	.3354	.2225	.3284	.3399	.3790
1.8	24.1	.2591	.2824	.1829	.2744	.2832	.3159
2.0	27.3	.2201	.2401	.1527	.2332	.2396	.2656
2.2	30.4	.1854	.2055	.1296	.1990	.2045	.2246
2.4	33.6	.1576	.1774	.1103	.1719	.1763	.1916
2.6	36.9	.1368	.1540	.0949	.1485	.1531	.1649
2.8	40.1	.1194	.1352	.0831	.1299	.1345	.1430
3.0	43.4	.1060	.1196	.0736	.1140	.1192	.1251
3.2	46.6	.0951	.1069	.0659	.1005	.1072	.1106
3.4	49.7	.0865	.0969	.0601	.0885	.0975	.0992
3.6	52.5	.0803	.0888	.0557	.0788	.0902	.0900
3.8	55.3	.0750	.0821	.0517	.0690	.0839	.0824
4.0	57.9	.0710	.0767	.0485	.0593	.0789	.0763
4.2	60.4	.0666	.0720	.0460	.0511	.0746	.0710
4.4	62.8	.0637	.0682	.0437	.0457	.0710	.0666
4.6	65.1	.0609	.0647	.0418	.0423	.0678	.0626
4.8	67.4	.0591	.0618	.0402	.0400	.0652	.0596
5.0	69.5	.0569	.0594	.0388	.0381	.0629	.0567
5.2	71.4	.0552	.0572	.0375	.0365	.0610	.0546
5.4	73.0	.0536	.0554	.0365	.0354	.0593	.0527
5.6	74.2	.0524	.0540	.0355	.0343	.0580	.0509
5.8	75.0	.0511	.0528	.0349	.0336	.0565	.0494
6.0	75.2	.0502	.0518	.0342	.0330	.0555	.0480
6.2	78.3	.0492	.0505	.0332	.0321	.0539	.0469
6.4	76.4	.0489	.0498	.0335	.0316	.0535	.0457
6.6	76.2	.0478	.0488	.0329	.0309	.0532	.0445
6.8	76.2	.0468	.0479	.0323	.0304	.0530	.0433
10.0	76.2	.0410	.0394	.0252	.0247	.0425	.0359
20.0	76.2	.0252	.0231	.0153	.0151	.0269	.0233
30.0	76.2	.0184	.0167	.0112	.0110	.0197	.0162
40.0	76.2	.0139	.0128	.0088	.0086	.0155	.0124
60.0	76.3	.0084	.0082	.0056	.0054	.0101	.0085
80.0	76.3	.0059	.0058	.0039	.0038	.0068	.0057
100.0	76.3	.0043	.0043	.0028	.0027	.0049	.0041

Table 16. Representative Results of Experiment 7. An 11.3 Second Stainless Steel Control Rod Insertion

Time (sec)	Depth (cm)	Fractional Changes for Detectors					
		1	2	3	4	5	6
.0	.0	1.0000	1.0000	1.0000	1.0000	1.0000	1.0000
.4	.8	1.0006	1.0018	.9899	.9878	1.0073	.9953
.8	3.0	.9352	.9366	.8732	.9102	.9314	.9243
1.2	5.5	.7403	.8461	.7359	.7807	.8127	.8234
1.6	8.1	.6428	.6948	.6095	.6798	.7084	.7214
2.0	10.8	.5408	.5913	.4981	.5943	.6067	.6222
2.4	13.4	.4508	.4929	.3783	.5013	.5119	.5311
2.8	16.1	.3748	.4062	.2932	.4163	.4291	.4500
3.2	18.9	.3146	.3387	.2354	.3388	.3569	.3802
3.6	21.6	.2634	.2876	.1922	.2845	.2984	.3207
4.0	24.4	.2222	.2444	.1597	.2410	.2522	.2709
4.4	27.2	.1838	.2068	.1345	.2042	.2132	.2295
4.8	29.9	.1577	.1769	.1125	.1751	.1819	.1950
5.2	32.7	.1357	.1529	.0964	.1512	.1563	.1667
5.6	35.5	.1170	.1326	.0821	.1304	.1355	.1435
6.0	38.3	.1013	.1159	.0716	.1133	.1180	.1245
6.4	41.1	.0892	.1018	.0622	.0993	.1040	.1086
6.8	44.0	.0790	.0900	.0561	.0867	.0924	.0955
7.2	46.8	.0707	.0803	.0498	.0763	.0827	.0843
7.6	49.6	.0640	.0722	.0450	.0671	.0747	.0750
8.0	52.5	.0591	.0656	.0412	.0593	.0682	.0675
8.4	55.3	.0537	.0597	.0377	.0514	.0626	.2086
8.8	58.1	.0500	.0549	.0349	.0435	.0580	.0554
9.2	60.9	.0471	.0509	.0323	.0365	.0542	.0514
9.6	63.7	.0440	.0475	.0304	.0321	.0508	.0480
10.0	66.6	.0420	.0446	.0284	.0292	.0480	.0450
10.4	69.4	.0401	.0422	.0280	.0273	.0457	.0425
10.8	72.2	.0430	.0400	.0267	.0257	.0449	.0404
11.2	75.0	.0422	.0383	.0261	.0246	.0434	.0387
11.6	76.2	.0411	.0402	.0258	.0239	.0423	.0374
12.0	76.2	.0402	.0391	.0249	.0231	.0411	.0364
15.0	76.2	.0337	.0323	.0207	.0206	.0349	.0305
20.0	76.2	.0274	.0256	.0167	.0165	.0282	.0242
30.0	76.3	.0194	.0181	.0115	.0119	.0206	.0163
40.0	76.3	.0146	.0135	.0092	.0091	.0160	.0132
50.0	76.3	.0113	.0108	.0073	.0072	.0131	.0105
60.0	76.3	.0091	.0088	.0059	.0059	.0105	.0085
70.0	76.3	.0075	.0074	.0049	.0049	.0087	.0070
80.0	76.3	.0063	.0062	.0041	.0040	.0072	.0058
90.0	76.3	.0053	.0053	.0034	.0034	.0060	.0049
100.0	76.3	.0046	.0046	.0029	.0029	.0053	.0043

Table 17. Representative Results of Experiment 8.
A 43 Second Stainless Steel Control Rod Insertion

Time	Depth	Fractional Changes for Detectors					
(sec)	(cm)	1	2	3	4	5	6
.0	.0	1.0000	1.0000	1.0000	1.0000	1.0000	1.0000
2.0	.2	.9235	.9219	.9161	.9246	.9157	.9287
4.0	5.8	.7516	.7597	.7562	.7239	.7407	.7569
6.0	9.6	.5056	.5934	.5887	.5725	.5615	.5840
8.0	13.3	.3791	.4117	.3530	.4356	.4016	.4368
10.0	17.1	.2819	.2993	.2257	.3154	.2946	.3220
12.0	20.8	.2057	.2164	.1509	.2281	.2142	.2373
14.0	24.5	.1496	.1580	.1057	.1673	.1572	.1765
16.0	28.2	.1102	.1177	.0792	.1245	.1178	.1340
18.0	31.9	.0957	.0965	.0599	.0946	.0922	.1037
20.0	35.6	.0753	.0757	.0464	.0772	.0716	.0821
22.0	39.3	.0604	.0605	.0369	.0612	.0566	.0662
24.0	43.0	.0481	.0488	.0298	.0490	.0458	.0464
26.0	46.7	.0401	.0404	.0247	.0402	.0379	.0388
28.0	50.4	.0335	.0336	.0208	.0328	.0320	.0330
30.0	54.1	.0291	.0285	.0180	.0270	.0275	.0285
32.0	57.7	.0248	.0245	.0158	.0218	.0242	.0251
34.0	61.3	.0226	.0215	.0141	.0159	.0215	.0223
36.0	65.0	.0204	.0191	.0128	.0139	.0193	.0200
38.0	68.6	.0188	.0172	.0117	.0122	.0175	.0181
40.0	72.2	.0173	.0156	.0108	.0109	.0162	.0166
42.0	75.6	.0163	.0144	.0101	.0102	.0151	.0154
44.0	76.2	.0156	.0137	.0096	.0097	.0143	.0146
46.0	76.2	.0147	.0130	.0091	.0092	.0136	.0140
48.0	76.2	.0142	.0124	.0087	.0088	.0129	.0133
50.0	76.2	.0133	.0118	.0083	.0083	.0123	.0126
55.0	76.2	.0018	.0105	.0073	.0074	.0110	.0105
60.0	76.2	.0106	.0095	.0065	.0067	.0100	.0094
65.0	76.2	.0096	.0086	.0059	.0060	.0090	.0085
70.0	76.2	.0087	.0078	.0053	.0055	.0081	.0077
75.0	76.2	.0078	.0071	.0048	.0050	.0074	.0069
80.0	76.2	.0072	.0065	.0044	.0046	.0068	.0064
85.0	76.2	.0064	.0060	.0040	.0042	.0062	.0059
90.0	76.2	.0059	.0055	.0037	.0039	.0057	.0054
95.0	76.2	.0054	.0051	.0034	.0035	.0053	.0050
100.0	76.2	.0049	.0047	.0031	.0033	.0049	.0046

Table 18. Representative Results of Experiment 9.
A 166 Second Stainless Steel Control Rod Insertion

Time (sec)	Depth (cm)	Fractional Changes for Detectors					
		1	2	3	4	5	6
.0	.0	1.0000	1.0000	1.0000	1.0000	1.0000	1.0000
4.0	1.9	.9595	.9424	.9177	.9217	.9240	.9235
8.0	3.8	.8148	.8254	.8158	.7943	.8027	.8045
12.0	5.6	.6850	.6978	.7115	.6748	.6714	.6800
16.0	7.5	.5759	.5928	.5817	.5823	.5519	.5637
20.0	9.3	.4664	.4719	.4254	.4682	.4414	.4578
24.0	11.1	.3761	.3758	.3214	.3732	.3518	.3669
28.0	12.9	.2979	.2980	.2432	.2963	.2797	.2934
32.0	14.8	.2434	.2402	.1817	.2364	.2228	.2325
36.0	16.6	.1905	.1863	.1350	.1866	.1768	.1884
40.0	18.4	.1565	.1512	.1035	.1496	.1425	.1549
44.0	20.2	.1225	.1201	.0802	.1194	.1147	.1121
48.0	22.0	.1001	.0984	.0635	.0971	.0932	.0910
52.0	23.8	.0807	.0799	.0505	.0785	.0755	.0742
56.0	25.6	.0652	.0650	.0408	.0633	.0614	.0612
60.0	27.5	.0538	.0540	.0333	.0524	.0506	.0507
64.0	29.3	.0440	.0444	.0273	.0432	.0416	.0422
68.0	31.1	.0362	.0369	.0226	.0360	.0346	.0356
72.0	32.9	.0300	.0304	.0188	.0298	.0289	.0301
76.0	34.8	.0255	.0255	.0159	.0252	.0245	.0259
80.0	36.6	.0216	.0216	.0134	.0215	.0208	.0222
84.0	38.4	.0185	.0187	.0116	.0187	.0179	.0193
88.0	40.2	.0163	.0160	.0100	.0160	.0154	.0169
92.0	42.1	.0139	.0138	.0086	.0138	.0134	.0149
96.0	43.9	.0120	.0120	.0074	.0119	.0117	.0112
100.0	45.8	.0106	.0106	.0065	.0104	.0103	.0099
104.0	47.6	.0094	.0093	.0058	.0091	.0090	.0087
108.0	49.5	.0085	.0084	.0052	.0081	.0080	.0077
112.0	51.3	.0076	.0076	.0046	.0072	.0072	.0069
116.0	53.2	.0069	.0069	.0042	.0065	.0065	.0062
120.0	55.0	.0062	.0063	.0038	.0057	.0059	.0056
124.0	56.9	.0054	.0057	.0034	.0050	.0054	.0051
128.0	58.8	.0049	.0051	.0031	.0042	.0049	.0046
136.0	62.5	.0042	.0044	.0027	.0032	.0042	.0039
144.0	66.2	.0036	.0037	.0023	.0026	.0037	.0034
152.0	70.0	.0032	.0033	.0021	.0022	.0033	.0030
160.0	73.7	.0028	.0028	.0018	.0019	.0029	.0027
168.0	76.2	.0026	.0026	.0017	.0017	.0027	.0024
176.0	76.2	.0024	.0024	.0016	.0016	.0025	.0023
184.0	76.2	.0022	.0022	.0015	.0015	.0024	.0021
192.0	76.2	.0021	.0020	.0014	.0014	.0022	.0020
200.0	76.2	.0020	.0019	.0013	.0013	.0021	.0019

Table 19. Representative Results of Experiment 10.
A 312 Second Stainless Steel Control Rod Insertion

Time (sec)	Depth (cm)	Fractional Changes for Detectors					
		1	2	3	4	5	6
.0	.0	1.0000	1.0000	1.0000	1.0000	1.0000	1.0000
8.0	.0	1.0046	1.0015	1.0050	1.0000	1.0181	1.0113
16.0	1.8	.9697	.9681	.9299	.9377	.9402	.9319
24.0	3.9	.7797	.8007	.7918	.7634	.7673	.7663
32.0	6.0	.6196	.6343	.6470	.6118	.6026	.6058
40.0	8.0	.4759	.4869	.4450	.4792	.4615	.4692
48.0	10.1	.3513	.3555	.3065	.3491	.3330	.3392
56.0	12.1	.2606	.2573	.2111	.2528	.2447	.2537
64.0	14.2	.1946	.1902	.1450	.1868	.1823	.1959
72.0	16.2	.1398	.1379	.0987	.1359	.1310	.1408
80.0	18.3	.0991	.0967	.0681	.0966	.0938	.1013
88.0	20.3	.0734	.0718	.0488	.0708	.0690	.0755
96.0	22.3	.0524	.0533	.0355	.0526	.0525	.0700
104.0	24.3	.0401	.0405	.0263	.0397	.0393	.0550
112.0	26.3	.0304	.0309	.0199	.0306	.0298	.0429
120.0	28.4	.0232	.0235	.0152	.0235	.0231	.0377
128.0	30.4	.0182	.0184	.0119	.0185	.0182	.0339
136.0	32.4	.0144	.0145	.0093	.0147	.0142	.0268
144.0	34.5	.0115	.0117	.0074	.0118	.0114	.0237
152.0	36.5	.0095	.0096	.0060	.0097	.0093	.0230
160.0	38.5	.0077	.0081	.0050	.0081	.0077	.0222
168.0	40.5	.0064	.0068	.0041	.0068	.0065	.0218
176.0	42.5	.0055	.0058	.0035	.0057	.0056	.0240
184.0	44.6	.0045	.0050	.0030	.0049	.0049	.0026
192.0	46.6	.0039	.0044	.0026	.0042	.0043	.0027
200.0	48.6	.0034	.0038	.0023	.0037	.0038	.0026
208.0	50.7	.0029	.0033	.0020	.0032	.0033	.0024
216.0	52.7	.0027	.0029	.0018	.0028	.0029	.0023
224.0	54.7	.0023	.0025	.0016	.0024	.0027	.0020
232.0	56.8	.0021	.0023	.0015	.0020	.0025	.0022
240.0	58.8	.0020	.0021	.0013	.0017	.0023	
248.0	60.8	.0018	.0018	.0012	.0015	.0021	
256.0	62.9	.0016	.0017	.0011	.0013	.0019	
264.0	64.9	.0016	.0016	.0011	.0011	.0018	
272.0	66.9	.0014	.0014	.0010	.0010	.0018	
280.0	69.0	.0014	.0013	.0010	.0009	.0017	
296.0	73.0	.0013	.0012	.0009	.0008	.0015	
312.0	76.2	.0012	.0011	.0008	.0008	.0014	
336.0	76.2	.0011	.0010	.0007	.0007	.0014	
360.0	76.2	.0010	.0009	.0007	.0006	.0012	
384.0	76.2	.0009	.0009	.0006	.0006	.0012	

APPENDIX C

KINETICS SIMULATIONS

This appendix contains the tabular presentation of the ten simulations discussed in Chapter V. The initial detector values can be found from the calculated distributions given in Chapter V. The kinetics parameters are also included in Chapter V. The power histories are those reported in Appendix B. The mathematical controls are given in Table 20. The space-time and adiabatic simulations versus time and control rod position are given in Tables 21 through 30.

Table 20. Mathematical Controls for the Experimental Simulations

Experiment Number	Theta	Maximum Fractional Change	Minimum Time Step (Sec)	Maximum Time Step (Sec)	Print Time Step (Sec)	Over-relaxation Time Step (Sec)	Outer Iteration Error
1	1.0	.01	.001	.07	.10	.05	.0005
2	1.0	.01	.001	.07	.10	.05	.0005
3	1.0	.02	.01	.3	.50	.30	.0005
4	1.0	.05	.01	7.0	10.0	5.0	.0005
5	1.0	.05	.001	.055	.10	.05	.001
6	1.0	.05	.001	.11	.20	.10	.001
7	1.0	.05	.001	.30	.50	.25	.001
8	1.0	.05	.001	.55	1.0	.50	.001
9	1.0	.05	.001	1.6	3.0	1.5	.001
10	1.0	.05	.001	3.2	6.0	3.0	.001

Table 21. Representative Results of the Kinetics Simulations of Experiment 1

Time	Depth	Prediction of Fractional Changes for Detectors											
(sec)	(cm)	Detector 1		Detector 2		Detector 3		Detector 4		Detector 5		Detector 6	
		S.T.	Adb.	S.T.	Adb.	S.T.	Adb.	S.T.	Adb.	S.T.	Adb.	S.T.	Adb.
.0	.0	1.0000	1.0000	1.0000	1.0000	1.0000	1.0000	1.0000	1.0000	1.0000	1.0000	1.0000	1.0000
.1	1.3	.9969	.9962	.9964	.9967	.9937	.9946	.9964	.9967	.9964	.9965	.9967	.9966
.2	2.4	.9861	.9914	.9864	.9922	.9834	.9883	.9861	.9922	.9866	.9920	.9872	.9921
.3	5.4	.9713	.9828	.9720	.9846	.9646	.9759	.9720	.9847	.9718	.9841	.9731	.9844
.4	9.3	.9526	.9688	.9539	.9720	.9328	.9485	.9537	.9722	.9536	.9710	.9551	.9716
.5	13.8	.9189	.9449	.9220	.9500	.8713	.8971	.9217	.9503	.9210	.9484	.9244	.9494
.6	18.5	.8695	.9115	.8746	.9185	.7983	.8394	.8743	.9189	.8728	.9161	.8772	.9175
.7	23.4	.8084	.8669	.8153	.8757	.7214	.7756	.8147	.8762	.8127	.8726	.8183	.8745
.8	28.3	.7432	.8128	.7511	.8227	.6564	.7200	.7506	.8230	.7480	.8189	.7541	.8212
.9	33.1	.6785	.7530	.6868	.7633	.5958	.6630	.6861	.7633	.6834	.7592	.6895	.7617
1.0	38.0	.6171	.6909	.6251	.7010	.5408	.6064	.6236	.7005	.6217	.6968	.6275	.6995
1.1	42.8	.5630	.6306	.5706	.6398	.4926	.5531	.5679	.6377	.5673	.6359	.5727	.6384
1.2	47.7	.5159	.5750	.5227	.5832	.4513	.5043	.5176	.5782	.5198	.5798	.5245	.5820
1.3	52.5	.4754	.5260	.4816	.5331	.4165	.4616	.4727	.5239	.4791	.5303	.4831	.5322
1.4	57.3	.4435	.4847	.4486	.4907	.3889	.4257	.4284	.4692	.4468	.4888	.4499	.4902
1.5	62.3	.4158	.4497	.4205	.4549	.3650	.3954	.3887	.4208	.4193	.4536	.4220	.4546
1.6	66.7	.3942	.4220	.3986	.4267	.3466	.3714	.3585	.3840	.3979	.4261	.3998	.4267
1.7	71.0	.3772	.3995	.3813	.4040	.3318	.3518	.3378	.3580	.3811	.4038	.3826	.4042
1.8	74.9	.3627	.3817	.3669	.3862	.3193	.3362	.3233	.3404	.3671	.3864	.3680	.3865
1.9	75.7	.3555	.3698	.3597	.3742	.3131	.3257	.3168	.3295	.3599	.3745	.3604	.3746
2.0	76.0	.3519	.3623	.3561	.3667	.3100	.3191	.3134	.3227	.3564	.3669	.3567	.3670
2.1	76.1	.3488	.3571	.3529	.3614	.3072	.3146	.3106	.3180	.3532	.3617	.3534	.3618
2.2	76.2	.3457	.3529	.3497	.3572	.3045	.3109	.3077	.3142	.3500	.3574	.3502	.3575
3.0	76.2	.3222	.3278	.3260	.3317	.2838	.2887	.2868	.2918	.3263	.3320	.3265	.3321
4.0	76.2	.2965	.3014	.3001	.3051	.2612	.2655	.2640	.2684	.3003	.3053	.3005	.3053
5.0	76.2	.2745	.2787	.2777	.2821	.2418	.2455	.2443	.2482	.2779	.2823	.2781	.2824
6.0	76.2	.2554	.2592	.2585	.2623	.2250	.2283	.2274	.2308	.2587	.2625	.2588	.2626

Table 22. Representative Results of the Kinetics Simulations of Experiment 2

Time	Depth	Prediction of Fractional Changes for Detectors											
		Detector 1		Detector 2		Detector 3		Detector 4		Detector 5		Detector 6	
(sec)	(cm)	S.T.	Adb.	S.T.	Adb.	S.T.	Adb.	S.T.	Adb.	S.T.	Adb.	S.T.	Adb.
.0	.0	1.0000	1.0000	1.0000	1.0000	1.0000	1.0000	1.0000	1.0000	1.0000	1.0000	1.0000	1.0000
.2	2.0	.9892	.9924	.9893	.9931	.9869	.9899	.9892	.9932	.9894	.9929	.9897	.9930
.4	6.1	.9627	.9773	.9639	.9793	.9545	.9696	.9638	.9794	.9636	.9788	.9648	.9791
.6	10.0	.9342	.9542	.9363	.9577	.9101	.9298	.9363	.9579	.9357	.9566	.9371	.9572
.8	13.5	.8970	.9227	.9009	.9275	.8525	.8778	.9007	.9278	.8997	.9260	.9016	.9269
1.0	17.0	.8589	.8867	.8638	.8929	.7970	.8244	.8639	.8932	.8622	.8908	.8643	.8921
1.2	20.4	.8115	.8439	.8177	.8512	.7375	.7679	.8174	.8516	.8154	.8487	.8182	.8502
1.4	23.9	.7643	.7986	.7714	.8069	.6821	.7137	.7713	.8073	.7687	.8039	.7718	.8057
1.6	27.4	.7140	.7492	.7216	.7581	.6327	.6649	.7216	.7584	.7187	.7547	.7222	.7568
1.8	30.9	.6666	.6998	.6747	.7090	.5871	.6170	.6747	.7092	.6716	.7054	.6750	.7076
2.0	34.4	.6201	.6508	.6281	.6599	.5455	.5725	.6274	.6597	.6248	.6562	.6284	.6585
2.2	37.9	.5766	.6045	.5844	.6134	.5060	.5306	.5835	.6129	.5811	.6096	.5845	.6120
2.4	41.4	.5370	.5614	.5444	.5696	.4705	.4925	.5428	.5681	.5413	.5661	.5446	.5683
2.6	44.9	.5002	.5220	.5070	.5296	.4380	.4578	.5045	.5272	.5041	.5264	.5071	.5285
2.8	48.3	.4676	.4876	.4738	.4945	.4095	.4276	.4688	.4897	.4712	.4916	.4739	.4935
3.0	51.7	.4399	.4568	.4456	.4630	.3855	.4008	.4384	.4556	.4433	.4605	.4458	.4621
3.2	55.0	.4148	.4298	.4200	.4354	.3638	.3773	.4072	.4226	.4181	.4334	.4201	.4347
3.4	58.4	.3929	.4069	.3975	.4119	.3449	.3575	.3772	.3909	.3960	.4103	.3978	.4114
3.6	61.8	.3720	.3851	.3763	.3896	.3268	.3386	.3492	.3615	.3751	.3885	.3766	.3893
3.8	65.1	.3562	.3671	.3602	.3713	.3133	.3230	.3270	.3375	.3595	.3705	.3605	.3712
4.0	68.4	.3409	.3511	.3446	.3549	.3000	.3091	.3066	.3159	.3442	.3546	.3451	.3550
4.2	71.6	.3267	.3364	.3304	.3402	.2877	.2962	.2926	.3012	.3303	.3401	.3310	.3404
4.4	74.4	.3154	.3241	.3192	.3280	.2776	.2855	.2817	.2892	.3192	.3281	.3197	.3282
4.6	75.3	.3080	.3151	.3117	.3189	.2713	.2776	.2745	.2809	.3118	.3191	.3121	.3192
4.8	76.2	.3019	.3079	.3056	.3116	.2660	.2712	.2687	.2742	.3058	.3119	.3060	.3119
5.0	76.2	.2966	.3021	.3001	.3058	.2611	.2662	.2640	.2690	.3003	.3060	.3005	.3061
6.0	76.2	.2746	.2791	.2779	.2825	.2419	.2459	.2445	.2485	.2781	.2827	.2783	.2828
7.0	76.2	.2555	.2595	.2586	.2626	.2251	.2286	.2275	.2310	.2587	.2628	.2589	.2629
8.0	76.2	.2389	.2425	.2418	.2454	.2105	.2136	.2127	.2159	.2420	.2456	.2421	.2456
9.0	76.2	.2245	.2276	.2272	.2304	.1978	.2005	.1999	.2027	.2274	.2306	.2275	.2306
10.0	76.2	.2119	.0000	.2144	.0000	.1866	.0000	.1886	.0000	.2146	.0000	.2147	.0000

Table 23. Representative Results of the Kinetics Simulations of Experiment 3

Time (sec)	Depth (cm)	Prediction of Fractional Changes for Detectors											
		Detector 1		Detector 2		Detector 3		Detector 4		Detector 5		Detector 6	
		S.T.	Adb.	S.T.	Adb.	S.T.	Adb.	S.T.	Adb.	S.T.	Adb.	S.T.	Adb.
.0	.0	1.0000	1.0000	1.0000	1.0000	1.0000	1.0000	1.0000	1.0000	1.0000	1.0000	1.0000	1.0000
.5	1.5	.9901	.9895	.9898	.9900	.9887	.9876	.9898	.9901	.9898	.9899	.9900	.9900
1.0	4.4	.9634	.9733	.9641	.9747	.9589	.9677	.9639	.9748	.9641	.9743	.9648	.9745
1.5	7.6	.9404	.9532	.9416	.9557	.9313	.9439	.9416	.9558	.9414	.9550	.9418	.9554
2.0	10.9	.9109	.9236	.9128	.9274	.8824	.8946	.9127	.9276	.9124	.9262	.9131	.9269
2.5	14.2	.8682	.8853	.8718	.8903	.8218	.8382	.8720	.8906	.8707	.8887	.8723	.8896
3.0	17.6	.8268	.8417	.8313	.8478	.7656	.7796	.8315	.8482	.8299	.8458	.8312	.8470
3.5	21.0	.7737	.7913	.7796	.7984	.7006	.7172	.7799	.7988	.7776	.7959	.7797	.7974
4.0	24.4	.7250	.7399	.7316	.7477	.6469	.6606	.7320	.7481	.7293	.7449	.7312	.7466
4.5	27.8	.6706	.6856	.6776	.6939	.5941	.6080	.6778	.6941	.6749	.6907	.6772	.6926
5.0	31.2	.6204	.6337	.6281	.6421	.5468	.5586	.6283	.6422	.6251	.6388	.6275	.6408
5.5	34.7	.5684	.5811	.5758	.5893	.5001	.5112	.5755	.5891	.5728	.5860	.5753	.5880
6.0	38.2	.5217	.5329	.5289	.5408	.4576	.4677	.5283	.5403	.5259	.5375	.5283	.5396
6.5	41.6	.4789	.4887	.4858	.4959	.4202	.4287	.4843	.4945	.4829	.4928	.4854	.4948
7.0	45.0	.4405	.4490	.4467	.4555	.3860	.3937	.4445	.4534	.4441	.4527	.4462	.4545
7.5	48.5	.4055	.4136	.4112	.4194	.3556	.3627	.4068	.4152	.4089	.4170	.4109	.4186
8.0	51.9	.3743	.3816	.3793	.3867	.3282	.3348	.3732	.3805	.3773	.3847	.3790	.3861
8.5	55.4	.3472	.3537	.3517	.3582	.3046	.3105	.3403	.3468	.3501	.3566	.3516	.3577
9.0	58.8	.3225	.3295	.3265	.3335	.2833	.2895	.3088	.3157	.3252	.3323	.3264	.3332
9.5	62.3	.3009	.3067	.3046	.3103	.2644	.2697	.2817	.2870	.3036	.3094	.3047	.3101
10.0	65.7	.2827	.2883	.2860	.2915	.2487	.2537	.2589	.2640	.2853	.2910	.2861	.2915
10.5	69.1	.2656	.2709	.2686	.2738	.2337	.2385	.2387	.2433	.2683	.2736	.2689	.2739
11.0	72.5	.2501	.2560	.2530	.2589	.2202	.2255	.2238	.2290	.2529	.2589	.2533	.2591
11.5	76.2	.2366	.2420	.2396	.2449	.2084	.2132	.2108	.2155	.2397	.2451	.2401	.2452
12.0	76.2	.2301	.2335	.2329	.2363	.2026	.2057	.2049	.2079	.2330	.2365	.2332	.2365
15.0	76.2	.1950	.1973	.1973	.1997	.1718	.1738	.1736	.1756	.1975	.1998	.1976	.1998
16.0	76.2	.1856	.1878	.1878	.1901	.1635	.1655	.1652	.1672	.1879	.1902	.1880	.1903
17.0	76.2	.1775	.1794	.1796	.1816	.1563	.1581	.1580	.1597	.1798	.1817	.1798	.1818
18.0	76.2	.1700	.1719	.1721	.1740	.1498	.1514	.1514	.1530	.1722	.1741	.1723	.1741
19.0	76.2	.1634	.1651	.1654	.1671	.1440	.1454	.1455	.1470	.1655	.1672	.1656	.1672
20.0	76.2	.1574	.1589	.1593	.1609	.1387	.1400	.1401	.1415	.1594	.1610	.1595	.1610
25.0	76.2	.1339	.1350	.1355	.1366	.1180	.1189	.1192	.1202	.1356	.1367	.1357	.1368

Table 24. Representative Results of the Kinetics Simulations of Experiment 4

Time (sec)	Depth (cm)	Prediction of Fractional Changes for Detectors											
		Detector 1		Detector 2		Detector 3		Detector 4		Detector 5		Detector 6	
		S.T.	Adb.	S.T.	Adb.	S.T.	Adb.	S.T.	Adb.	S.T.	Adb.	S.T.	Adb.
.0	.0	1.0000	1.0000	1.0000	1.0000	1.0000	1.0000	1.0000	1.0000	1.0000	1.0000	1.0000	1.0000
20.0	3.6	.9332	.9446	.9339	.9458	.9285	.9402	.9339	.9459	.9337	.9455	.9339	.9457
40.0	6.7	.8666	.8775	.8682	.8795	.8587	.8699	.8682	.8796	.8678	.8789	.8681	.8792
60.0	9.7	.7833	.7895	.7854	.7923	.7649	.7709	.7857	.7924	.7848	.7914	.7854	.7919
80.0	12.7	.6816	.6842	.6844	.6876	.6524	.6546	.6846	.6877	.6836	.6865	.6842	.6871
100.0	15.7	.5653	.5782	.5684	.5818	.5295	.5417	.5686	.5820	.5675	.5807	.5681	.5814
120.0	18.7	.4536	.4548	.4569	.4583	.4176	.4183	.4570	.4585	.4558	.4571	.4566	.4578
140.0	21.6	.3535	.3514	.3566	.3547	.3193	.3173	.3567	.3549	.3555	.3535	.3564	.3542
160.0	24.5	.2653	.2662	.2680	.2690	.2369	.2376	.2682	.2691	.2670	.2679	.2677	.2686
180.0	27.4	.1947	.1956	.1968	.1979	.1726	.1736	.1969	.1980	.1960	.1971	.1965	.1976
200.0	30.3	.1411	.1423	.1429	.1442	.1245	.1255	.1429	.1442	.1422	.1434	.1427	.1439
220.0	33.2	.1024	.1026	.1038	.1040	.0902	.0903	.1038	.1040	.1032	.1035	.1036	.1038
240.0	36.1	.0739	.0741	.0749	.0752	.0649	.0651	.0749	.0751	.0745	.0748	.0748	.0750
260.0	39.0	.0542	.0540	.0550	.0548	.0475	.0474	.0549	.0547	.0546	.0545	.0548	.0547
280.0	41.8	.0399	.0399	.0405	.0404	.0350	.0350	.0404	.0403	.0403	.0402	.0404	.0404
300.0	44.7	.0306	.0299	.0310	.0303	.0268	.0262	.0309	.0302	.0308	.0301	.0309	.0303
320.0	47.5	.0233	.0230	.0236	.0233	.0204	.0201	.0234	.0231	.0234	.0232	.0235	.0233
340.0	50.4	.0182	.0182	.0184	.0185	.0159	.0160	.0182	.0182	.0183	.0184	.0184	.0184
360.0	53.2	.0145	.0144	.0147	.0146	.0127	.0126	.0144	.0143	.0146	.0145	.0146	.0146
380.0	56.1	.0117	.0117	.0118	.0119	.0103	.0103	.0114	.0114	.0118	.0118	.0118	.0119
400.0	58.9	.0097	.0097	.0098	.0098	.0085	.0085	.0093	.0093	.0098	.0098	.0098	.0098
420.0	61.7	.0081	.0082	.0082	.0083	.0072	.0072	.0076	.0077	.0082	.0082	.0082	.0083
440.0	64.6	.0071	.0071	.0072	.0071	.0063	.0062	.0066	.0065	.0072	.0071	.0072	.0071
460.0	67.4	.0062	.0062	.0062	.0062	.0054	.0054	.0056	.0056	.0062	.0062	.0062	.0062
480.0	70.2	.0054	.0054	.0055	.0055	.0047	.0048	.0048	.0048	.0054	.0055	.0055	.0055
500.0	73.0	.0048	.0048	.0049	.0049	.0042	.0042	.0043	.0043	.0049	.0049	.0049	.0049
520.0	75.6	.0043	.0043	.0044	.0044	.0038	.0038	.0039	.0039	.0044	.0044	.0044	.0044
540.0	76.2	.0040	.0040	.0040	.0041	.0035	.0035	.0036	.0036	.0040	.0041	.0040	.0041
560.0	76.2	.0037	.0037	.0038	.0038	.0033	.0033	.0033	.0033	.0038	.0038	.0038	.0038
580.0	76.2	.0035	.0035	.0036	.0036	.0031	.0031	.0031	.0031	.0036	.0036	.0036	.0036
600.0	76.2	.0033	.0033	.0034	.0034	.0029	.0029	.0030	.0030	.0034	.0034	.0034	.0034

Table 25. Representative Results of the Kinetics Simulations of Experiment 5

Time (sec)	Depth (cm)	Prediction of Fractional Changes for Detectors											
		Detector 1		Detector 2		Detector 3		Detector 4		Detector 5		Detector 6	
		S.T	Adb.	S.T.	Adb.	S.T.	Adb.	S.T.	Adb.	S.T.	Adb.	S.T.	Adb.
.0	.0	1.0000	1.0000	1.0000	1.0000	1.0000	1.0000	1.0000	1.0000	1.0000	1.0000	1.0000	1.0000
.1	.2	.9941	.9954	.9949	.9960	.9948	.9943	.9949	.9961	.9949	.9959	.9950	.9960
.2	.4	.9859	.9888	.9871	.9899	.9850	.9865	.9870	.9900	.9873	.9897	.9875	.9898
.3	1.9	.9512	.9631	.9541	.9685	.9402	.9525	.9537	.9688	.9539	.9673	.9563	.9680
.4	3.6	.8825	.9226	.8891	.9326	.8628	.9034	.8887	.9330	.8882	.9303	.8931	.9316
.5	7.0	.7866	.8624	.7993	.8806	.7535	.8272	.7989	.8814	.7971	.8764	.8043	.8788
.6	11.2	.6640	.7677	.6834	.7960	.5636	.6620	.6829	.7974	.6792	.7886	.6897	.7929
.7	15.9	.5191	.6417	.5426	.6773	.3801	.4742	.5421	.6791	.5366	.6673	.5481	.6731
.8	20.8	.3900	.4979	.4151	.5355	.2370	.3080	.4148	.5374	.4077	.5238	.4195	.5307
.9	25.8	.2969	.3722	.3210	.4070	.1613	.2044	.3211	.4086	.3132	.3952	.3230	.4023
1.0	30.7	.2302	.2746	.2522	.3047	.1192	.1428	.2523	.3058	.2444	.2937	.2525	.3004
1.1	35.7	.1855	.2071	.2045	.2312	.0943	.1059	.2034	.2311	.1972	.2217	.2045	.2276
1.2	40.7	.1526	.1639	.1687	.1831	.0771	.0829	.1665	.1813	.1621	.1751	.1684	.1801
1.3	45.6	.1293	.1352	.1423	.1502	.0649	.0680	.1391	.1467	.1367	.1437	.1418	.1478
1.4	50.6	.1120	.1158	.1214	.1266	.0563	.0582	.1129	.1182	.1173	.1218	.1212	.1249
1.5	56.3	.0995	.1016	.1053	.1085	.0501	.0510	.0861	.0899	.1029	.1055	.1054	.1075
1.6	60.9	.0908	.0926	.0948	.0966	.0458	.0465	.0666	.0678	.0932	.0951	.0950	.0962
1.7	65.2	.0857	.0868	.0874	.0884	.0432	.0436	.0526	.0538	.0870	.0881	.0878	.0885
1.8	69.3	.0817	.0829	.0818	.0825	.0412	.0416	.0435	.0427	.0822	.0832	.0824	.0830
1.9	72.4	.0791	.0802	.0779	.0787	.0399	.0403	.0404	.0407	.0790	.0800	.0787	.0793
2.0	74.5	.0774	.0784	.0756	.0761	.0390	.0394	.0385	.0388	.0770	.0778	.0764	.0769
2.1	75.5	.0761	.0770	.0740	.0745	.0384	.0387	.0375	.0376	.0756	.0763	.0749	.0753
2.2	75.9	.0751	.0759	.0728	.0732	.0379	.0382	.0369	.0369	.0745	.0751	.0736	.0741
2.3	76.0	.0741	.0748	.0717	.0722	.0374	.0376	.0363	.0363	.0734	.0741	.0725	.0730
2.4	76.1	.0731	.0738	.0707	.0712	.0369	.0371	.0357	.0358	.0724	.0731	.0715	.0720
2.5	76.2	.0721	.0729	.0696	.0702	.0364	.0367	.0352	.0353	.0714	.0721	.0704	.0710
3.0	76.2	.0676	.0683	.0654	.0658	.0342	.0344	.0330	.0331	.0670	.0676	.0662	.0666
3.5	76.2	.0636	.0642	.0614	.0618	.0321	.0323	.0310	.0311	.0630	.0635	.0622	.0626
4.0	76.2	.0599	.0605	.0579	.0583	.0303	.0304	.0292	.0293	.0593	.0598	.0586	.0589
5.0	76.2	.0536	.0540	.0518	.0521	.0271	.0272	.0262	.0261	.0531	.0535	.0524	.0527
6.0	76.2	.0484	.0487	.0468	.0470	.0244	.0245	.0236	.0236	.0479	.0482	.0473	.0475

Table 26. Representative Results of the Kinetics Simulations of Experiment 6

Time (sec)	Depth (cm)	Prediction of Fractional Changes for Detectors											
		Detector 1		Detector 2		Detector 3		Detector 4		Detector 5		Detector 6	
		S.T.	Adb.	S.T.	Adb.	S.T.	Adb.	S.T.	Adb.	S.T.	Adb.	S.T.	Adb.
.0	.0	1.0000	1.0000	1.0000	1.0000	1.0000	1.0000	1.0000	1.0000	1.0000	1.0000	1.0000	1.0000
.4	1.0	.9481	.9649	.9508	.9678	.9425	.9594	.9503	.9680	.9507	.9672	.9520	.9675
.8	6.5	.7533	.8249	.7653	.8411	.7245	.7938	.7655	.8418	.7631	.8374	.7672	.8395
1.2	14.1	.5129	.5902	.5345	.6187	.3996	.4636	.5350	.6201	.5291	.6109	.5355	.6155
1.6	20.9	.3445	.3833	.3679	.4124	.2096	.2361	.3687	.4139	.3610	.4033	.3673	.4087
2.0	27.3	.2426	.2578	.2639	.2832	.1301	.1392	.2645	.2843	.2567	.2744	.2626	.2797
2.4	33.6	.1790	.1837	.1973	.2046	.0916	.0946	.1969	.2048	.1905	.1966	.1957	.2015
2.8	40.1	.1347	.1368	.1492	.1529	.0681	.0692	.1484	.1516	.1433	.1462	.1478	.1503
3.2	46.6	.1056	.1064	.1162	.1179	.0533	.0536	.1127	.1142	.1117	.1129	.1151	.1161
3.6	52.6	.0873	.0878	.0943	.0953	.0441	.0441	.0864	.0873	.0912	.0920	.0936	.0942
4.0	57.9	.0753	.0761	.0797	.0805	.0381	.0382	.0619	.0632	.0778	.0787	.0793	.0799
4.4	62.8	.0678	.0681	.0700	.0703	.0342	.0342	.0459	.0464	.0692	.0696	.0699	.0702
4.8	67.4	.0618	.0625	.0626	.0628	.0312	.0313	.0350	.0352	.0626	.0631	.0629	.0631
5.2	71.4	.0577	.0583	.0572	.0575	.0291	.0293	.0298	.0300	.0579	.0583	.0577	.0579
5.6	74.2	.0547	.0552	.0535	.0537	.0276	.0278	.0274	.0274	.0545	.0549	.0541	.0543
6.0	75.2	.0523	.0528	.0508	.0511	.0264	.0265	.0259	.0259	.0520	.0523	.0514	.0517
6.4	76.2	.0500	.0506	.0484	.0487	.0253	.0254	.0245	.0245	.0496	.0500	.0490	.0493
6.8	76.2	.0481	.0486	.0465	.0468	.0243	.0244	.0235	.0235	.0476	.0481	.0470	.0474
7.2	76.2	.0463	.0467	.0448	.0450	.0234	.0235	.0226	.0226	.0459	.0462	.0453	.0456
7.6	76.2	.0446	.0450	.0432	.0434	.0225	.0226	.0218	.0218	.0442	.0446	.0437	.0439
8.0	76.2	.0431	.0434	.0416	.0419	.0217	.0219	.0210	.0210	.0427	.0430	.0421	.0423
8.4	76.2	.0416	.0420	.0402	.0404	.0210	.0211	.0203	.0203	.0412	.0415	.0407	.0409
8.8	76.2	.0403	.0406	.0389	.0391	.0203	.0204	.0197	.0196	.0399	.0402	.0394	.0396
9.2	76.2	.0390	.0393	.0377	.0379	.0197	.0198	.0190	.0190	.0386	.0389	.0381	.0383
9.6	76.2	.0378	.0381	.0366	.0367	.0191	.0192	.0185	.0184	.0375	.0377	.0370	.0372
10.0	76.2	.0367	.0370	.0355	.0356	.0186	.0186	.0179	.0179	.0364	.0366	.0359	.0361
10.4	76.2	.0357	.0360	.0345	.0346	.0180	.0181	.0174	.0174	.0354	.0356	.0349	.0351
10.8	76.2	.0348	.0350	.0336	.0337	.0176	.0176	.0170	.0169	.0344	.0346	.0340	.0341
11.2	76.2	.0339	.0341	.0327	.0328	.0171	.0171	.0165	.0165	.0335	.0337	.0331	.0332
11.6	76.2	.0330	.0332	.0319	.0320	.0167	.0167	.0161	.0161	.0327	.0329	.0323	.0324
12.0	76.2	.0322	.0324	.0311	.0312	.0163	.0163	.0157	.0157	.0319	.0321	.0315	.0316

Table 27. Representative Results of the Kinetics Simulations of Experiment 7

Time (sec)	Depth (cm)	Prediction of Fractional Changes for Detectors											
		Detector 1		Detector 2		Detector 3		Detector 4		Detector 5		Detector 6	
		S.T.	Adb.	S.T.	Adb.	S.T.	Adb.	S.T.	Adb.	S.T.	Adb.	S.T.	Adb.
.0	.0	1.0000	1.0000	1.0000	1.0000	1.0000	1.0000	1.0000	1.0000	1.0000	1.0000	1.0000	1.0000
.5	1.3	.9310	.9499	.9337	.9536	.9256	.9428	.9333	.9538	.9338	.9528	.9350	.9533
1.0	4.2	.8023	.8502	.8113	.8609	.7811	.8295	.8120	.8614	.8096	.8584	.8126	.8598
1.5	7.5	.7014	.7544	.7143	.7716	.6720	.7215	.7149	.7723	.7119	.7676	.7144	.7699
2.0	10.8	.5775	.6228	.5949	.6448	.4984	.5436	.5956	.6459	.5910	.6391	.5951	.6424
2.5	14.1	.4735	.5085	.4942	.5331	.3698	.3994	.4953	.5343	.4890	.5264	.4932	.5303
3.0	17.5	.3884	.4099	.4096	.4352	.2688	.2869	.4103	.4365	.4038	.4278	.4085	.4322
3.5	20.9	.3072	.3243	.3281	.3489	.1873	.1998	.3289	.3502	.3219	.3412	.3263	.3458
4.0	24.4	.2522	.2612	.2723	.2845	.1399	.1457	.2731	.2856	.2660	.2767	.2704	.2814
4.5	27.8	.2002	.2076	.2183	.2284	.1069	.1114	.2190	.2292	.2122	.2211	.2164	.2255
5.0	31.3	.1669	.1712	.1834	.1904	.0863	.0882	.1837	.1910	.1776	.1833	.1817	.1876
5.5	34.8	.1352	.1381	.1493	.1540	.0693	.0708	.1491	.1540	.1439	.1478	.1477	.1516
6.0	38.3	.1152	.1160	.1276	.1300	.0582	.0588	.1270	.1296	.1227	.1243	.1260	.1278
6.5	47.9	.0819	.0828	.0893	.0913	.0413	.0417	.0852	.0874	.0861	.0876	.0886	.0900
7.0	45.4	.0801	.0825	.0877	.0917	.0404	.0415	.0857	.0898	.0845	.0877	.0864	.0902
7.5	48.9	.0713	.0721	.0778	.0793	.0360	.0363	.0736	.0752	.0750	.0762	.0770	.0782
8.0	52.5	.0636	.0636	.0687	.0691	.0321	.0320	.0630	.0634	.0665	.0667	.0682	.0683
8.5	56.0	.0565	.0568	.0601	.0607	.0285	.0285	.0498	.0508	.0586	.0590	.0597	.0601
9.0	59.5	.0514	.0515	.0539	.0541	.0259	.0258	.0397	.0401	.0529	.0530	.0537	.0538
9.5	63.0	.0472	.0473	.0486	.0487	.0238	.0237	.0316	.0320	.0481	.0482	.0487	.0486
10.0	66.6	.0438	.0438	.0445	.0443	.0221	.0220	.0255	.0256	.0444	.0443	.0445	.0444
10.5	70.1	.0410	.0414	.0409	.0411	.0207	.0208	.0216	.0205	.0412	.0415	.0411	.0413
11.0	73.6	.0388	.0391	.0381	.0382	.0196	.0197	.0196	.0196	.0387	.0389	.0384	.0385
11.5	74.9	.0372	.0375	.0363	.0364	.0187	.0189	.0185	.0185	.0370	.0372	.0367	.0368
12.0	76.2	.0357	.0361	.0347	.0348	.0180	.0182	.0175	.0175	.0355	.0357	.0351	.0352
13.0	76.2	.0334	.0337	.0323	.0325	.0169	.0170	.0163	.0163	.0331	.0334	.0327	.0329
14.0	76.2	.0314	.0317	.0304	.0305	.0159	.0159	.0154	.0153	.0312	.0314	.0307	.0309
15.0	76.2	.0297	.0299	.0287	.0288	.0150	.0151	.0145	.0145	.0295	.0296	.0291	.0292
20.0	76.2	.0238	.0239	.0230	.0230	.0120	.0120	.0116	.0116	.0236	.0236	.0233	.0233
25.0	76.2	.0201	.0202	.0194	.0194	.0102	.0102	.0098	.0098	.0199	.0200	.0197	.0197
30.0	76.2	.0174	.0175	.0168	.0168	.0088	.0088	.0085	.0085	.0173	.0173	.0170	.0170

Table 28. Representative Results of the Kinetics Simulations of Experiment 8

Time (sec)	Depth (cm)	Prediction of Fractional Changes for Detectors											
		Detector 1		Detector 2		Detector 3		Detector 4		Detector 5		Detector 6	
		S.T.	Adb.	S.T.	Adb.	S.T.	Adb.	S.T.	Adb.	S.T.	Adb.	S.T.	Adb.
.0	.0	1.0000	1.0000	1.0000	1.0000	1.0000	1.0000	1.0000	1.0000	1.0000	1.0000	1.0000	1.0000
2.0	2.2	.8618	.8850	.8661	.8908	.8510	.8738	.8664	.8911	.8656	.8895	.8663	.8902
4.0	5.8	.7122	.7415	.7227	.7544	.6887	.7165	.7231	.7550	.7207	.7514	.7223	.7531
6.0	9.6	.5569	.5827	.5717	.6006	.4996	.5269	.5725	.6015	.5685	.5961	.5711	.5987
8.0	13.3	.4155	.4347	.4325	.4543	.3322	.3507	.4334	.4553	.4282	.4490	.4312	.4521
10.0	17.1	.3037	.3170	.3208	.3362	.2138	.2250	.3217	.3371	.3161	.3306	.3196	.3339
12.0	20.8	.2190	.2274	.2345	.2445	.1341	.1406	.2353	.2454	.2298	.2392	.2331	.2424
14.0	24.5	.1616	.1659	.1751	.1807	.0897	.0924	.1757	.1814	.1707	.1758	.1736	.1787
16.0	28.2	.1183	.1209	.1295	.1332	.0632	.0646	.1298	.1337	.1257	.1288	.1283	.1315
18.0	31.9	.0904	.0911	.0997	.1012	.0467	.0472	.0999	.1015	.0963	.0974	.0985	.0997
20.0	35.6	.0687	.0694	.0761	.0775	.0351	.0355	.0760	.0774	.0732	.0743	.0751	.0762
22.0	39.3	.0546	.0548	.0606	.0613	.0277	.0278	.0602	.0610	.0582	.0586	.0598	.0603
24.0	43.0	.0440	.0439	.0487	.0489	.0223	.0222	.0477	.0481	.0467	.0468	.0481	.0481
26.0	46.7	.0364	.0363	.0400	.0402	.0184	.0183	.0386	.0389	.0384	.0385	.0395	.0396
28.0	50.4	.0308	.0306	.0336	.0335	.0156	.0154	.0314	.0313	.0324	.0322	.0332	.0331
30.0	54.0	.0267	.0265	.0287	.0286	.0135	.0133	.0256	.0259	.0278	.0277	.0285	.0283
32.0	57.7	.0233	.0232	.0247	.0246	.0118	.0116	.0193	.0194	.0241	.0240	.0245	.0244
34.0	61.3	.0208	.0207	.0217	.0216	.0105	.0104	.0150	.0149	.0213	.0212	.0216	.0215
36.0	65.0	.0187	.0187	.0192	.0191	.0094	.0094	.0116	.0117	.0190	.0190	.0192	.0191
38.0	68.6	.0171	.0172	.0173	.0172	.0086	.0086	.0093	.0092	.0173	.0173	.0173	.0173
40.0	72.2	.0159	.0159	.0157	.0157	.0080	.0080	.0081	.0081	.0159	.0159	.0158	.0158
42.0	75.6	.0149	.0150	.0145	.0145	.0075	.0075	.0073	.0073	.0148	.0148	.0146	.0146
44.0	76.2	.0141	.0142	.0136	.0136	.0071	.0071	.0069	.0069	.0140	.0140	.0138	.0138
46.0	76.2	.0134	.0134	.0129	.0130	.0067	.0068	.0065	.0065	.0132	.0133	.0131	.0131
48.0	76.2	.0127	.0128	.0123	.0123	.0064	.0064	.0062	.0062	.0126	.0126	.0124	.0125
50.0	76.2	.0121	.0122	.0117	.0117	.0061	.0061	.0059	.0059	.0120	.0120	.0118	.0119
52.0	76.2	.0115	.0116	.0111	.0112	.0058	.0058	.0056	.0056	.0114	.0115	.0113	.0113
54.0	76.2	.0110	.0111	.0106	.0106	.0055	.0056	.0054	.0053	.0109	.0109	.0107	.0108
56.0	76.2	.0105	.0105	.0101	.0102	.0053	.0053	.0051	.0051	.0104	.0104	.0102	.0103
58.0	76.2	.0100	.0101	.0097	.0097	.0051	.0051	.0049	.0049	.0099	.0100	.0098	.0098
60.0	76.2	.0096	.0096	.0093	.0093	.0048	.0048	.0047	.0047	.0095	.0095	.0094	.0094

Table 29. Representative Results of the Kinetics Simulations of Experiment 9

Time (sec)	Depth (cm)	Prediction of Fractional Changes for Detectors											
		Detector 1		Detector 2		Detector 3		Detector 4		Detector 5		Detector 6	
		S.T.	Adb.	S.T.	Adb.	S.T.	Adb.	S.T.	Adb.	S.T.	Adb.	S.T.	Adb.
.0	.0	1.0000	1.0000	1.0000	1.0000	1.0000	1.0000	1.0000	1.0000	1.0000	1.0000	1.0000	1.0000
6.0	2.9	.8003	.8241	.8063	.8312	.7861	.8105	.8066	.8315	.8052	.8295	.8066	.8305
12.0	5.7	.6379	.6574	.6485	.6687	.6157	.6358	.6487	.6692	.6460	.6661	.6483	.6675
18.0	8.4	.4967	.5125	.5086	.5258	.4635	.4794	.5091	.5264	.5060	.5226	.5079	.5245
24.0	11.1	.3468	.3599	.3591	.3731	.2967	.3109	.3597	.3737	.3560	.3696	.3582	.3716
30.0	13.9	.2500	.2590	.2613	.2713	.1963	.2050	.2619	.2719	.2584	.2679	.2602	.2699
36.0	16.6	.1794	.1837	.1892	.1944	.1285	.1326	.1897	.1949	.1865	.1913	.1882	.1931
42.0	19.3	.1243	.1278	.1326	.1366	.0804	.0837	.1330	.1371	.1302	.1339	.1318	.1355
48.0	22.1	.0906	.0929	.0976	.1004	.0531	.0545	.0980	.1008	.0955	.0981	.0969	.0995
54.0	24.8	.0658	.0671	.0715	.0731	.0364	.0372	.0718	.0734	.0696	.0711	.0708	.0723
60.0	27.5	.0481	.0490	.0526	.0538	.0259	.0264	.0527	.0540	.0510	.0521	.0520	.0531
66.0	30.2	.0372	.0372	.0410	.0413	.0194	.0194	.0411	.0414	.0396	.0398	.0404	.0407
72.0	32.9	.0280	.0280	.0309	.0311	.0144	.0144	.0309	.0312	.0298	.0299	.0305	.0307
78.0	35.6	.0215	.0217	.0238	.0242	.0110	.0111	.0238	.0242	.0229	.0232	.0235	.0239
84.0	38.4	.0170	.0171	.0189	.0192	.0086	.0087	.0189	.0191	.0182	.0183	.0186	.0188
90.0	41.1	.0134	.0135	.0149	.0151	.0068	.0068	.0147	.0149	.0143	.0144	.0147	.0148
96.0	43.9	.0108	.0109	.0120	.0121	.0055	.0055	.0118	.0119	.0115	.0116	.0118	.0119
102.0	46.7	.0089	.0089	.0098	.0099	.0045	.0045	.0095	.0096	.0094	.0095	.0097	.0097
108.0	49.5	.0074	.0074	.0080	.0081	.0037	.0037	.0076	.0076	.0077	.0078	.0079	.0080
114.0	42.3	.0062	.0062	.0067	.0068	.0032	.0031	.0062	.0062	.0065	.0065	.0067	.0067
120.0	55.1	.0054	.0053	.0058	.0057	.0027	.0027	.0049	.0049	.0056	.0056	.0057	.0057
126.0	57.8	.0047	.0047	.0050	.0049	.0024	.0023	.0039	.0039	.0048	.0048	.0049	.0049
132.0	60.6	.0041	.0041	.0043	.0043	.0021	.0021	.0031	.0030	.0042	.0042	.0043	.0043
138.0	63.4	.0036	.0036	.0038	.0037	.0018	.0018	.0024	.0024	.0037	.0037	.0038	.0037
144.0	66.2	.0033	.0033	.0033	.0033	.0016	.0016	.0019	.0019	.0033	.0033	.0033	.0033
150.0	69.1	.0030	.0030	.0030	.0030	.0015	.0015	.0016	.0016	.0030	.0030	.0030	.0030
156.0	71.9	.0027	.0027	.0027	.0027	.0014	.0014	.0014	.0014	.0027	.0027	.0027	.0027
162.0	74.6	.0025	.0025	.0025	.0025	.0013	.0013	.0013	.0012	.0025	.0025	.0025	.0025
168.0	75.7	.0024	.0024	.0023	.0023	.0012	.0012	.0012	.0012	.0023	.0023	.0023	.0023
174.0	76.2	.0022	.0022	.0021	.0021	.0011	.0011	.0011	.0011	.0022	.0022	.0022	.0022
180.0	76.2	.0021	.0021	.0020	.0020	.0011	.0011	.0010	.0010	.0021	.0021	.0020	.0021

Table 30. Representative Results of the Kinetics Simulations of Experiment 10

Time (sec)	Depth (cm)	Prediction of Fractional Changes for Detectors											
		Detector 1		Detector 2		Detector 3		Detector 4		Detector 5		Detector 6	
		S.T.	Adb.	S.T.	Adb.	S.T.	Adb.	S.T.	Adb.	S.T.	Adb.	S.T.	Adb.
.0	.0	1.0000	1.0000	1.0000	1.0000	1.0000	1.0000	1.0000	1.0000	1.0000	1.0000	1.0000	1.0000
12.0	.6	.9313	.9382	.9328	.9399	.9279	.9349	.9326	.9399	.9328	.9395	.9329	.9397
24.0	3.9	.6952	.7041	.7038	.7123	.6780	.6882	.7038	.7127	.7021	.7104	.7025	.7115
36.0	7.0	.5016	.5144	.5115	.5252	.4797	.4934	.5118	.5257	.5090	.5227	.5106	.5242
48.0	10.1	.3210	.3314	.3311	.3422	.2824	.2953	.3316	.3427	.3285	.3394	.3301	.3410
60.0	13.1	.2020	.2072	.2107	.2164	.1619	.1680	.2111	.2169	.2084	.2140	.2098	.2154
72.0	16.2	.1285	.1315	.1356	.1390	.0935	.0962	.1360	.1394	.1337	.1369	.1349	.1381
84.0	19.2	.0785	.0804	.0838	.0859	.0510	.0528	.0840	.0862	.0822	.0843	.0832	.0852
96.0	22.3	.0509	.0522	.0549	.0564	.0294	.0303	.0551	.0566	.0537	.0551	.0544	.0559
108.0	25.3	.0329	.0334	.0358	.0365	.0181	.0184	.0359	.0366	.0348	.0355	.0354	.0361
120.0	28.4	.0218	.0222	.0240	.0245	.0116	.0118	.0241	.0246	.0232	.0237	.0237	.0242
132.0	31.5	.0153	.0155	.0169	.0172	.0080	.0080	.0170	.0172	.0164	.0166	.0167	.0169
144.0	34.5	.0108	.0108	.0119	.0121	.0055	.0056	.0119	.0121	.0115	.0116	.0118	.0119
156.0	37.5	.0079	.0080	.0088	.0089	.0040	.0041	.0088	.0089	.0085	.0085	.0087	.0088
168.0	40.5	.0060	.0060	.0066	.0067	.0030	.0030	.0066	.0066	.0064	.0064	.0066	.0066
180.0	43.5	.0047	.0047	.0052	.0052	.0024	.0024	.0051	.0051	.0050	.0050	.0051	.0051
192.0	46.6	.0037	.0037	.0041	.0041	.0019	.0019	.0040	.0040	.0039	.0039	.0041	.0041
204.0	49.6	.0030	.0030	.0033	.0033	.0015	.0015	.0031	.0031	.0032	.0032	.0033	.0033
216.0	52.7	.0025	.0025	.0027	.0027	.0013	.0013	.0025	.0025	.0027	.0026	.0027	.0027
228.0	55.7	.0022	.0021	.0023	.0023	.0011	.0011	.0019	.0019	.0022	.0022	.0023	.0023
240.0	58.8	.0019	.0019	.0020	.0020	.0010	.0009	.0015	.0015	.0020	.0019	.0020	.0020
252.0	61.8	.0017	.0017	.0017	.0017	.0008	.0008	.0012	.0012	.0017	.0017	.0017	.0017
264.0	64.9	.0015	.0015	.0015	.0015	.0008	.0007	.0009	.0009	.0015	.0015	.0015	.0015
276.0	67.9	.0013	.0013	.0014	.0013	.0007	.0007	.0007	.0007	.0014	.0014	.0014	.0014
288.0	71.0	.0012	.0012	.0012	.0012	.0006	.0006	.0006	.0006	.0012	.0012	.0012	.0012
300.0	74.0	.0011	.0011	.0011	.0011	.0006	.0006	.0006	.0006	.0011	.0011	.0011	.0011
312.0	76.2	.0011	.0011	.0010	.0010	.0005	.0005	.0005	.0005	.0011	.0011	.0010	.0010
324.0	76.2	.0010	.0010	.0010	.0010	.0005	.0005	.0005	.0005	.0010	.0010	.0010	.0010
336.0	76.2	.0010	.0010	.0009	.0009	.0005	.0005	.0005	.0005	.0009	.0009	.0009	.0009
348.0	76.2	.0009	.0009	.0009	.0009	.0005	.0005	.0004	.0004	.0009	.0009	.0009	.0009
360.0	76.2	.0009	.0009	.0008	.0008	.0004	.0004	.0004	.0004	.0009	.0009	.0008	.0008

BIBLIOGRAPHY

1. T. J. Thompson and J. G. Beckerly, The Technology of Nuclear Reactor Safety, The M.I.T. Press, Cambridge, Massachusetts, 1964.

2. S. Kaplan, et al, "Space-Time Reactor Dynamics," Proceedings of the Third United Nations International Conference on the Peaceful Uses of Atomic Energy, 1964, Vol. 4, 41-50, United Nations, New York.

3. D. K. Butler and D. A. Meneley, "Recent Developments in Fast Reactor Kinetics," Nuclear Safety, 9, 125 (March-April) 1968.

4. A. F. Henry, "Analytical Methods in Reactor Kinetics," WAPD-OP-10.

5. T. W. Kerlin, "Status of Space-Time Analysis," Nuclear Safety, 6 (4), 395-398 (Summer 1965).

6. J. B. Yasinsky, "Notes on Nuclear Reactor Kinetics," WAPD-TM-960, Atomic Power Laboratory (July 1970).

7. A. F. Henry, "Neutron Kinetics," Selected Basic Technique, Naval Reactors Physics Handbook, A. Radkowsky (Ed.) Vol. I, U.S. Atomic Energy Commission (1964).

8. J. B. Yasinsky, op. cit.

9. J. B. Yasinsky and A. F. Henry, "Some Numerical Experiments Concerning Space-Time Reactor Kinetics Behavior," Nuclear Science and Engineering, 22, 171-181 (1965).

10. A. F. Henry and N. J. Curlee, "Verification of a Method for Treating Neutron Space-Time Problems," Nuclear Science and Engineering, 4, (6), 727-744 (December 1958).

11. S. Kaplan, "Some New Methods of Flux Synthesis," Nuclear Science and Engineering, 13, 22-31 (1962).

12. W. M. Stacey, Jr., "A General Modal-Expansion Method for Obtaining Approximate Equations for Linear Systems," Nuclear Science and Engineering, 28, 438-442 (1967).

13. J. B. Yasinsky, "Numerical Studies of Combined Space-Time Synthesis," Nuclear Science and Engineering, 34, 158-168 (1968).

14. K. F. Hansen, A Comparative Review of Two-Dimensional Kinetics Methods, GA-8169, General Atomic (1967).

BIBLIOGRAPHY (Continued)

15. A. F. Henry and A. V. Vota, "WIGL2-A Program for the Solution of the One-Dimensional, Two-Group Space-Time Diffusion Equations Accounting for Temperature, Xenon, and Control Feedback," WAPD-TM-532, Bettis Atomic Power Laboratory (1965).

16. R. S. Varga, Matrix Iterative Analysis, Prentice-Hall, Inc., Englewood Cliffs, N. J. (1962).

17. J. A. Thie, Reactor Noise, Rowman and Littlefield, New York, 1963.

18. J. E. Grund, Self-Limiting Excursion Tests of a Highly Enriched Plate-Type D_2O Moderated Reactor Part I, Initial Test Series, USAEC Report IDO-16891, Phillips Petroleum Co. (July 1963).

19. P. T. Kaneson and L. R. Foulke, "Investigations in Spatial Reactor Kinetics," Nuclear Science and Engineering, 17 (4) pp. 528-533 (December 1963).

20. R. J. Johnson, Investigations of the Space-Dependent Zero Power Reactor Source Transfer Function, Ph.D. Dissertation, Georgia Institute of Technology, Atlanta, Georgia (September 1966).

21. N. J. Diaz and M. J. Ohanian, "Space-Time Kinetics Studies in a Large, Close to Critical H_2O-UO_2 Assembly," Transactions of the American Nuclear Society, 13, 236 (1970).

22. R. A. Rydin, J. A. Burke, W. E. Moore, and K. W. Seemann, "Space-Time Experiments and Calculations for a Loosely Coupled Core," Transactions of the American Nuclear Society, 13 (2), 698 (1970).

23. A. F. Henry, "Review of Computational Methods for Space-Time Kinetics," Proceedings of the Conference in the Effective Use of Computers in Nuclear Industry, Knoxville, Tennessee, CONF-690401

24. K. F. Hansen, Private Communications (April 1969).

25. "Safeguards Report for the Georgia Tech Research Reactor," Georgia Institute of Technology, Atlanta, Georgia (Unpublished) (January 1960).

26. "Safety Analysis Report for the 5 Mw Georgia Tech Research Reactor," Georgia Institute of Technology, Atlanta, Georgia (Unpublished) (December 1967).

BIBLIOGRAPHY (Concluded)

27. "Fluid Power Data Book," Womack Machine Supply Company, Dallas, Texas (1967).

28. T. M. Apostol, Mathematical Analysis-A Modern Approach to Advanced Calculus, Addison-Wesley Publishing Company, Inc., Reading, Massachusetts, 1957, page 339.

29. E. L. Wachspress, Iterative Solution of Elliptic Systems and Applications to the Neutron Diffusion Equations of Reactor Physics, Prentice-Hall Publishing Company, Inc., Englewood Cliffs, N. J. (1966).

30. G. G. Bilodeau, et al., "PDQ--An IBM-704 Code to Solve the Two-Dimensional Few-Group Neutron-Diffusion Equations," WAPD-TM-70, Westinghouse (August 1957).

31. J. B. Yasinsky, M. Natelson, L. A. Hageman, "TWIGL--A Program to Solve the Two-Dimensional, Two-Group, Space-Time Neutron Diffusion Equations with Temperature Feedback," WAPD-TM-743

32. G. Bilodeau and L. Hageman, "A Survey of Numerical Methods in the Solution of Diffusion Problems," WAPD-TM-64, Bettis Atomic Power Laboratory (July 1957).

33. T. B. Fowler, M. L. Tobias, and D. R. Vondy, "EXTERMINATOR--A Multigroup Code for Solving Neutron Diffusion Equations in One and Two Dimensions," USAEC Report ORNL-TM-842, Oak Ridge National Laboratory (1965).

34. J. J. Seidler, J. D. Clement, and W. R. Klein, Reactor Physics Calculations for the 5 Mw Georgia Tech Research Reactor, Technical Report GT-NE-9, Nuclear Engineering Series, Georgia Institute of Technology, Atlanta, Georgia (September 1968).

35. R. H. Shudde and J. Dyer, "TEMPEST, A Neutron Thermalization Code," NAA Program Description, Decks No. 3W-354 (September 1960).

36. D. J. McGoff, "FORM--A Fourier Transform Fast Spectrum Code for the IBM-709," NAA-SR-Memo-5766 (September 1960).

37. W. W. Graham and D. S. Harmer, The Determination of Effective Delayed Neutron and Photoneutron Kinetics Parameters in a Highly Enriched Heavy Water Reactor, Technical Report GT-NE-3, Nuclear Engineering Series, Georgia Institute of Technology, Atlanta, Georgia (August 1965).

38. Report RE-129, AMD Program Library, Argonne National Laboratory.

VITA

Gabriel Howard Weaver was born on November 26, 1943 in Humacao, Puerto Rico. He attended public school in Quitman, Georgia and graduated from Brook County High School in 1962. In 1966 Mr. Weaver received the Bachelor of Science in Physics from the Georgia Institute of Technology. While an undergraduate he worked for the Georgia Tech Engineering Experiment Station and participated in the development of ceramic radomes and platinum-deposited radar antennas. Between 1966 and 1971 Mr. Weaver was engaged in graduate study in the School of Nuclear Engineering. While completing his Doctor of Philosophy degree, he worked for Technical Analysis Corporation, developing airline scheduling and tariff research systems.

Mr. Weaver is married to the former Elizabeth Anne Sherwood of Atlanta, Georgia and has two children, Robert and David. He is a member of the American Nuclear Society, Tau Beta Pi, and Sigma Xi.